Design of Ultra-large-pore Ordered Mesoporous Silicas and Grafting of Organic Groups on Their Surfaces

by

Liang Huang

A dissertation submitted to the Graduate Faculty in Chemistry in partial fulfillment of the requirements for the degree of Doctor of Philosophy,

The City University of New York

2012

This manuscript have been read and accepted for the

Graduate Faculty in Chemistry in satisfaction of the dissertation requirement for the degree of Doctor of Philosophy.

Dr. Michal Kruk

Date	Chair of Examining Committee

Dr. Maria C. Tamargo

Date	Executive Officer

Dr. Shuiqin Zhou

Dr. Jong I. Lee

Dr. Krishnaswami Raja

Dr. Michal Kruk

Supervisory Committee

THE CITY UNIVERSITY OF NEW YORK

Abstract

Design of Ultra-large Pore Ordered Mesoporous Silicas and Grafting of Organic Groups on their Surfaces

by

Liang Huang

Advisor: Dr. Michal Kruk

Developing novel methods to synthesize ordered mesoporous silicas with ultra-large pores and exploring robust approaches to functionalize their surfaces are two attractive topics in material science. Focused on these two aspects, this dissertation includes the selection of swelling agents for the synthesis of ordered mesoporous silicas templated by commercially available surfactants, and the development of diverse surface modification strategies to graft functional molecules on the surface of ordered mesoporous silicas.

In Chapter 2, the synthesis of FDU-12 silicas with face-centered cubic structure of ultra-large spherical mesopores was described. Xylene was identified as a superior micelle swelling agent, which worked perfectly with Pluronic F127 ($EO_{106}PO_{70}EO_{106}$). The unit-cell parameter of FDU-12 silicas was expanded up to 56 nm, and the pore diameter reached 36 nm without the loss of structural ordering. The acid treatment effectively suppressed the structural shrinkage. Ethylbenzene was proven to be another powerful swelling agent comparable with xylene. Highly ordered closed-pore FDU-12 silicas were prepared via a simple thermally-induced pore closure process at temperatures as low as 400-450 °C.

In Chapter 3, grafting of organic groups on surfaces of ordered mesoporous silicas was discussed. Polymers were grafted either by growing them from the initiation sites on the surface of the solid support ("grafting from" method) or attached to the surface by forming covalent bond between the chain ends and the functional groups on the surface ("grafting to" method). Polymer/FDU-12 silica composites were obtained by surface-initiated atom transfer radical polymerization (SI-ATRP) or surface-initiated atom transfer radical polymerization with activators regenerated by electron transfer (SI-ARGET ATRP). Good control of the polymerizations was observed in organic and protic media. The Huisgen azide-alkyne cycloaddition "click" reaction and thiol-ene "click" reaction were employed for grafting organic groups to the surfaces of SBA-15 silicas. The alkyne-azide "click" reaction was highly effective for grafting various azide molecules including low-molecular weight polymers to the inner surface of mesopores. The thiol-ene "click" was found less effective, but still suitable for the "grafting to" attachment of orgnic groups, including polymers, in nanopores.

This dissertation is dedicated to

my grandparents: Huang, Houkuan and Ju, Guilian

(黄厚宽 与 俱桂莲)

my parents: Huang, Qidong and Shen, Xiaokang

(黄其东 与 沈晓康)

and my husband: Liao, Yuanxi

(廖远熹)

Acknowledgements

I would like to sincerely and gratefully thank my advisor, Dr. Michal Kruk, for his guidance, encouragement, understanding, patience and kindness during my graduate studies at College of Staten Island/CUNY. His wisdom, knowledge and support helped me solve many puzzles in my research, overcome crisis situations and finish this dissertation. I am deeply thankful to him for carefully reading and correcting this manuscript.

I owe my gratitude to my thesis committee members, Dr. Krishnaswami Raja, Dr. Jong I. Lee and Dr. Shuiqin Zhou for their time, advice and support.

I would also like to thank all those people who have made this dissertation possible, Dr. Sukanta Dolai for the cooperation in part of my research; Dr. Liang Cao, Dr. Xuewu Yan, Dr. Manik Mandal and Chinming Hui for sharing experimental techniques and experiences; Mr. Tai Park for maintaining the instruments of TGA and GPC. I am also thankful to Dr. Krzysztof Matyjaszewski for offering the opportunity to get training in his laboratory and Dr. Hongchen Dong for teaching me how to effectively carry out ATRP.

I would like to express my gratitude to my parents for being the constant source of love, concern, strength and support all these years. I am also grateful to my husband for his tolerance, support and care.

Finally, I appreciate the financial support from the College of Staten Island, the Graduate Center of the City University of New York and Center for Engineered Polymeric Materials. The financial support from NSF and PRF is also acknowledged.

Table of Contents

List of Schemes

List of Figures

List of Tables

Chapter 1. Introduction

1.1. Ordered Mesoporous Silicas

When pores are created in a solid material, new features are introduced. Comparing to its peer nonporous material, the porous material usually has a larger specific surface area, lower bulk density, and the capacity to accommodate guest molecules (or other species) inside it. The advent of well-defined nanoporous materials has opened great opportunities in a variety of applications, such as adsorption, separation, heterogeneous catalysis, sensors and drug delivery systems.[1-2] According to the IUPAC definition[3], porous materials can be classified into three categories depending on their pore diameters. Mesoporous materials are those with pore diameter (or width) between 2 to 50 nm. As for the pore diameter below 2 nm or above 50 nm, these porous materials are defined as microporous and macroporous, respectively.

Among the well-defined nanoporous materials, ordered mesoporous materials have attracted much attention because their mesopores offer high specific surface area and high pore volume, which are important for the high-capacity adsorbents and allow them to accommodate large molecules, such as proteins or polymers, usually the sizes which are beyond the upper limit of the pore size for microporous materials. The first family of ordered mesoporous materials was ordered mesoporous silicas (OMSs) independently reported by Kuroda and coworkers (FSM-16)[4] and Mobil Corporation scientists (M41S family of materials)[5] in the early 1990s. These OMSs ended the long-standing pore-size constraint of zeolites, which are exclusively microporous as far as their primary pore system is concerned. Since then, the research in this field has rapidly grown.

The synthesis of OMSs primarily involves polycondensation of silica precursor in the presence of a surfactant template. Silica precursors undergo hydrolysis and condensation forming silica/surfactant ion pairs for cationic surfactants.[6] For nonionic surfactants, silica condenses in the corona area of the micelles. The above silica/surfactant ion-pairs or silica/micelle building blocks can assemble into ordered "liquid crystal" arrays.[7] In some cases, the rearrangements of the micellar structures within the composites may take place. As the condensation progresses, the silica framework replicates the structure of the surfactant micelle arrays, which may or may not correspond to micellar structures originally present in the surfactant solution. After that, the surfactant template can be removed by calcination or solvent extraction making the ordered mesopore spaces free in the final material. The hydrophilic/hydrophobic ratio of the surfactant, reaction temperature, concentrations (including pH) and the addition of salts are important parameters in the synthesis of OMSs. By adjusting these conditions, the mesostructures can be 2-dimensional (2-D) hexagonal, 3-dimensional (3-D) cubic, lamellar or disordered, and the geometry of the mesopores can be cylindrical, spherical or bicontinous gyroidal.

In aqueous solutions, the effective surfactant packing parameter g, ($g = V/a_0 l$), is a useful parameter to characterize the geometry of the mesophase products, where V is the total volume of the surfactant chains plus any organic cosolvent between the chains, a_0 is the effective head group area at the micelle surface, and l is the hydrophobic tail length of the surfactant.[8] Stucky and co-workers studied the relationship between g value and mesophase structure. The surfactant with relatively large hydrophilic part (large a_0) tends to associate in a spherical structure, and the cylinder or lamellar packing is favored if the

hydrophilic part is relatively smaller. As *g* is smaller than 1/3, cubic *Pm3n* structure is formed; when *g* is between 1/3 and 1/2, 2-D hexagonal (*p6mm*) structure is produced; cubic (*Ia3d*) phase is generated as $1/2<g<2/3$ and when *g* is close to 1, the lamellar phase is obtained.[8] These considerations for surfactant micelles prompted the use of different surfactants to tailor the structure of the surfactant-templated materials.

Alkylammonium surfactants were first used as templates and afforded OMSs with cylindrical pores (MCM-41 silica[5,9] and FSM-16 silica[4] of p6mm symmetry, and MCM-48 silica[5] of Ia3d symmetry). By increasing the size of ionic head groups of alkylammonium surfactants, spherical mesopores were obtained for SBA-1 silica[10-11] of Pm3n symmetry and SBA-2 silica[12] of $P6_3/mmc$ symmetry. The layered structures (MCM-50 silicas[5]) were favored when surfactants with large hydrophobic tails were used. However, the adjustment of the synthesis conditions may allow one to form a variety of structures with spherical, and cylindrical pores, as well as layered structures using a single alkylammonium surfactant. [6-8]

The limitation of common ionic surfactant templates (alkylammounium surfactants) is that the short length of the alkyl tail limits the size of micelles and results in moderate pore size (typically 2-7 nm). [8-9] On the other hand, the wall thickness of OMSs templated by ionic surfactants is typically in the range of 0.7-1.5 nm.[13] The non-ionic block-copolymer surfactants have larger hydrophilic and hydrophobic domains than the alkylammounium and other typical ionic surfactants, and therefore they can template OMSs with larger pore size and thicker walls. Moreover, the hydrophilic/hydrophobic domain volume ratio for the block copolymers can be easily tailored by simply adjusting

the length of the blocks and thus to template OMSs with different pore shape, structural symmetry, and pore size.

The introduction of commercially available Pluronic® block copolymers (poly(ethylene oxide)-poly(propylene oxide)-poly(ethylene oxide) triblock copolymers[14-16]) as surfactant templates, added new members with ordered cylindrical and spherical pores to the family of OMSs. The material with cylindrical mesopores include SBA-15 silica with 2-D hexagonal array of cylindrical mesopores with inter connections.[17-19] The ordered silicas with spherical mesopores (OSSMs) exhibit cage-like pores arranged in diverse structures, including SBA-16 of body-centered cubic structure (Im3m symmetry),[19] and SBA-12,[20] FDU-1,[21-22] FDU-12,[23] and KIT-5[24] of face-centered cubic (Fm3m symmetry) or mixed cubic close-packed structures.

OSSMs exhibit remarkable features, such as superior hydrothermal stability,[21-22] tunable pore cage diameters (within the range from ~5 to ~30 nm and beyond, as discussed in this Dissertation)[22,25] pore-entrance sizes (from below 1 nm to the diameter close to the pore cage size)[22] and 3-D pore connectivity.[11,23] These features provide advantages over their widely known counterparts with approximately cylindrical mesopores (such as MCM-41,[5,9] FSM-16,[4] SBA-15,[15-16,19] MCM-48[5,9,26] and KIT-6,[27-30] the latter two having Ia3d symmetry and pores with three-way intersections). For example, the narrow pore entrances of cage-like pores are beneficial to prevent the leaching of guest molecules from the OMS host, which is challenging for the cylindrical pores.[31] The three-dimensional pore connectivity provides faster mass transport and more accessible entrances to the pore cage than the two-dimensional pore system, and therefore

OSSMs are attractive solid hosts for heterogeneous catalysis[32] and enzymatic catalysis.[33] In addition, OSSMs can be synthesized in the form of powders,[15] thin films,[16] fibers,[34] and monoliths[35] to fulfill different requirements of applications. OSSMs were used as media for immobilization of biomolecules[36-38] and as supports for high-surface-area polymer brushes[39]. OSSMs were also found suitable as templates for isolated nanoparticles (including nanospheres)[40] and for ordered arrays of nanospheres of a variety of compositions.[23,25,41-42] Moreover, the transition between open-pore[16] and closed-pore[43-44] systems makes OSSMs promising low-dielectric-constant materials[45-47] for the development of on-chip electronics.

The adjustment of pore diameters, pore entrance size, and the maximization of the mesopore volume is important for the development of OSSMs. To obtain spherical pore structures, the block copolymer surfactants with large hydrophilic block(s) and relatively small hydrophobic block should be employed. Therefore, intrinsically the pore size which is the void space produced by the hydrophobic core of the micelles is typically small relative to the unit-cell volume. Several ways can be used to increase the size of the mesopores.

One straightforward method is to select a surfactant of a suitable molecular size [9,16], which affects the size of the formed micelles and the resulting templated pores. Another alternative way is to use micelle expander[9,19] that is solubilized in the micelles, thereby increasing their size. The application of micelle expander offers a convenient way to tune the pore size, and for instance, the pore diameter can be increased by simply increasing the amount of micelle expander added.[9,19] The selection of the micelle expander and

optimization of its amount in the synthesis may require careful consideration, because the organic addictives are able to change the shape of surfactant micelles and/or introduce their size nonuniformly, so the disordered structures can form.[48-49] The studies of the synthesis of large-pore SBA-15 (LP-SBA-15) [50] and large-pore FDU-12 (LP-FDU-12) [51] revealed that in some cases of low-temperature syntheses,[25] although pore size in the ordered structure was enlarged by adding micelle expanders, the uptake of micelle expanders by micelles was not significant. It was postulated that in such a case if the extent of solubilization of a micelle expander in the surfactant micelles can be made higher, and the addition of the micelle expander still does not disrupt the structure of the material, it might be possible to enhance the swelling and thus increase the pore size even further.[52] The prior extensive study on the extent of solubilization of aliphatic and aromatic hydrocarbons in the micelles of Pluronic block copolymers[53-54] provides useful reference for the selection of suitable micelle expander.[52] For example, the uptake of benzene derivatives in Pluronic block copolymer micelles was reported to decrease as the size and number of alkyl substituents on the benzene ring increased [53-54]. 1,3,5-trimethyl benzene (TMB) has been used as the micelle expander for the synthesis of SBA-15 to successfully increase the pore diameter to about 12 nm.[55] However, the further addition of TMB to the synthesis mixture[55] resulted in the phase transition from SBA-15 to mesocellular foams.[56] After TMB was identified as a "too strong" micelle expander for Pluronic P123 ($EO_{20}PO_{70}EO_{20}$) surfactant, 1,3,5-triisopropylbenzene (TIPB) which has larger substituents, was found to be a superior micelle expander for the synthesis of 2-D hexagonal materials (e.g. SBA-15) with cylindrical mesopores templated by Pluronic P123 [52]. The extent of solubilization of TIPB in P123 is expected to be lower than the

extent of solubilization of TMB. However, since the hydrophobic fraction in Pluronic P123 is high (70 wt.%), which makes this surfactant easy to be swollen,[53] the high uptake of TMB tends to result in the disordered structures, while the moderate uptake of TIPB expands the micelles and retains the periodic structure of the materials.

Based on the above reasoning, the selection of micelle expander should always involve consideration of the properties of the surfactant and the desired structure of the material. The surfactants used as templates for OSSMs usually have large hydrophilic proportion and small hydrophobic fraction, such as Pluronic F127 ($EO_{106}PO_{70}EO_{106}$). With a lower hydrophobic part content (30 wt.%), Pluronic F127 is less swollen comparing to Pluronic P123.[53] TMB turned out to be a good swelling agent for the F127-templated synthesis of LP-FDU-12 silica with face-centered cubic structure.[25] Aromatic hydrocarbons with fewer substituents on the benzene ring and thus have higher extent of solubilization in comparison to TMB could be promising candidates to further increase of the pore size of OSSMs. In our studies, [57,141] xylenes (dimethylbenzenes) and ethylbenzene were selected as swelling agent candidates for Pluronic F127 and they were applied to synthesize new generations of face-centered cubic silicas, which are referred to herein as ultra-large-pore FDU-12 (ULP-FDU-12). In addition, it was shown that highly ordered closed-pore silicas can be obtained using one-step low-temperature synthesis and remarkably low calcination temperature. The details of the synthesis of ULP-FDU-12 and the corresponding closed-pore OSSMs are discussed in Chapter 2.

1.2. Ordered Mesoporous Polymer/Silica Composites

Ordered mesoporous silicas are excellent solid supports for the synthesis of polymer/silica composites, because they have ordered structure, large surface area, high pore volume and large pore size. The mesopores can accommodate macromolecules, such as biomolecules[58-59] and polymers.[39,42,60-64] OMSs constitute an excellent model system to study the surface functionalization in nanopores,[2,65-67] because besides the characterization of the attached functional groups by using conventional analytical methods, the distribution of the functional groups on the surfaces can be readily studied by measuring the changes in the pore diameter, surface area and surface properties.[39,68] Mesoporous silica/polymer composites can be prepared via various methods.

1.2.1. Physical blending

The simplest way is directly mixing mesoporous silicas into polymers either by melt blending or solution blending. The physical properties of polymers can be greatly changed by adding a very low amount of mesoporous silicas into the polymer matrix. For example, when adding 3 wt.% of MCM-41 to polypropylene (PP)/polystyrene (PS) immiscible blend, the elastic modulus and tensile strength of the composites were higher than in the case of adding nanoscale silica particles (nonporous) at the same content because the high surface area and the existence of channels of MCM-41 improved adhesion between PP and PS phases.[69] The pore geometry and structure also showed some impact on the properties of polymer/silica composites. Comparing to FSM-16 (2-D hexagonal p6m symmetry), KIT-6 (cubic Ia3d approximately cylindrical pores with three-way intersections) was found more effective to decrease the coefficient of linear

thermal expansion of the epoxy polymer because the interfacial interaction between the polymer and the surface of KIT-6 silica was increased in the 3D gyroid mesopores.[70]

However, the effective dispersion of mesoporous silicas in the polymer matrix is challenging, because of the strong tendency of silica particles to agglomerate in polymer melts or polymer solutions.[71] The surface modification of silicas by organic groups is usually used to improve the dispersion or increase the interaction between polymers and silicas. By introducing proper functional groups on the surfaces of silicas, covalent bonds can be formed between polymers and the surfaces of silicas.

1.2.2. "Grafting from" method

When initiation sites are attached to the surfaces of a solid support, polymers can be grown from the surface via surface-initiated polymerization. This is called "grafting from" method. Grafting polymers from the surfaces of mesopores is challenging because the uncontrolled growth of polymers may block the mesopores and result in unevenly grafted composites. The development of controlled/living polymerizations provides versatile methods for surface-initiated grafting. Among various controlled polymerization techniques, atom transfer radical polymerization (ATRP) is a powerful tool, which can be used under mild reaction conditions and applied to a wide range of monomers. ATRP is based on a reversible halogen radical transfer between a dormant species (the initiator or the dormant propagating chain end) and a transition metal complex at a lower oxidation state (Mt^m/L_n, Mt^m is a transition metal at oxidation state m) to produce propagating radicals and the transition metal complex at the higher oxidation state (Mt^{m+1}/L_n) (the mechanism is shown in Scheme 1). Note that L refers to the ligands coordinated to the

transition metal and n is the number of the ligands in the complex.[72] During the polymerization, the equilibrium is strongly shifted to the dormant species. Therefore the concentration of radicals is maintained at a low level, which minimizes termination reactions. If the initiation is fast, all the chains grow over the same period of time, and the polymerization is typically well controlled. These properties of ATRP are very important for the grafting of polymers from nanoporous materials due to the limited space in the pores. Surface-initiated atom transfer radical polymerization (SI-ATRP) has been applied to graft polymers on flat surfaces or on spherical particles.[71,73] To improve the control of the polymerization and to reduce the number of dead grafted chains produced, sacrificial initiators were used to assist in controlling polymerization from surfaces, while the free polymer chains were unavoidably formed as the side product. By adding deactivor (Cu(II)) species at the beginning of polymerizations, Kruk and coworkers first achieved the successfully controlled SI-ATRP in ordered mesopores silicas.[39] In their work, polyacrylonitrile, poly(2-(dimethylamino)ethyl methacrylate) and polystyrene were grafted on the concave surfaces of SBA-15 silica with cylindrical pores of diameter 10 nm and FDU-1 silica with spherical pores of diameter 15 nm. The polymer film thicknesses were in the range up to 1−2 nm. In some cases, the polymers cleaved from the composites showed narrow molecular weight distributions with very low polydispersity (~1.06). The use of a larger-pore support was beneficial with respect to the polymer loading, because in the study of polymer grafting from the surface of typical SBA-15 with pore diameter of 10 nm, prominent pore blocking was observed above the polymer loading of 22 wt.%,[39] while the use of large-pore SBA-15 with pore diameter of 15 nm as a support for polymer grafting by ATRP allowed one to introduce high loadings

of polymer (up to 27-28 wt.%) without any major pore blockage[74-75]. As a result of the use of large-pore OMSs supports, various monomers have been successfully polymerized via "grafting from" strategy on the silicas with well defined cylindrical[39,76] or spherical mesopores[42] via SI-ATRP, such as styrene,[29,61,77] methyl methacrylate,[61,76] N-isopropylacrylamide,[64] acrylonitrile[39,42] and sodium p-styrenesulfonate.[77] The polymer loading and molecular weight were controlled by selecting polymerization time or other conditions.

One drawback of SI-ATRP is that a large amount of catalyst is required to achieve good control over the polymerization. The residue of the Cu catalyst adsorbed by high-surface area mesoporous silicas[78] or deposited within grafted polymer chains results in colored polymer/silica composites. A new method, atom transfer radical polymerization with activators regenerated by electron transfer (ARGET ATRP) greatly decreases the amount of copper to 10~100 ppm level without any appreciable loss of control over the polymerization.[79] In ARGET ATRP, $Cu(II)X_2/L_n$ (where X is halogen) is added at the beginning and continuously reduced by a reducing reagent to form the activator ($Cu(I)X/L_n$) in situ (the mechanism is shown in Scheme 1). The presence of the reducing reagent also makes ARGET ATRP tolerant to initial presence of air, which greatly simplifies the work in comparison to normal ATRP. SI-ARGET ATRP has been successfully applied to grow polymers on surfaces of mesopores of SBA-15 silicas. By using ultra-large pore SBA-15 (pore size ~22 nm) as the solid support, a high loading of PMMA (~36 wt%) was achieved via SI-ARGET ATRP without any major pore blockage and the corresponding thickness of PMMA layer was up to 2 nm. [76]

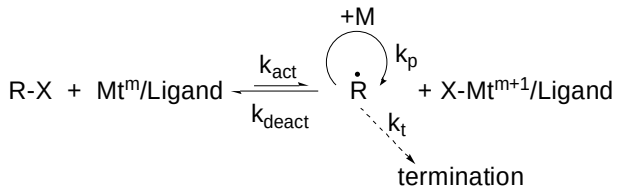

ATRP mechanism

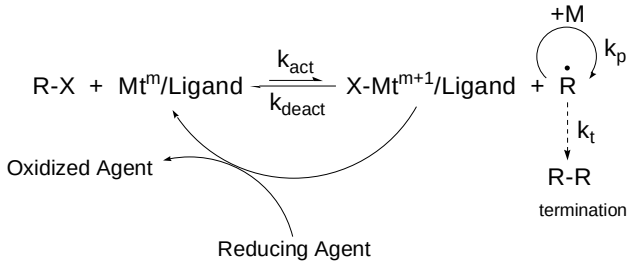

ARGET ATRP mechanism

R-X= dormant species or initiator
X=halogen atom
R•=propagating radicals
Mt^m=transition metal at lower oxidation state m
Mt^{m+1}=transition metal at higher oxidation state m+1
M= monomer

Scheme 1. Mechanism of atom transfer radical polymerization (ATRP)[72] and atom transfer radical polymerization with activators regenerated by electron transfer (ARGET ATRP)[79]

FDU-12 silicas with spherical pores and face centered cubic symmetry are attractive solid supports for the synthesis of polymer/silica composites. The spherical pores of FDU-12 silicas are connected to each other and form a 3-D matrix. The size of passages between the mesopores is smaller than the size of pore cages. Such 3-D pore connectivity provides many transport pathways to pores and is beneficial for fast mass transport.[23]

FDU-12 silicas were used as supports for the grafting of polyacrylonitrile (PAN) via SI-ATRP.[80] The grafted PAN was carbonized to prepare mesoporous carbon after silica dissolution. The mesoporous carbon exhibited ordered mesoporous structure as a replica of the FDU-12 support. However, since the connections between the mesopores of FDU-12 silica are often quite narrow, there is an increased risk of pore blocking during the polymerization if the polymerization proceeds uniformly throughout the surface of the material. From this point of view, the SI-ATRP or SI-ARGET ATRP in FDU-12 silicas is more complicated and challenging than in the case of cylindrical mesopores. In our study, we grafted temperature-responsive polymers from the surfaces of ultra-large pore FDU-12 silicas via both SI-ATRP and SI-ARGET ATRP. The polymerizations proceeded with good control in the mesopores, and the loadings of polymers were controlled by adjusting the polymerization time and other conditions.

1.2.3. "Grafting to" method

The main limitations of surface-initiated ATRP or ARGET ATRP and other polymerizations are the difficulty to characterize the grafted polymers and the side reactions, which limit the scope of monomers that can be successfully used. In contrast, the advantages of "grafting to" method are that a wide range of polymers can be prepared by using suitable polymerization approaches and the preformed polymers can be easily characterized. However, the main disadvantages of "grafting to" method include the high steric hindrance between the attached polymer chains and the incoming chains, and thus the low efficiency and the lack of chemical orthogonality of the coupling methods.

The development of the "click" chemistry provides promising coupling methods to solve the above problems in the "grafting to" approach. The "click" chemistry[81] is

defined as a set of modular and broadly applicable reactions that proceed with high stereospecificity and very high yield under benign conditions without offensive by-products. The "click" chemistry offers a powerful method to build up substances by joining small modular units together, which mimics the way of generating molecules in nature. Therefore since the advent of this concept, the "click" chemistry has attracted much attention and led to advancement in diverse areas of chemistry,[82-86] including the synthesis of organic compounds,[87] polymers,[88-93] nanocomposites,[94] therapeutic agents,[95] and bioconjugates.[96-102]

The Huisgen cycloaddition which involves a reaction between an azide group and a propargyl group to form a triazole linkage has been known as one of the powerful "click" reactions and attracted much attention. The process of this "click" reaction is described as "spring-loaded" for a single trajectory with a high thermodynamic driving force, usually greater than 20 kcal mol^{-1}.[81] The Cu(I)-catalyzed cycloaddition of azides to terminal alkynes exhibits broad scope and provides 1,4-disubstituted 1,2,3-triazoles in excellent yields and high region selectivity.[81] The mechanism of the Huisgen cycloaddition reaction is postulated as shown in Scheme 2, and the reaction is thought to proceed in a stepwise manner (A→B-1→B-2→B-3).[103]

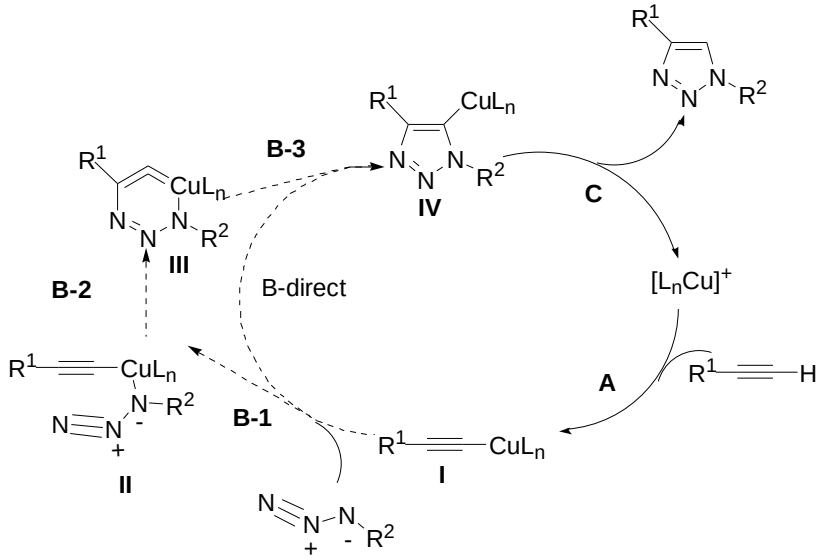

Scheme 2. Postulated catalytic cycle for azide-alkyne coupling[103]: L: a ligand or a counterion associated with copper (I/II). $[CuL_n]^+$: bi- or polynuclear Cu(I) species.

Huisgen cycloaddition has been applied to surface modification of porous materials,[104-116] including attachment of molecules to porous silicon for mass spectrometry application, modification of porous silicon with small molecules, oligomers and polymer [106,109,114-115], click functionalization of silica gels,[105,110,113] and the preparation of polymer-based stationary phases for HPLC.[104] In addition, "click" attachment of functional groups to ordered mesoporous materials[107-108,117-118] and metal-organic frameworks[111,116] was reported. The "clickable" OMSs can be prepared via co-condensation[108] and postsynthetic grafting approaches[107]. In the co-condensation method, organosilanes with desired functional groups are added during the initial step of the synthesis of OMSs, the condensation reaction takes place between the organosilanes and inorganic silica precursors and thus the functional groups are incorporated on the surfaces

or in the framework of OMSs. After the removal of surfactants by solvent-extraction, the functionalized ("clickable") OMSs are ready for use. The postsynthetic grafting method introduces functional groups after the synthesis of OMSs by silylation reaction between organosilane and the silanol groups on the surfaces of OMSs. While the co-condensation approach is convenient, it restricts opportunities for the pore size and pore structure symmetry adjustment. In the case of post-functionalization of pure-silica materials, a wide range of pore diameters and structure types is available. The reported "clickable" SBA-15 silicas prepared by co-condensation method exhibited pore diameter ~6 nm.[107,112] Recently, a successful "click" grafting of poly-L-lysine (PLL) to SBA-15 (pore diameter ~12 nm) was reported. Appreciable loadings (15-25 wt.%) was achieved without any major pore blockage.[117]

In our study, large-pore SBA-15 was used as the solid support with very uniform cylindrical mesopores and the "clickable" SBA-15 was prepared via postsynthetic functionalization.[119] Various azide molecules, including oligo(ethylene glycol), monosaccharides and poly(methyl methacrylate) were "click"-grafted to the surfaces of pores. It was demonstrated for the first time that the Huisgen cycloaddition can serve as a highly efficient method to attach polymers to the surface of ordered nanopores in the "grafting to" approach.

Although Huisgen cycloaddition reaction serves as a robust method for a covalent attachment of molecules and biomolecules to solid surfaces, the removal of residual of copper catalyst and ligand may still be a challenge. The presence of copper residue may limit the application of this "click" reaction in the biological area[120] and also induce the appearance of color of the resulting materials. Thiol-ene reaction recently emerged as

another typical “click” reaction, which satisfies the criteria of the “click chemistry”, such as tolerance to most functional groups, wide range of substrates, high regioselectivity and diverse reaction conditions. More importantly, this thiol-ene “click” reaction is “metal-free”, which makes it attractive for immobilization of biomolecules.[121]

The thiol-ene reaction is the hydrothiolation of a carbon-carbon double bond, which can proceed via the anti-Markovnikov’s radical addition pathway (Scheme 3) or the catalytic processes mediated by bases or nucleophiles.[121] The radical conditions are generally adopted for the thiol-ene reaction. The reaction is initiated by using azo initiator (radical generator) at elevated temperature or photoinitiators under irradiation to form the thiyl radical. Then the thiyl radical directly adds to the end of C=C bond to produce the intermediate radical. The intermediate radical undergoes chain transfer to a second thiol molecule yielding the product with anti-Markovnikov orientation and a new thiyl radical. Such propagation could be terminated by bi-radical coupling process.[121-122]

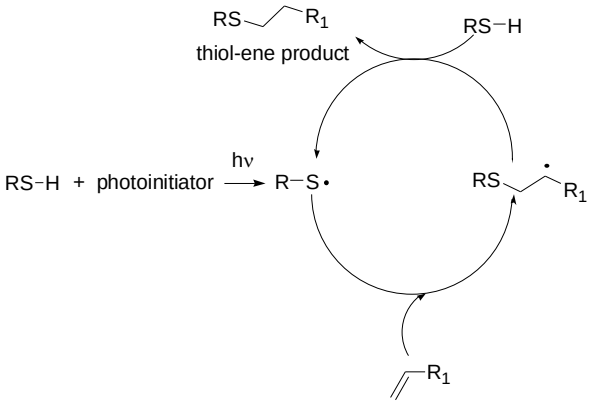

Scheme 3. The mechanism for the hydrothiolation of a C=C bond in the presence of a photoinitiator and hυ.[121]

The thiol-ene reaction has been employed extensively in the polymer and materials fields, such as the preparation of dendrimers[123], post-polymerization modification of polymers[124-125], surface modification of nanoparticles[126-128] and bioconjugations[129-133]. Recently, the first application of thiol-ene "click" reaction to the surface modification of OMSs was reported.[120] SBA-15 of 8.5 nm pore diameter was used as the support. Methacrylate-functionalized SBA-15 was prepared by postsynthetic grafting method, and then reacted with a variety of thiol containing molecules, amino acids and disulfide-containing molecules. The thermogravimetric analysis results showed low to moderate loadings of thiol-containing groups in the final materials. Also, the authors only reported the N_2 adsorption measurements for the "click" attachments of small thiol molecules and the changes of pore diameters after thiol-ene "click" were quite small (0.1-0.2 nm), which might be due to the low loading of the small thiol molecules or because the small thiol molecules were grafted preferentially on the external surfaces instead of internal surfaces of pores. The pore size distribution and pore accessibility after the grafting of large thiol molecules were not clarified.

We studied the thiol-ene "click" grafting based on large-pore SBA-15 silicas. Vinyl-group-functionalized SBA-15 was prepared via postsynthetic functionalization. Small thiol molecule and thiol-containing polystyrene were grafted to the surface of SBA-15 via thiol-ene reaction through the radical addition pathway. Our results indicated the first successful thiol-ene "click" grafting of polymers in the nanopores of ordered mesoporous silicas.

Chapter 2. Synthesis of FDU-12 Silicas with Face-Centered Cubic Structure of Ultra-large Mesopores

2.1. Introduction

FDU-12 silica with spherical mesopores was first reported in 2003 as the first pure face-centered-cubic (fcc) mesoporous material without intergrowth of 3D hexaganol mesophase.[23] The 3-dimensional pore system of FDU-12 and other similar materials exhibits advantages over the 2-D channels in faster mass transport, and therefore is more attractive as a solid host for heterogeneous catalysis[32] and enzymatic catalysis.[33] The large pore size (~12 nm), tunable pore entrance size and 3-D pore system has made FDU-12 an attractive material since its advent. Heterogeneous catalysts based on large-pore ordered mesoporous materials, including LP-SBA-15 and LP-FDU-12, showed considerably improved performance.[134-135] The efforts to obtain FDU-12 silica with larger pore size is important, as seen from recent publications.[69,134,136]

The first reported FDU-12 silica (pore diameter 10~12 nm) was synthesized at the initial temperature of 40 ^{o}C by using Pluronic F127 as the template and TMB as the micelle expander in the presence of KCl. Later, large-pore FDU-12 (LP-FDU-12) (pore diameter 22~27 nm) was synthesized as the initial temperature was lowered to 15 ^{o}C.[25] At the low temperature, it was hypothesized that the Pluronic block copolymer was hydrated and extended more than at a higher temperature, inorganic salt lowered the critical micelle concentration and helped the surfactant to form micelles. Under such condition, it was argued that the micelle had smaller association number and less tight packing, which was claimed to be beneficial for the penetration of micelle expander to enter the hydrophobic cores and to increase the micelle size, causing the pore size increase.[25]

Ultra-large-pore FDU-12 silica (the unit-cell parameter for as-synthesized sample was 56.7 nm) was synthesized by using PEO-PS diblock copolymer as the template.[136] However, such customer-made surfactants need to be selected carefully to achieve the desired well-ordered mesophase. In contrast, the commercially available surfactants and abundant choices of micelle expanders provide vast opportunities to explore facile and convenient way to tune the pore size of OMSs.

In addition to the directly increasing the size of micelles and thereby enlarging pores in as-synthesized materials, the suppressing of the structural shrinkage during calcination by a hydrothermal treatment is another step needed to get larger pores. The hydrothermal treatment is a step following the initial synthesis step, and involves the heating of the reaction mixture at a higher temperature (e.g., 100 °C) for an extended period of time. The shrinkage of the silica framework upon removal of the surfactant template (for instance by calcination) may reduce the size of pores to different extents.[50-51,137] Among several methods used to remove the surfactants, the widely used calcination method may result in substantial structural shrinkage (unit-cell parameter decrease up to about 20%). However, such shrinkage could be decreased to about 2% if the hydrothermal treatment at 100-130 °C or higher temperature is employed [50-51].

The purpose of this project was to identify superior micelle expanders for the synthesis of ultra-large-pore FDU-12 silicas and to enhance the ability to successfully predict swelling agent candidates in the micelle-templated synthesis.[52,138-140] On the basis of the solubilization behavior of aromatics, xylene (dimethylbenzene) and ethylbenzene were

selected as swelling agent candidates and were indeed shown to be superior to TMB [57,138,140] in the silica [25,134,138] and organosilica [140-141] synthesis.

2.2. Synthesis of ULP-FDU-12 Silica by using Xylene as the Micelle Expander [138]

2.2.1. Materials and Methods

2.2.1.1. Synthesis

Synthesis of ULP-FDU-12 silicas In a typical synthesis procedure, 1.00 g of Pluronic F127 ($EO_{106}PO_{70}EO_{106}$) and 2.5 g of KCl were dissolved in 60 mL of 2 M HCl in a glass container with magnetic stirring, and then a certain amount (see text) of xylenes (mixed isomers with some ethylbenzene possibly present, which will be referred to as xylene throughout this chapter) was added and the mixture was stirred at 350 rpm at 14 °C for one day in a covered container. Next, 4.5 g of tetraethyl orthosilicate (TEOS) was added. In some cases, tetramethyl orthosilicate (TMOS) was used instead of TEOS. The reaction mixture was stirred at 14 °C for one day, and then it was transferred to a polypropylene bottle and kept at 100 °C for one day. The product was filtered and dried in a vacuum oven at 60 °C. The resulting as-synthesized material was calcined at 550 °C under air for 5 h to remove the surfactant template. The resulting samples are denoted EHx or MHx, where E stands for TEOS, M stands for TMOS, H denotes the hydrothermal treatment at 100 °C, and x is the sample number. In some cases, a part of the dried as-synthesized material was subjected to an acid treatment, in which 0.5 g of the as-synthesized sample was placed in 30 mL of 2 M HCl solution and heated at 100 °C (in a polypropylene bottle) or 130 °C (in a Teflon-lined autoclave) for one to four days. The

resulting materials were filtered and dried. The acid-treated samples are denoted using the EHx (or MHx) with –ATt ending, where A denotes the acid treatment, T indicates the treatment temperature in °C and t shows the treatment time in days.

Synthesis of Closed-pore FDU-12 Silicas Closed-pore silicas were prepared via the low-temperature synthesis. 1.00 g of Pluronic F127 ($EO_{106}PO_{70}EO_{106}$) and 2.5 g of KCl were dissolved in 60 mL of 2 M HCl in a glass container with magnetic stirring, and then 4.5g xylenes was added. Subsequently 4.5 g of tetraethyl orthosilicate (TEOS) was added. The sample was filtered out after one day of stirring at 14 °C. After drying at 60 °C in a vacuum oven, the as-synthesized material was calcined under air for 5 hours at different temperatures in the range 300-450 °C. The calcined samples were denoted E4'-T, where T represents the calcination temperature.

A series of FDU-12 silicas was also prepared in the absence of KCl. The synthesis was done in a semi-closed polypropylene bottle with the mechanical stirring (the method was similar to that discussed in Dr. Liang Cao's dissertation).[80] 1 g of F127 was dissolved in 60 mL of HCl at room temperature, and then the solution was moved to 14 ^{o}C refrigerated water bath. 3 hours later, 2.35 mL of xylenes were added to the solution. The mixture was stirred for 16.5 hours. Then 4.35 mL of TEOS was added and the mixture was stirred at 14 ^{o}C for 1 day. The product was filtered and dried in a vacuum oven. The resulting powder was calcined at 550-650 °C in air for 5 h to remove the template. The calcined samples were denoted E0-T, where T represents the calcination temperature.

2.2.1.2. Measurements

Small-angle X-ray scattering (SAXS) measurements were performed using a Bruker Nanostar U SAXS/wide-angle X-ray scattering instrument with a rotating anode X-ray

source and Vantec-2000 two-dimensional detector. The instrument was in high flux mode. Nitrogen adsorption measurements were performed at −196 °C on a Micromeritics ASAP 2020 volumetric adsorption analyzer. Before the analysis, samples were outgassed under vacuum at 200 °C for 2 h in the port of the adsorption analyzer. Transmission electron microscopy (TEM) images were acquired on a FEI Tecnai Spirit microscope operated at 120 kV. Before the imaging, the samples were dispersed in ethanol using sonication, and subsequently deposited on carbon-coated copper grid.

2.2.1.3. Calculations

The specific surface area was calculated using the BET method in the relative pressure range from 0.04 to 0.2.[3] The total pore volume, V_t, was estimated from the amount adsorbed at a relative pressure of 0.99.[3] The micropore volume, V_{mi}, was evaluated using the α_s plot method.[3,142] For many OMSs,[17,51] the sum of the mesopore volume, V_p, and the micropore volume can be estimated from the α_s plot method from data corresponding to pressures above the capillary condensation pressure. However, the pore diameter for the present materials was so large that the capillary condensation takes place very close to the saturation vapor pressure, making such calculations inaccurate or impossible. Therefore, $V_p + V_{mi}$ was estimated as $0.957 \times V_t$, the proportionality factor being estimated from the data for LP-FDU-12.[51,143] The pore size distribution (PSD) was calculated using the KJS method for cylindrical mesopores[144] with the statistical film thickness curve for a macroporous silica gel.[142] This implementation of the PSD calculation is known to underestimate the pore diameter for large spherical mesopores by at least 2 nm,[22,51] but reflects well the width of the mesopore size distribution and allows one to reliably compare the pore size among different samples with the same pore

geometry. To obtain a more accurate assessment of the pore diameter, an equation relating the unit-cell parameter, a, the mesopore volume, V_p, and the micropore volume was used:[145]

$$w_d = a\left(\frac{6}{\pi v}\,\frac{V_p\rho}{1+V_p\rho+V_{mi}\rho}\right)^{\frac{1}{3}} \quad (1)$$

where a is determined from the position of (111) peak on SAXS pattern, ρ is the density of silica framework (assumed to be 2.2 g cm^{-3}) and v = 4 is the number of spherical pores in the unit cell.

2.2.2. Results and Discussion

2.2.2.1. Optimization of synthesis conditions

Several series of samples were synthesized with different reaction mixture compositions and stirring speeds. It was found that the initial step of the synthesis should be performed in a semi-closed container (glass container with glass cover) and magnetic stirring, as the use of an open container with mechanical stirring tended to afford materials with lower unit-cell size or even those devoid of the structural ordering. This may be due to volatility of xylene. In the case of the semi-closed setup described above, the stirring speed needed to be optimized, and 350 rpm was found to be suitable to obtain materials with the largest unit-cell parameters (see below). With a fixed amount of xylene, the amount of TEOS was increased from the originally used 4.1 g to 4.5 g, because when the original molar ratio (TEOS : F127 : KCl : HCl : H_2O = 1.0 : 0.004 : 1.68 : 6 : 157) was used, additional porosity appeared in smaller pore size range (~10 nm), which could be observed in the adsorption branch where a small capillary

condensation step was seen in a relative pressure range 0.77-0.83, followed by a more prominent capillary condensation step related to the capillary condensation in the uniform mesopores of the materials (Figure 2.1). Such additional porosity was thought to be another population of mesopores existing in the material in addition to the main mesopores structure. However, the SAXS pattern in Figure 2.2 (a) showed clearly resolved peaks indicating ordered face-centered-cubic (fcc) structure with unit-cell parameter of 44.3 nm for the calcined sample. In addition, this unit-cell parameter was in agreement with the larger mesopore size (~24.1 nm) measured by N_2 adsorption, and there were no additional peaks corresponding to the ~10 nm pore size in the SAXS pattern (Figure 2.2 (a)).

By adding 10% more TEOS in the synthesis mixture, this additional porosity was completely or nearly completely eliminated (Figure 2.1), while the SAXS pattern (Figure 2.2 (b)) revealed ordered fcc structure. These results indicated that the additional porosity could be attributed to the void space between the closed-packed spheres.[146] Yuan and co-workers studied the packing of monodisperse silica spheres, and observed similar bimodal mesopores size distribution. By using TEM of ultra-microtomed samples and electron tomography techniques, the two sets of mesopores were imaged. The hard silica spheres were packed in a face-centered-cubic structure and the smaller mesopores were attributed to the octahedral cavities between the packed spheres.[146]

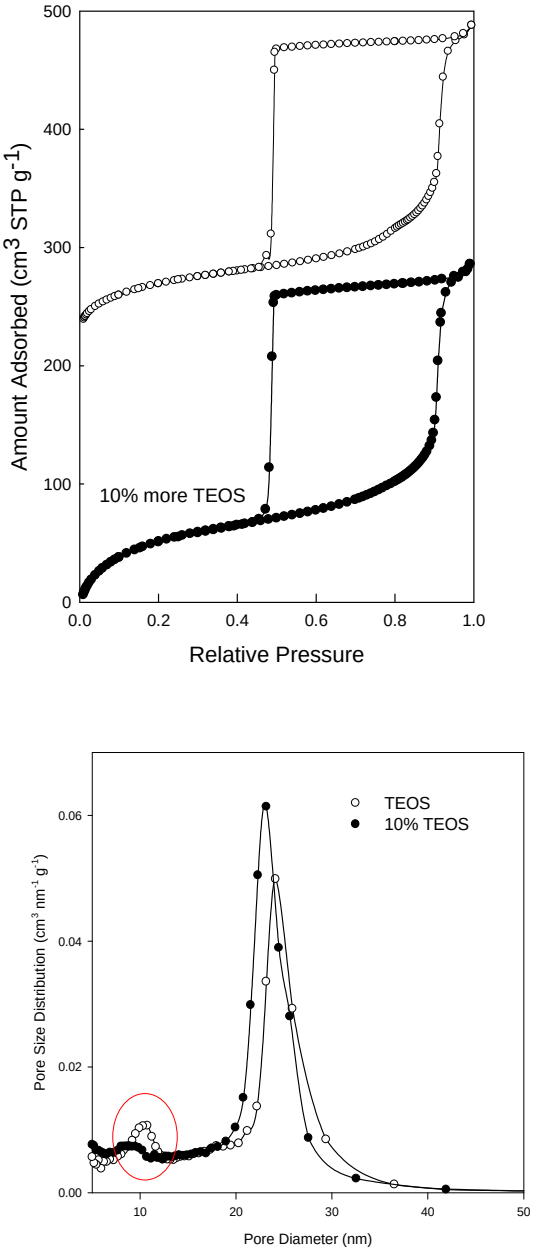

Figure 2.1. N_2 adsorption isotherms and pore size distributions for calcined sample prepared with initially selected and increased by 10% amount of TEOS.

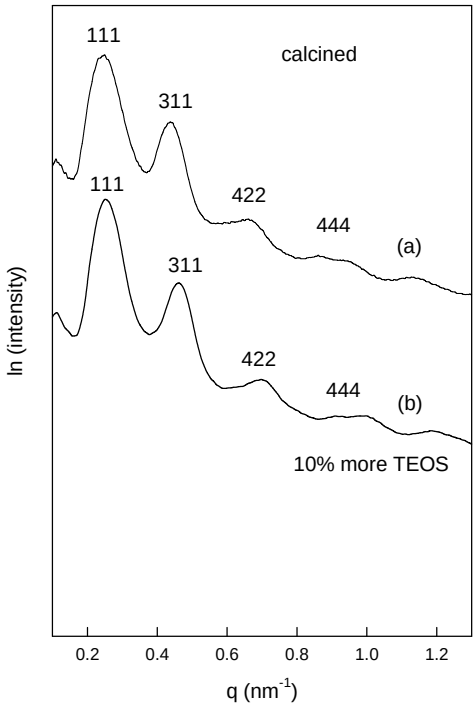

Figure 2.2. SAXS pattern for FDU-12 silicas prepared with (a) initially selected and (b) increased by 10% amount of TEOS.

2.2.2.2. Synthesis of Fm3m structure with ultra-large unit-cell size[138]

The replacement of TMB by xylene in the synthesis analogous to that of LP-FDU-12 afforded a highly ordered face-centered cubic structure with large unit-cell parameter of 50 nm for as-synthesized material.[138] Twelve well-resolved reflections characteristic of Fm3m structure were accurately identified for the as-synthesized sample, while the assignment of the last four peaks (indexes 551 and higher) for the calcined sample was somewhat less clear, although it can be done convincingly by referring to the data for as-synthesized sample.[138] The stirring was maintained throughout the low-temperature step of the synthesis. A series of samples was synthesized a stirring speed of 350 rpm with

different amounts of xylene and fixed molar ratio of the other components: TEOS : F127 : KCl : HCl : H_2O = 1.1 : 0.004 : 1.68 : 6 : 157.

The data for the entire series of samples are shown in Figures 2.3 and 2.4, and the structural parameters derived from these data are summarized in Table 2.1. With the increase in the amount of xylenes, the unit cell parameter of the face-centered cubic structure increased until the mass of xylenes was 6 g per 1 g of Pluronic F127. It should be noted that in all cases, the available amount of xylene had to be much higher than the actual uptake of xylene by the micelles of F127, because otherwise the pore volume generated in the final material would be much higher. The largest unit cell parameter (~55.8 nm) obtained for as-synthesized samples EH5 or EH6 was much larger than the unit-cell size reported for LP-FDU-12 synthesized in the presence of TMB[25,51,134,147] and comparable to that reported for face-centered cubic silicas templated by PEO-PS diblock copolymer.[136]

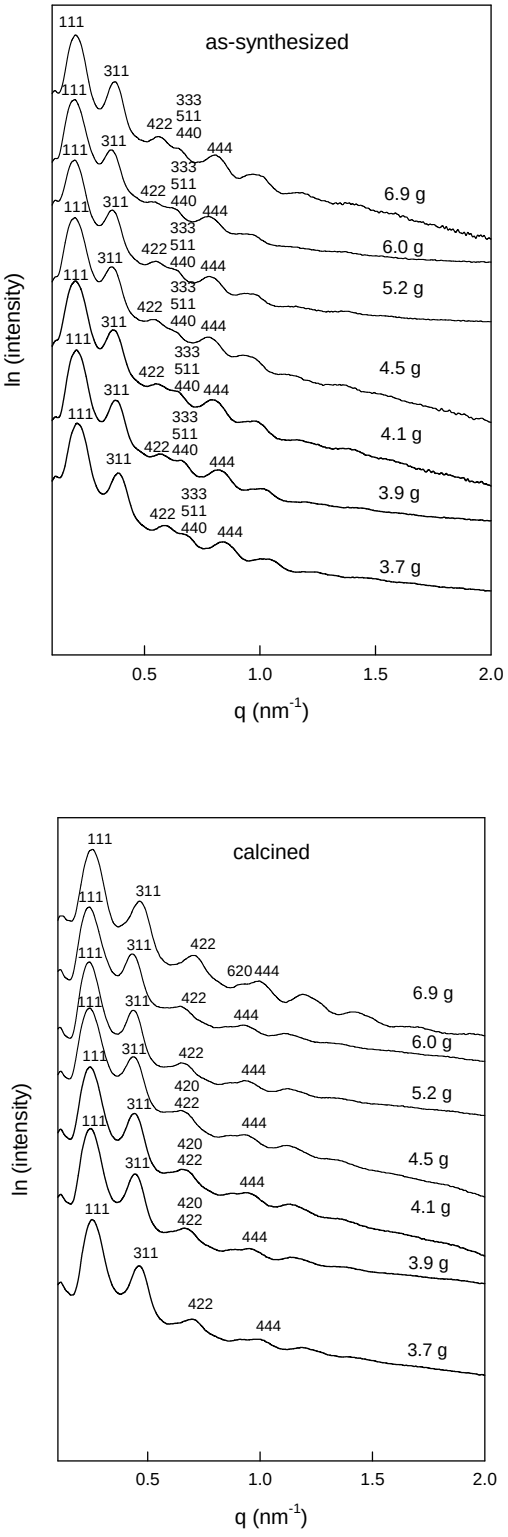

Figure 2.3. SAXS pattern of FDU-12 synthesized with different amounts of xylene.[138]

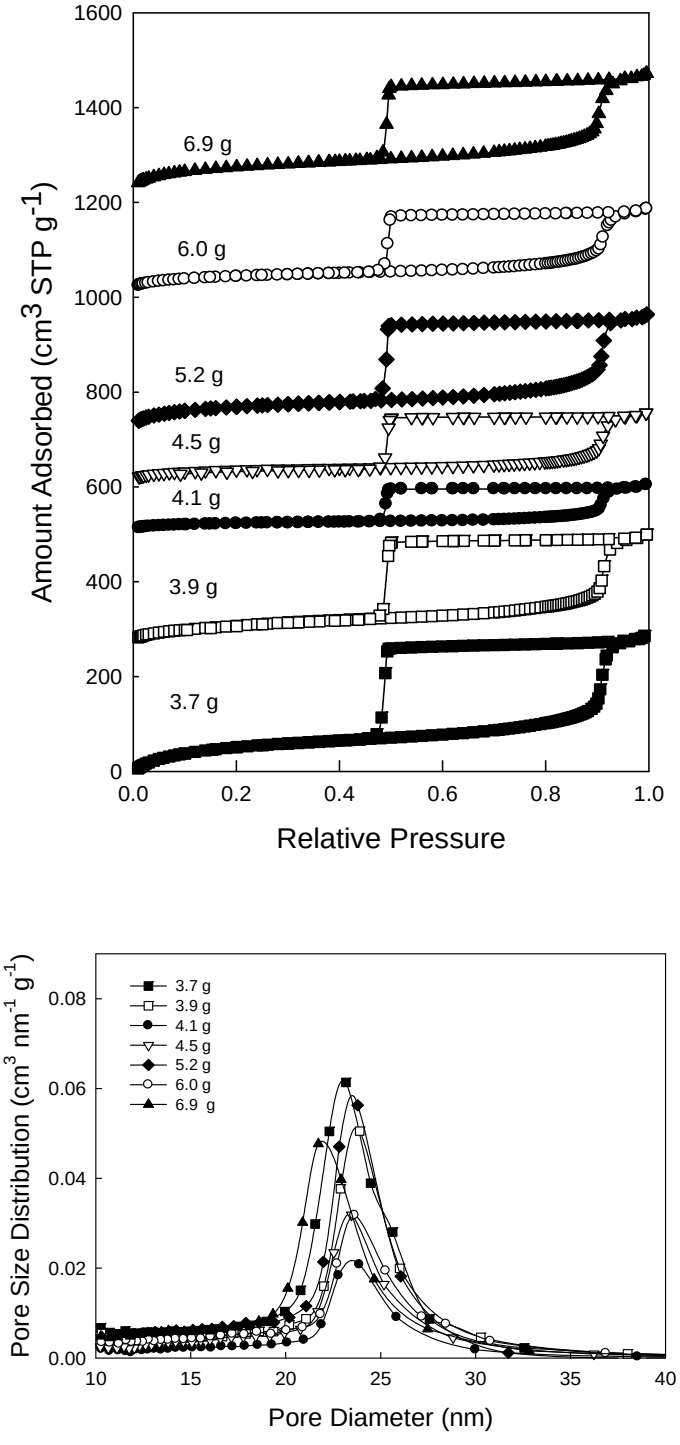

Figure 2.4. N_2 adsorption isotherms and pore size distributions for FDU-12 silica synthesized with different amount of xylene.[138]

After calcination at 550 °C, the shrinkage was large (the unit cell parameter decreased by ~18%), which is similar to the case of LP-FDU-12 silicas prepared in the presence of TMB.[51] Even after this significant shrinkage, the unit-cell size still was 45-46 nm for some of the samples, being higher than the unit-cell parameter for LP-FDU-12 silica[25] with the template removed through the microwave digestion that is known to greatly reduce the structural shrinkage (unlike the calcination that was used for our samples). The specific surface areas and total pore volumes of the FDU-12 silicas were relatively low, especially for EH3, which indicates that some mesopores may have closed during the calcination due to the structural shrinkage that reduced the pore entrance diameter to such an extent that nitrogen adsorbate molecules were unable to access the pore interiors,[44] which is known for similarly hydrothermally treated LP-FDU-12.[44]

Our previous study of LP-FDU-12 has shown[51] that the acid treatment, which was introduced by Fan et al.[25] and Kleitz et al.,[148] greatly reduces the shrinkage upon calcination, allowing one to significantly increase the total pore volume and pore diameter. Therefore, as-synthesized ULP-FDU-12 samples were treated in 2 M HCl solution at 100 or 130 °C for periods of time from one to four days. SAXS patterns for a selected series of as-synthesized and calcined samples, as well as nitrogen adsorption isotherms and PSDs are shown in Figures 2.5 and 2.6. The corresponding structural parameters for these and some additional acid-treated ULP-FDU-12 silicas are listed in Table 2.2. After the acid treatment at 100 °C for 2 days, the shrinkage upon calcination at 550 °C decreased to 8 %, while the pore size and the total pore volume increased significantly. The N_2 adsorption isotherm retained the same shape as before the acid

treatment, which indicates the cage-like mesopores with narrow entrances (diameter below 5 nm in the narrowest point).[149]

Table 2.1. Structural parameters for FDU-12 silicas.[a] [138]

Sample	Mass of xylenes (g) per 1 g F127	Unit cell parameter			w_{KJS} (nm)	S_{BET} (m^2/g)	V_t (cm^3/g)
		a_{as} (nm)	a_c (nm)	a_c/a_{as}			
EH1	3.7	52.2	43.1	0.83	23.1	367	0.51
EH2	3.9	52.6	44.3	0.84	24.1	307	0.37
EH3	4.1	54.5	44.6	0.82	23.5	80	0.16
EH4	4.5	55.2	45.3	0.82	23.5	130	0.24
EH5	5.2	55.8	45.9	0.82	23.5	249	0.40
EH6	6.0	55.8	45.9	0.82	23.6	157	0.29
EH7	6.9	51.3	41.9	0.82	22.0	271	0.41

[a] Notation: Composition of the synthesis mixture: 4.5 g (21.6 mmol) TEOS, 1 g F127 and 2.5 g KCl in 60 ml of 2 M HCl solution. a_{as}, unit cell parameter for as-synthesized sample; a_c, unit cell parameter for calcined sample; w_{KJS}, pore diameter calculated by using KJS method; S_{BET}, BET specific surface area; V_t, total pore volume.

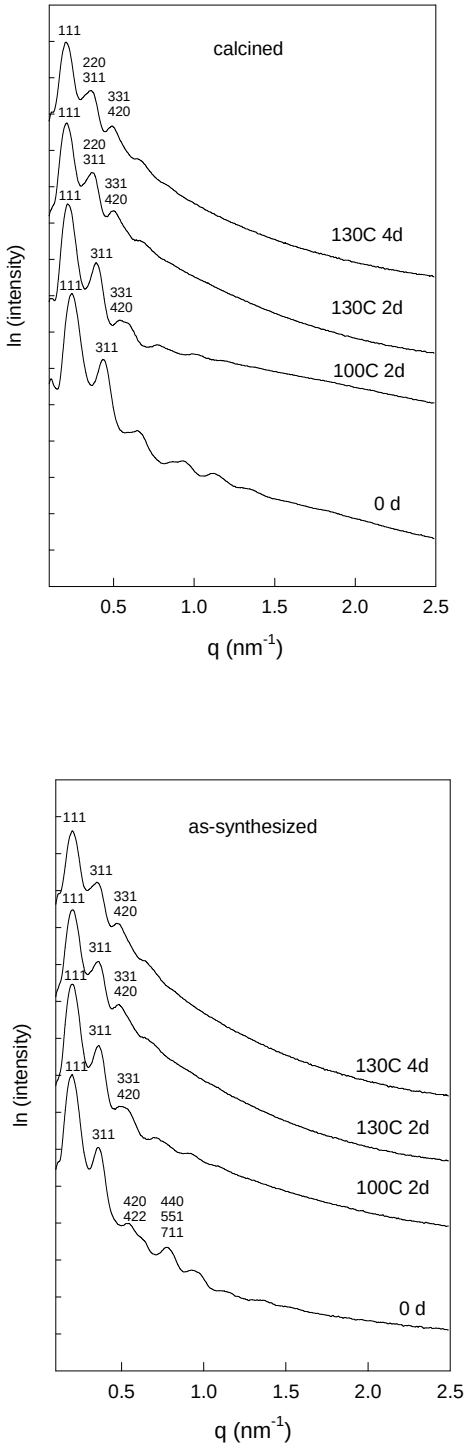

Figure 2.5. SAXS patterns for as-synthesized and calcined sample EH4 before (0 d) and after acid treatment for different periods of time.[141]

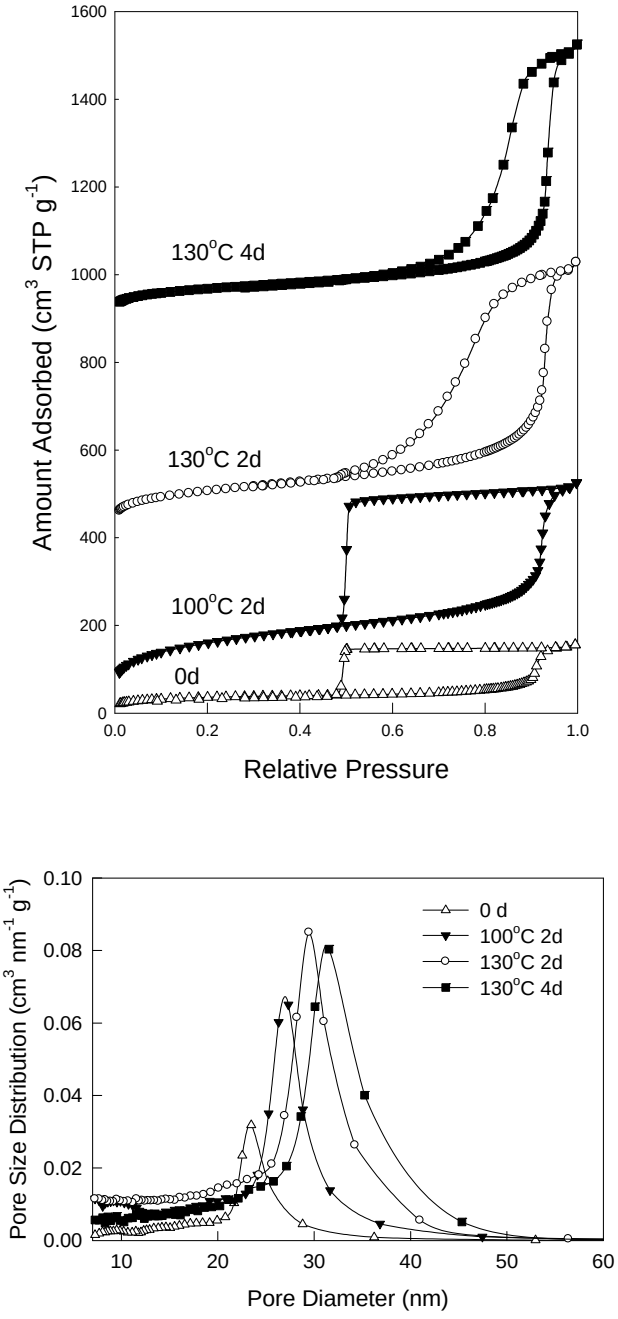

Figure 2.6. N_2 adsorption isotherms and pore size distributions for calcined sample EH4 before (0 d) and after acid treatment for different periods of time. The adsorption isotherms for samples acid-treated at 130 °C for 2 and 4 days were shifted vertically by 400 and 900 cm^3 STP g^{-1}.[138]

Table 2.2. Structural parameters for FDU-12 samples after the acid treatment [a] [138]

Sample	Unit cell parameter			w_{KJS}	S_{BET}	V_t	V_{mi}	w_d
	a_{as} (nm)	a_c (nm)	a_c /a_{as}	(nm)	(m^2/g)	cm^3/g	(cm^3/g)	(nm)
EH4-A100C2d	54.4	50.2	0.92	27.0	575	0.81	0.14	31.5
EH4-A130C2d	54.4	52.6	0.97	29.5	380	0.97	0.04	35.5
EH4-A130C4d	54.4	53.3	0.99	31.6	246	0.97	0.02	36.3
EH5-A100C2d	54.4	49.7	0.91	26.2	558	0.77	0.14	30.9
EH5-A130C2d	54.4	53.1	0.98	31.4	363	1.04	0.04	36.2
EH5-A130C4d	54.4	53.5	0.98	31.7	236	1.00	0.00	36.7

[a] Notation: a_{as}, unit cell parameter for as-synthesized sample; a_c, unit cell parameter for calcined sample; w_{KJS}, pore diameter calculated by using KJS method; S_{BET}, BET specific surface area; V_t, total pore volume; V_{mi}, micropore volume; w_d, pore diameter calculated by using Equation 1.

For the samples treated at 130 °C, the shrinkage upon calcination at 550 °C decreased to 1-4 %. Consequently, the pore size and the total pore volume of these samples were larger than those of the samples treated at 100 °C. The KJS pore diameter approached 32 nm. It should be noted that the original BdB work[150] for spherical mesopores indicates the pore diameter of 43-46 nm for the capillary condensation at relative pressures of 0.9325-0.9375, which correspond to the largest capillary condensation relative pressures observed for our samples (0.935-0.938). The use of eq 1 allows one to assess the pore diameters of 31 to 37 nm for our acid-treated samples (see Table 2.2). Equation 1 is expected to closely reflect the actual pore diameter, and therefore the BdB “spherical”

pore diameters appear to overestimate and the KJS "cylindrical" pore diameters appear to underestimate the actual diameter of very large spherical mesopores. The hysteresis loops on nitrogen adsorption isotherms for the considered samples became narrower when the acid treatment was performed at 130 °C, and the narrowing became even more pronounced as the acid treatment was prolonged. This provides evidence of a significant pore entrance widening. In fact, the hysteresis loops observed for the samples subjected to the acid treatment at 130 °C for 4 days were so narrow that the pore entrance diameter is likely to approach the pore cage diameter. The specific surface area decreased as the temperature and time of acid treatment were increased, as already reported for LP-FDU-12.[51] The acid-treated samples still show several strong peaks on their SAXS patterns, indicating that the ordered Fm3m structure was well preserved, although some reflections (for instance, (220) and (311)) were not well-separated in some cases and the relative intensity of peaks changed (which was also observed earlier)[51,151]. The latter can be attributed to changes in the relation between the mesopore diameter and the unit-cell parameter. TEM (Figure 2.7) also confirms that the acid-treated materials have a highly ordered structure.

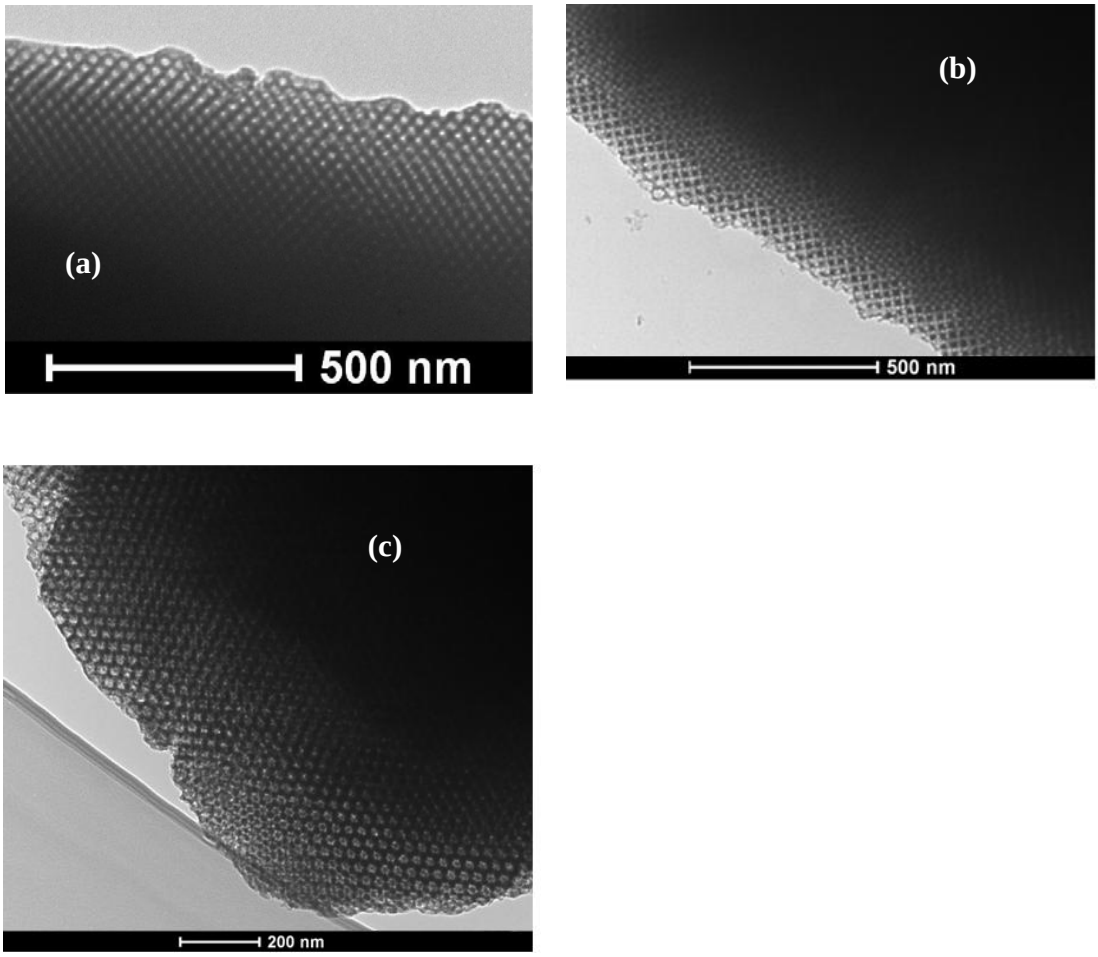

Figure 2.7. TEM images of ULP-FDU-12: (a) calcined EH4 sample ([110] incidence); (b) and (c) calcined EH6-A130C4d sample ([100] and [110] incidence).[138]

2.2.2.3. ULP-FDU-12 prepared with TMOS[138]

Tetramethyl orthosilicate (TMOS) is a faster hydrolyzing silica source when compared to TEOS. The same procedure as that introduced above was used to prepare ULP-FDU-12 from TMOS. Structural parameters determined by SAXS and N_2 adsorption are listed in Table 2.3. For comparison, samples MH1 and EH4 were prepared with the same molar composition of the components of the synthesis mixture and at the same stirring speed. The sample prepared using TMOS exhibited a smaller unit-cell parameter. The acid

treatment effectively reduced the shrinkage caused by calcination and increased the specific surface area and total pore volume. SAXS patterns for these samples (Figure 2.8) revealed ordered cubic Fm3m structures and N_2 adsorption isotherms exhibited narrow pore size distributions (Figure 2.9).

Table 2.3. Structural parameters for FDU-12 samples [a] [138]

Sample[b]	Unit cell parameter			w_{KJS} (nm)	S_{BET} (m^2/g)	V_t (cm^3/g)	V_{mi} (cm^3/g)	w_d (nm)
	a_{as} (nm)	a_c (nm)	a_c/a_{as}					
MH1	50.8	42.2	0.83	21.8	211.0	0.34	D	c
MH1-A-130C-2d	51.8	49.9	0.96	26.6	297.1	0.85	0.011	33.5
MH1-A-130C-4d	52.1	50.4	0.97	28.4	253.4	0.85	0.005	33.9
MH2	52.8	44.2	0.84	22.0	231.5	0.30	D	c
MH2-A-130C-1d	51.8	49.5	0.96	27.0	424.6	0.83	0.051	32.5
MH2-A-130C-2d	52.1	51.1	0.98	27.2	317.0	0.83	0.014	34.1
MH2-A-130C-4d	52.6	51.3	0.98	29.1	255.6	0.86	0.005	34.6

[a] Notation: a_{as}, unit cell parameter for as-synthesized sample; a_c, unit cell parameter for calcined sample; w_{KJS}, pore diameter calculated by using KJS method; S_{BET}, BET specific surface area; V_t, total pore volume; V_{mi}, micropore volume; w_d, pore diameter calculated by using Equation 1. [b] Sample MH1 was prepared with 3.3 g TMOS, 4.5 g xylene, 1 g F127 and 2.5 g KCl in 60 ml of 2 M HCl solution at 350 rpm; Sample MH2 was prepared with 3.7 g TMOS, 4.1 g xylene, 1 g F127 and 2.5 g KCl in 60 ml of 2 M HCl solution at 300 rpm. [c] w_d was not calculated because this sample may contain some closed-pore structures. [d] V_{mi} was not calculated.

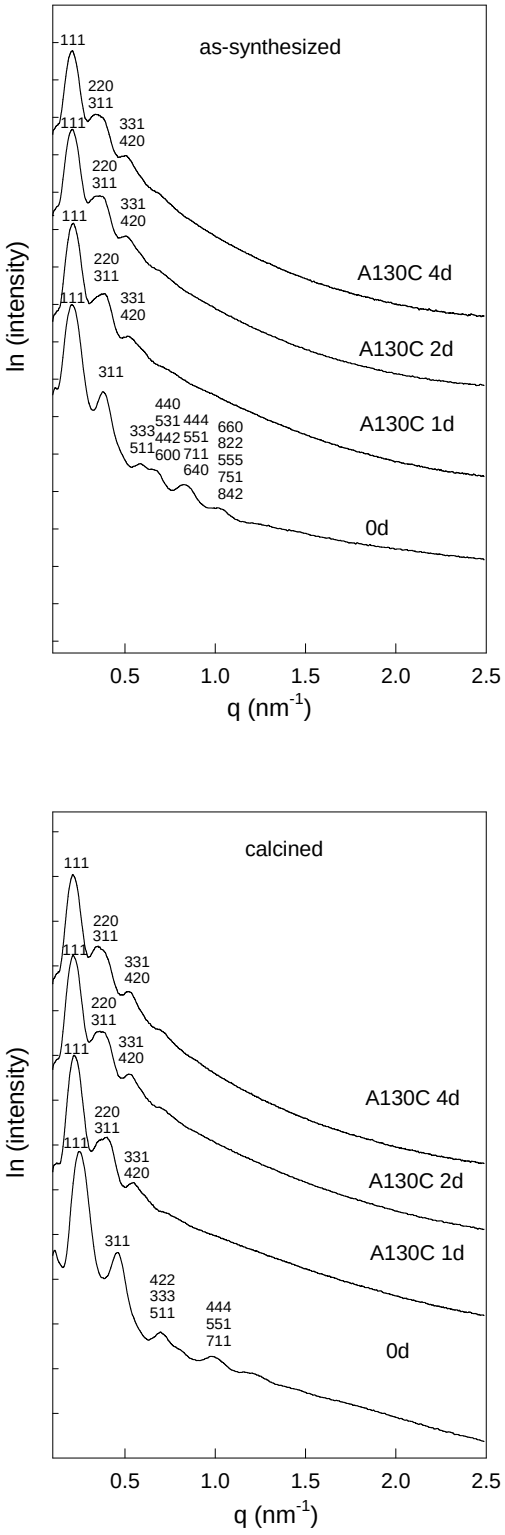

Figure 2.8. SAXS pattern for MH-2 sample. [138]

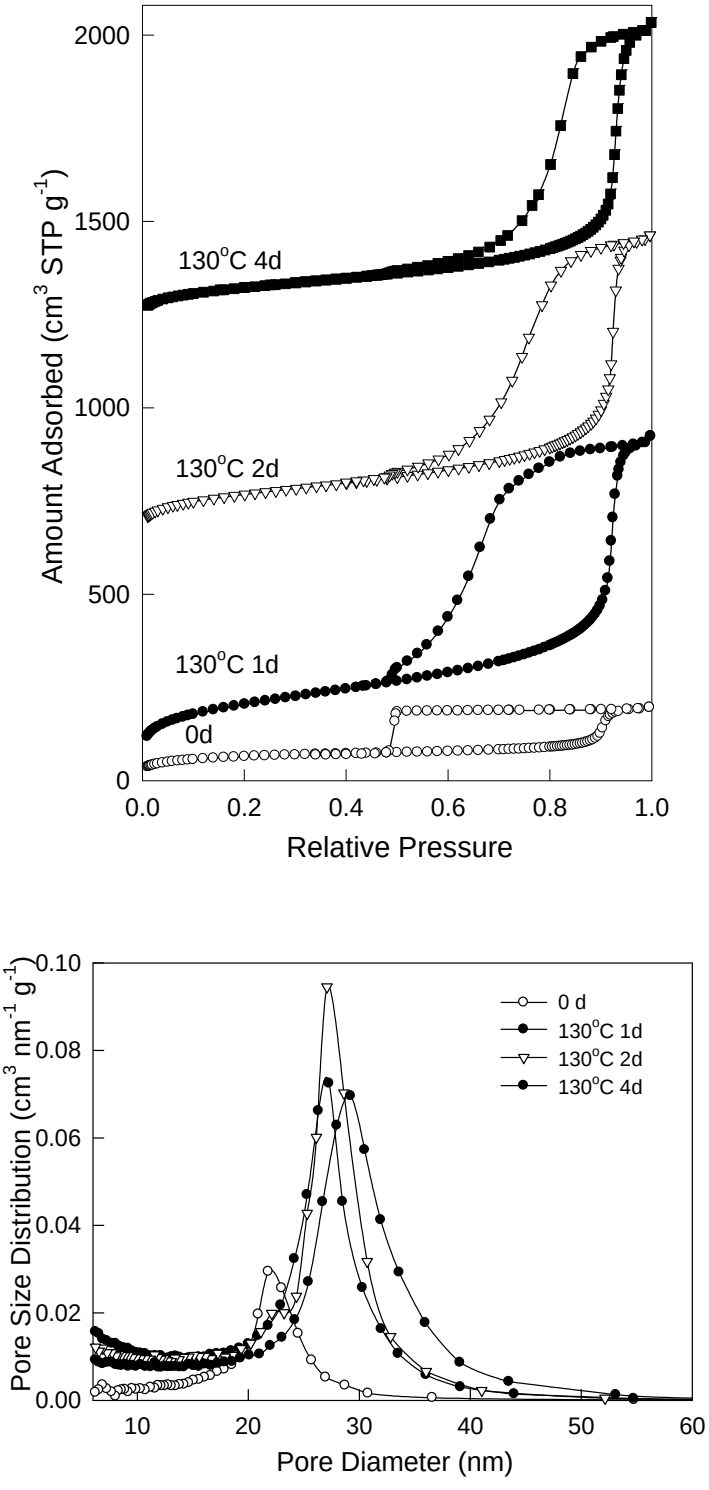

Figure 2.9. N_2 adsorption isotherms and pore size distributions for MH-2 samples. [138]

2.2.2.4. Synthesis of closed-pore silicas with xylene as the micelle expander[138]

Figure 2.10 shows N_2 adsorption isotherms for ULP-FDU-12 silica prepared in the same manner as the sample EH4, but at 14 °C only (without further heating of the synthesis mixture). It is noteworthy that the as-synthesized sample E4' prepared without the hydrothermal treatment had somewhat lower unit-cell size than the as-synthesized sample EH4 prepared with the hydrothermal treatment (compare Tables 2.1 and 2.4). A similar behavior was already observed for LP-FDU-12 and related materials.[51,136] With the increase in the calcination temperature in the 300-400 °C range, the specific surface area, the total pore volume and the pore diameter decreased (Table 2.4). The isotherm of the sample calcined at 450 °C indicated no accessible mesoporosity. On the other hand, the SAXS patterns shown in Figure 2.11 revealed that all the considered materials had highly ordered face-centered cubic structures, whose unit-cell parameter decreased as the calcination temperature increased. The unit-cell parameter of the as-synthesized E4' ULP-FDU-12 was 49.7 nm, whereas the samples calcined at 300 to 450 °C exhibited unit-cell sizes from 41.7 to 38.5 nm. An approximately linear relationship is shown in Figure 2.12 between the total pore volume and the unit cell volume of E4' ULP-FDU-12 silica calcined at different temperatures. The total pore volume of the closed-pore sample, E4'-450C, estimated by extrapolation[143] was 0.270 cm^3/g. It was thus demonstrated that closed-pore ordered silica with spherical mesopores (OSSM) with an appreciable volume of ordered mesopores can be synthesized without a hydrothermal treatment and turned into a closed-pore material via calcination at as low as 450 °C. In an earlier study, the pore closing of LP-FDU-12 prepared with hydrothermal treatment was observed at 550-640 °C, which is at least 100 °C higher.[44] While LP-FDU-12 synthesized without

hydrothermal treatment was a closed-pore material after calcination at 550 °C,[51] the exact pore closing temperature was not investigated.

In the presence of 2.5 g of KCl per 60 mL of solution, the closed-pore FDU-12 silica can be obtained after calcination at 450 ^{o}C. For the sample prepared without KCl, (the sample was denoted E0), the pores were not closed after the calcination at 550 ^{o}C, as could be observed from its N_2 adsorption isotherm (Figure 2.13). The pores were not completely closed even after calcination at 600 ^{o}C, but a large proportion of pores were not accessible to N_2 molecules and the pore volume and surface area decreased greatly (Table 2.5). When the temperature increased to 650 ^{o}C, the pores were not accessible to N_2 anymore, but the ordered structure was retained which could be observed from the well resolved peaks in SAXS pattern (Figure 2.14). The reason can be the decrease of the shrinkage during the calcination at a particular temperature as the salt was eliminated from the synthesis mixture. It appears that the loss of pore accessibility to nitrogen molecules appears when the shrinkage reaches about 20% (a_c/a_{as} = 0.80), which is similar to what was reported earlier for LP-FDU-12 silica prepared in the presence of TMB as a swelling agent.[152]

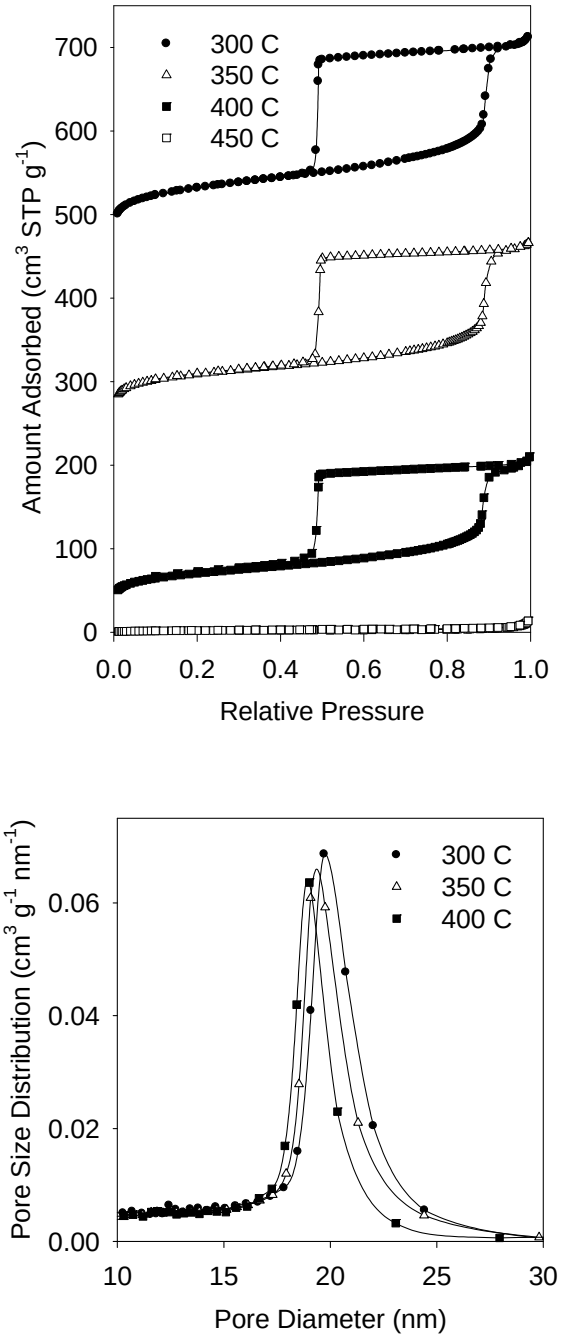

Figure 2.10. N_2 adsorption isotherms (top) and pore size distributions (bottom) of E4' ULP-FDU-12 silicas calcined at different temperatures. The adsorption isotherms for the samples calcined at 300, and 350 °C were shifted vertically by 400 and 200 cm^3 STP g^{-1}.

138

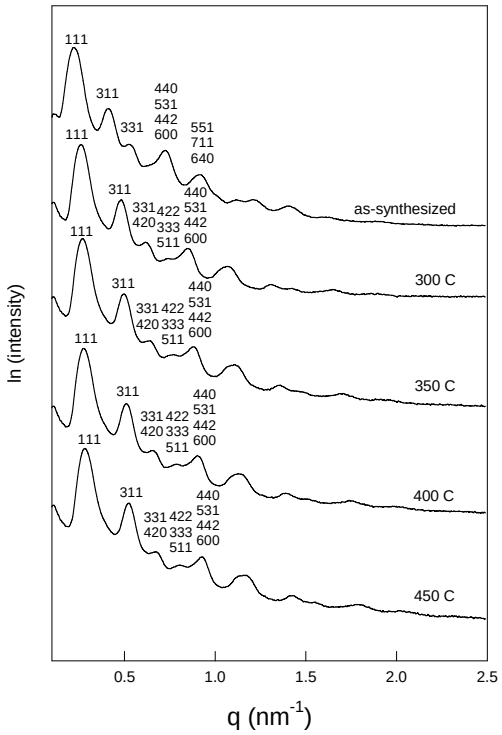

Figure 2.11. Small angle X-ray scattering patterns for E4' ULP-FDU-12 silica calcined at different temperatures.[138]

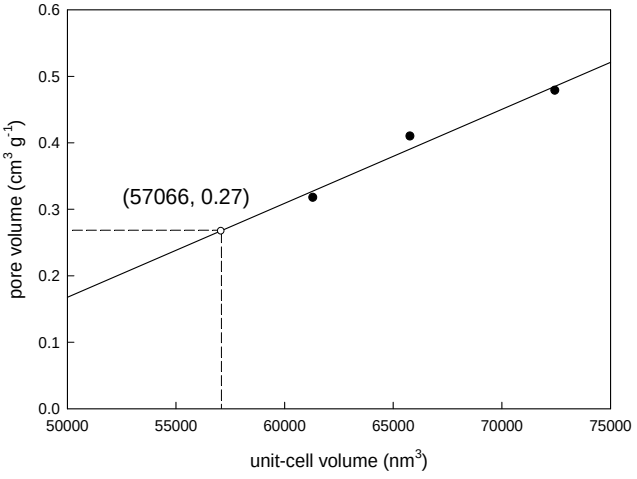

Figure 2.12. Pore volume vs. unit-cell volume for E4' calcined at different temperatures.[138] Regression function: $y = 1.41\times10^{-5} x - 0.539$

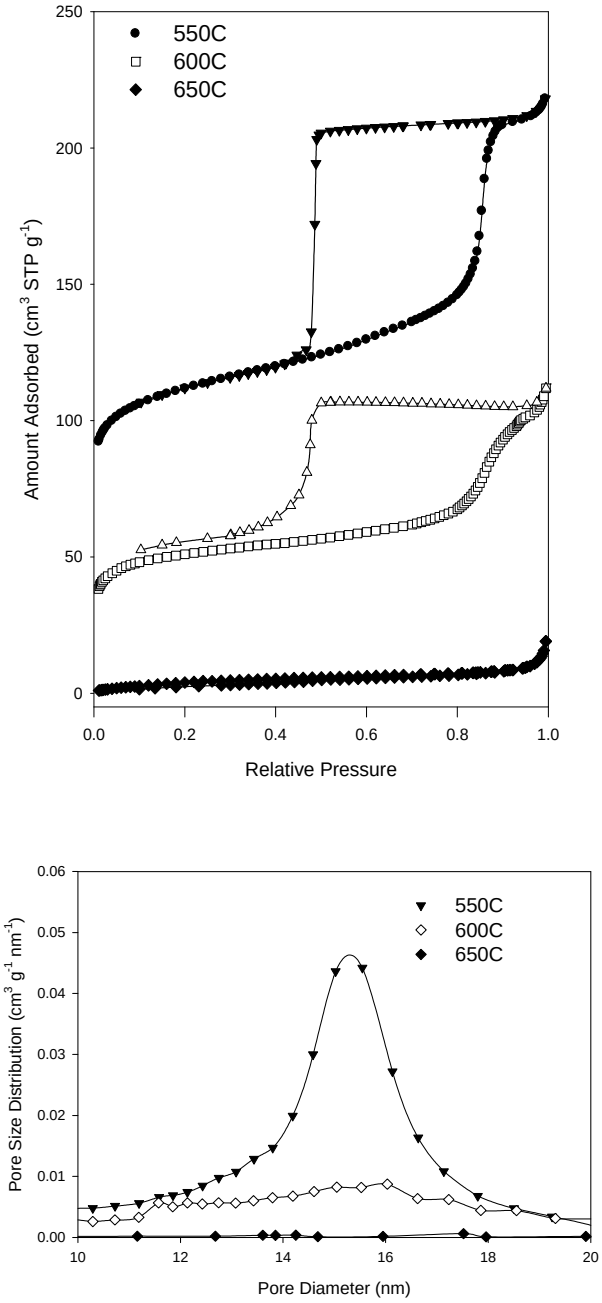

Figure 2.13. N_2 adsorption isotherms (top) and pore size distribution (bottom) of FDU-12 silica synthesized without KCl and calcined at 550 – 650 ^{o}C.

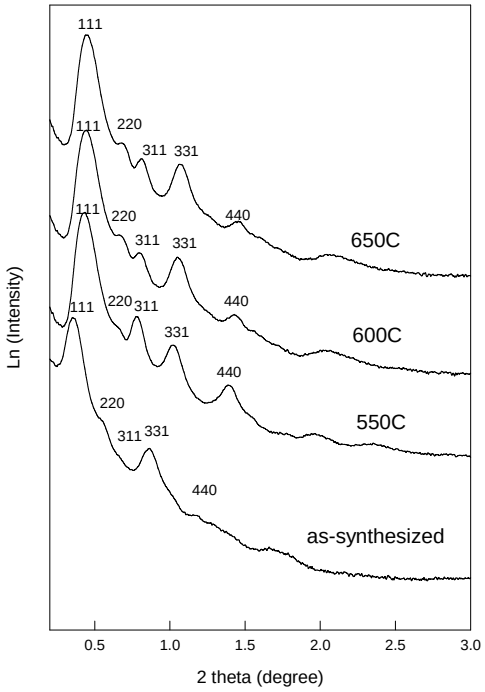

Figure 2.14. Small-angle X-ray scattering patterns for FDU-12 silicas prepared without KCl and calcined at different temperatures.

Table 2.4. Structural parameters for FDU-12 silicas calcined at different temperatures. [138]

Sample	a_{as} (nm)	a_c (nm)	a_c/a_{as}	w_{KJS} (nm)	S_{BET} (m^2/g)	V_t (cm^3/g)
E4'-300C	49.7	41.7	0.84	19.8	458	0.478
E4'-350C	49.7	40.3	0.81	19.4	378	0.409
E4'-400C	49.7	39.5	0.79	18.9	247	0.317
E4'-450C	49.7	38.5	0.77	b	b	0.270[a]

[a] The pore volume was calculated through extrapolation. [b]the value could not be calculated due to the lack of pore accessibility.

Table 2.5. Structural parameters for FDU-12 silicas prepared without KCl and calcined at different temperatures.

Sample	a_{as} (nm)	a_c (nm)	a_c/a_{as}	w_{KJS} (nm)	S_{BET} (m^2/g)	V_t (cm^3/g)
E0-550C	42.9	35.6	0.83	15.3	285	0.29
E0-600C	42.9	34.7	0.81	(16.0) [a]	178	0.17
E0-650C	42.9	34.5	0.80	b	17	0.02

[a] Notation: Most of mesopores seemed to be closed in this material, and w_{KJH} could not be reliably calculated. [b]The value could not be calculated due to the lack of pore accessibility

2.2.3. Conclusions

Our research on the synthesis of ultra-large pore FDU-12 established a facile and highly reproducible method to effectively extend the range of the unit-cell parameters and the diameters achievable in ordered silicas with spherical mesopores (OSSMs) templated by commercially available surfactants. The successful identification of xylene as the micelle expander was based on the data for the extent of solubilization of compounds in surfactant micelles and their extrapolation within families of compounds. Xylene was found to be a superior swelling agent for Pluronic F127 because this surfactant has smaller hydrophobic proportion than Pluronic P123, and the swelling of F127 in the presence of xylene was within a proper range which afforded desired pore size expansion without the loss of structural ordering. Significant structural shrinkage of the resulting ultra-large-pore silicas during calcination was observed. Such structural shrinkage could

be greatly decreased by the post-synthesis acid treatment. The selection of an appropriate hydrothermal treatment (temperature and the length of time) allows one to generate silicas with a range of pore diameters and to tune the size of pore entrance from a single synthesis mixture. The samples prepared in a one-step low-temperature synthesis were transformed to closed-pore ordered mesoporous silicas with appreciable pore volume (as evaluated by extrapolation) by calcination at as low as 450 °C. The absence of the inorganic salt (KCl) in the synthesis increased the pore-closing temperature, possibly by diminishing the structural shrinkage during the calcination.

2.3. Synthesis of Ultra-Large-Pore FDU-12 Silica Using Ethylbenzene as Micelle Expander

The performance of xylene in the surfactant-templated synthesis of ordered mesoporous materials exceeded the performance of 1,3,5-trimethylbenzene (TMB) and validated the hypothesis[52] for the selection of micelle expanders, which states that the swelling agent with moderate extent of solubilization in micelles of a particular surfactant template are likely to be superior micelle expanders. Besides the reported data on the extent of solubilization of several benzene derivatives in Pluronic surfactants,[53,54] the number or size of alkyl substituents on the benzene ring could be used as a guide to deduce the behavior of other benzene derivatives[53,54]. A general trend is that the extent of solubilization in Plurionic surfactants decreases as the number or size of substituents increases.[52] Therefore, with one methyl group less, xylene exhibits higher extent of solubilization than TMB. However, the influence of the number versus the size of the substituents was not clear. So as for the pair of ethylbenzene and xylene, it is difficult to predict which one has higher extent of solubilization by simply counting the number or comparing the size of substituents. The studies on solubilization of xylene and ethylbenzene in poly(ethylene oxide)-poly(propylene oxide)-type surfactant micelles indicated that their extent of solubilization[53-54] was similar. To enhance our ability for predicting swelling agent candidates and to extend the library of the swelling agents with superior performance [52,138-140], we investigated the suitability of ethylbenzene as a micelle expander for the synthesis of ULP-FDU-12 by using the conditions established with xylene (mixture of xylene isomers, possibly containing some ethylbenzene).[57] For better

comparison, we also examined three xylene isomers. Interestingly, under the conditions that we studied, ethylbenzene exhibited comparable swelling ability to the xylene mixture and better than any individual xylene isomer. The obtained highly ordered ULP-FDU-12 silica proved that ethylbenzene is another powerful swelling agent. Xylene isomers were also suitable micelle expanders for the synthesis of ULP-FDU-12 silicas, although they afforded slightly lower unit-cell sizes than ethylbenzene or xylene mixture.

2.3.1. Experimental section[57]

2.3.1.1. Materials

Pluronic F127 ($EO_{106}PO_{70}EO_{106}$) was received as a research sample from BASF. Ethylbenzene (99.8 %) and m-xylene (99+ %) were acquired from Fisher, o-xylene (99%) and p-xylene (99%) were from Alfa Aesar and tetraethyl orthosilicate was obtained from Acros. The synthesis was similar to that developed earlier for xylenes [138], but either ethylbenzene or one of xylene isomers (o-xylene, m-xylene and p-xylene) was used. In a typical synthesis procedure, 1.00 g of Pluronic F127 and 2.50 g of KCl were dissolved at 14.0 °C in 60 mL of 2.0 M HCl in a glass container with magnetic stirring. Then 5.2 g (6.0 mL) ethylbenzene was added and the mixture was stirred at 350 rpm at 14.0 °C for one day in a container covered with parafilm. It should be noted that the proportion of the swelling agent was selected to match the proportion of xylenes that allowed to achieve the highest unit-cell size in our earlier study [138]. Next, 4.5 g (4.8 mL) of TEOS was added. The reaction mixture was stirred at 14.0 °C in a covered container for another day, and then transferred to a polypropylene bottle and maintained at 100 °C for one day. The product was filtered, and dried in a vacuum oven at 60 °C. The resulting as-synthesized

material was calcined at 550 °C (heating ramp 2 °C/min) under air for 5 h to remove the surfactant template. A part of the dried as-synthesized sample was subjected to an acid treatment, in which 0.5 g of the as-synthesized sample was placed in 30 mL of 2.0 M HCl solution and heated at 130 °C in a Teflon-lined autoclave for 4 days. The resulting sample was filtered, dried and calcined at 550 ^{o}C. The synthesis was also performed without any hydrothermal treatment or acid treatment step, that is, the sample was filtered out after one day of stirring at low temperature. After drying at 60 °C in a vacuum oven, the as-synthesized material was calcined at different temperatures in the range 300-650 °C under air for 5 h (heating ramp 2 ^{o}C/min).

2.3.1.2. Measurements

Small-angle X-ray scattering (SAXS) patterns were acquired using a Bruker Nanostar U SAXS/WAXS instrument with a rotating anode X-ray source (Cu K_{α} radiation) and Vantec-2000 two-dimensional detector. Nitrogen adsorption isotherms were measured at −196 °C on a Micromeritics ASAP 2020 volumetric adsorption analyzer. Before the analysis, the samples were outgassed under vacuum at 200 °C for 2 h in the port of the adsorption analyzer. Transmission electron microscopy (TEM) images were acquired on a FEI Tecnai Spirit microscope operated at 120 kV. Before the imaging, the samples were dispersed in ethanol using sonication, and subsequently deposited on carbon-coated copper grid.

2.3.1.3. Calculations

See section 2.2.1.3

2.3.2. Results and discussion[57]

2.3.2.1. Synthesis of ultra-large pore FDU-12 with Fm3m structure

By using the condition explored with xylene, a series of samples were synthesized using ethylbenzene and xylene isomers (o-xylene, m-xylene and p-xylene) as swelling agents. The mixture composition was TEOS : F127 : KCl : HCl : H_2O = 1.1 : 0.004 : 1.68 : 6 : 157 and the proportion of micelle expander was the same as that of xylene (mixture of isomers, which may contain some ethylbenzene) used in the synthesis of the sample EH5 (Table 2.1). These samples were synthesized at low temperature (14 °C) and hydrothermally treated at 100 °C for 1 d.

The SAXS patterns for as-synthesized and calcined samples are shown in Figures 2.15 (a) and (b). Patterns for EH5 sample synthesized as described earlier [138] were included for comparison. All the SAXS patterns showed well resolved peaks and can be identified as those of the face-centered cubic structure of Fm3m symmetry. N_2 adsorption isotherms of these samples (Figure 2.16) showed large mesopores with narrow pore size distributions. The structural parameters obtained from SAXS and N_2 adsorption measurements were summarized in Table 2.6. The unit-cell parameter for the as-synthesized material prepared in the presence of ethylbenzene reached 55.6 nm, which is comparable to the highest value observed when xylenes were employed as a swelling agent [138]. This value is also comparable to the unit-cell size attained for face-centered cubic silica templated by poly(ethylene oxide)-polystyrene block copolymer (56.7 nm) [136]. The unit-cell parameters for as-synthesized samples synthesized in the presence of o-xylene, m-xylene and p-xylene were 50.6, 51.9 and 51.9 nm, being 7-9 % lower than those for the ethylbenzene and the xylenes mixture.

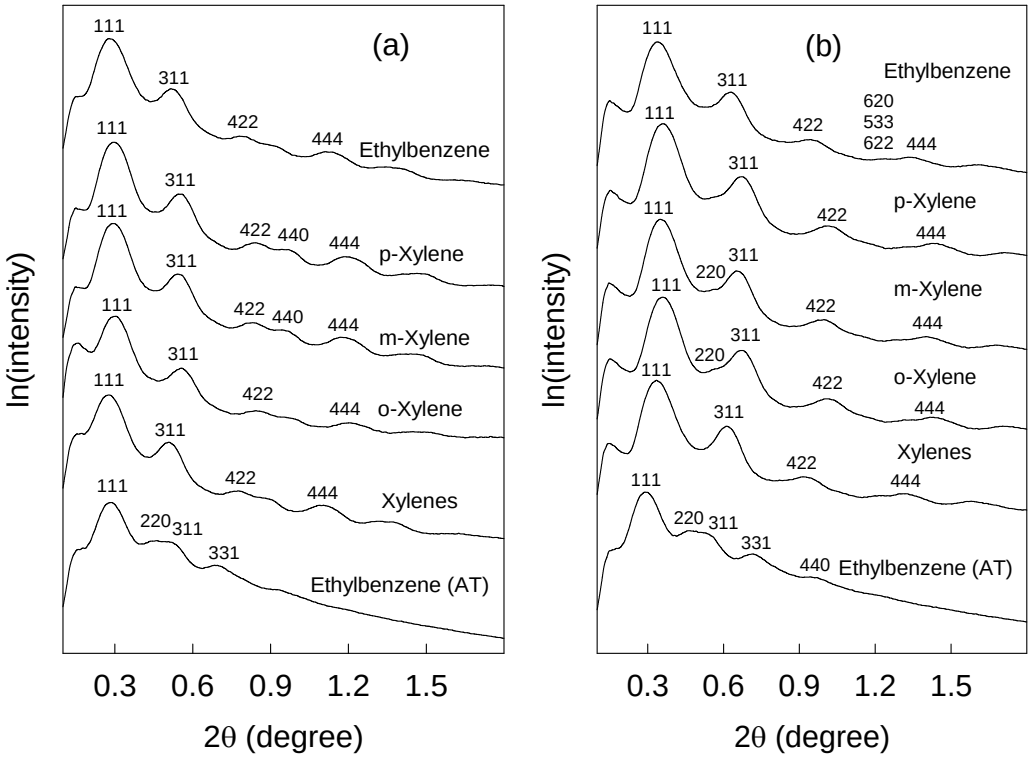

Figure 2.15. SAXS patterns for: (a) as-synthesized and (b) calcined ULP-FDU-12 samples. The sample denoted (AT) was subjected to acid treatment at 130 °C for 4 d. The data for the sample prepared with xylenes were reported elsewhere, wherein the sample was denoted EH5 [138]. [57]

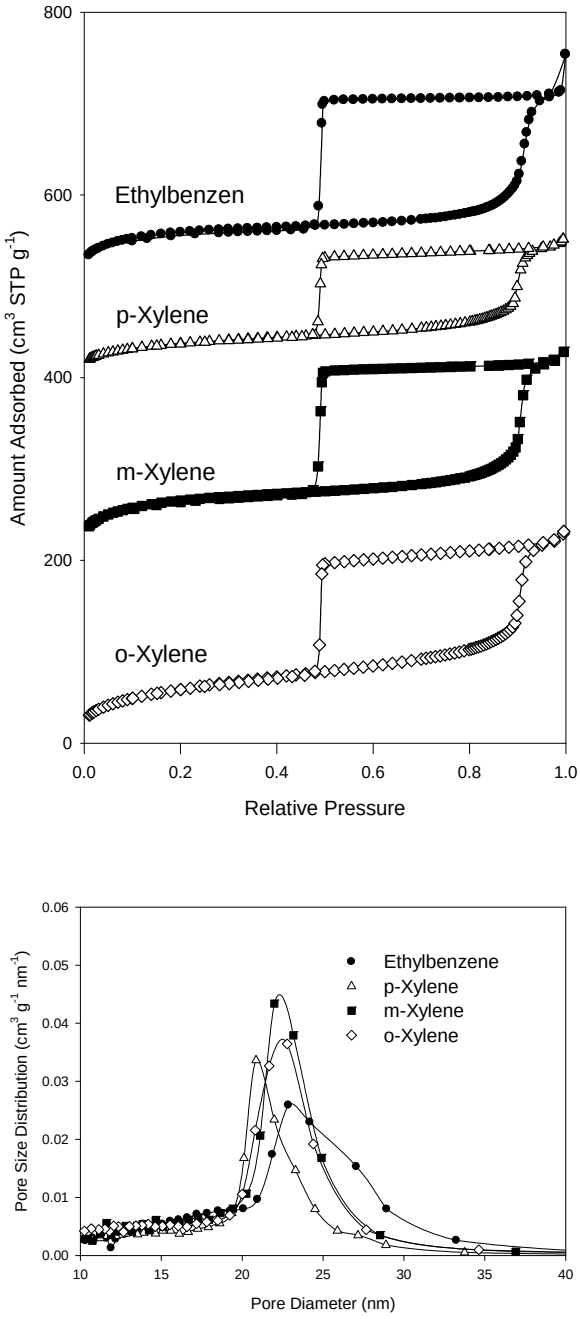

Figure 2.16. N_2 adsorption isotherms (top) and pore size distribution (bottom) for samples prepared with ethylbenzene and xylene isomers as micelle expanders. The isotherms were vertically shifted by 200, 400 and 500 cm^3 STP g^{-1}.

Table 2.6. Structural parameters for FDU-12 silicas prepared with ethylbenzene and xylene isomers[a]

Micelle expander	a_{as} (nm)	a_c (nm)	a_c/a_{as}	w_{KJS} (nm)	S_{BET} (m^2/g)	V_t (cm^3/g)
ethylbenzene	55.6	45.1	0.81	23.0	213	0.33
o-xylene	50.6	42.6	0.84	22.4	216	0.35
p-xylene	51.9	42.5	0.82	20.9	137	0.23
m-xylene	51.9	43.3	0.83	22.3	237	0.35

[a] Notation: a_{as}, unit cell parameter for as-synthesized sample; a_c, unit cell parameter for calcined sample; w_{KJS}, pore diameter calculated by using KJS method; S_{BET}, BET specific surface area; V_t, total pore volume.

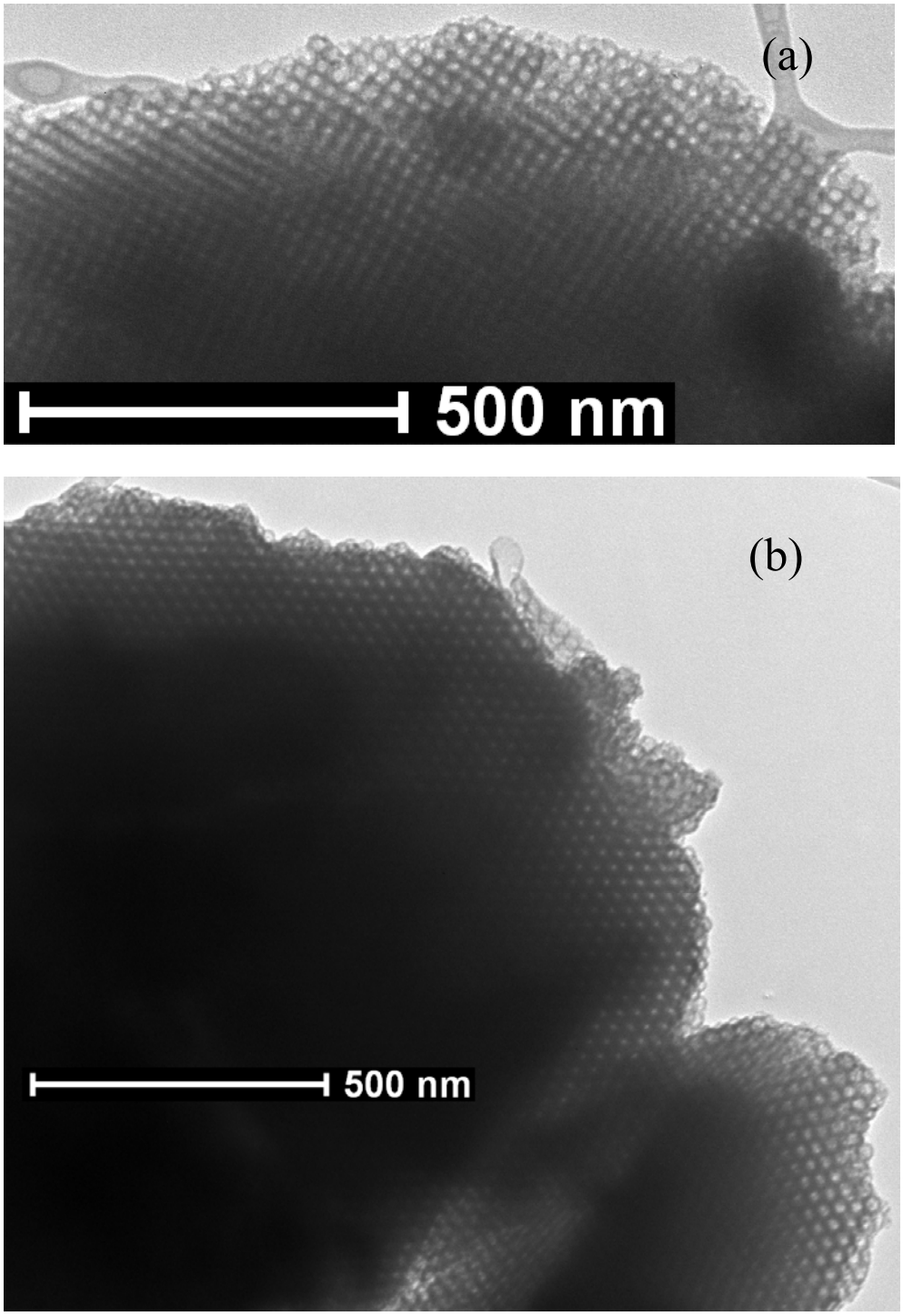

Figure 2.17. Transmission electron microscopy images of ULP-FDU-12 showing: (a) [100] projection, and (b) [110] projection. [57]

Shown in Figure 2.17 are TEM images of the calcined ULP-FDU-12 sample prepared in the presence of ethylbenzene (without the acid treatment), which show [100] and [110] projections for the face-centered cubic structure. While stacking sequences characteristic of face centered cubic and 3-D hexagonal structures are seen in many closed-packed structures with spherical mesopores [22], no clear evidence of 3-D hexagonal intergrowth was seen in the present case.

Similar trend of the structural shrinkage upon calcination of the sample prepared with ethylbenzene was observed as in the synthesis with xylenes[141]. After calcination at 550 °C, the unit-cell parameter of the sample synthesized with ethylbenzene decreased significantly (to 45.0 nm). When the as-synthesized material was additionally subjected to the acid treatment at 130 °C for 4 d, the shrinkage upon calcination was largely suppressed and the unit-cell parameter of the surfactant-free material reached 52.3 nm (down from 53.7 nm before the calcination), being nearly the same as the highest value achieved with xylenes for the calcined material (53.5 nm) [138]. The unit-cell parameter of 52.3 nm exceeds that attained for surfactant-free LP-FDU-12 synthesized using TMB as a swelling agent (up to 50.5 nm) [25,134], even though in the latter cases, a microwave digestion, which is known to lead to small shrinkage[137], was used to remove the surfactant. It should be noted that the relative peak intensity on SAXS patterns changed dramatically as a result of the acid treatment, which was already seen in the case of syntheses of FDU-12 with TMB and xylenes [51,138].

Figure 2.18(a) shows nitrogen adsorption isotherms for calcined silicas prepared in the presence of ethylbenzene, one being for the sample prepared without the acid treatment, and the other one with the acid treatment at 130 °C for 4 d. The former sample showed a

steep step of capillary condensation at a relative pressure of ~0.915 and a capillary evaporation delayed to the lower limit of adsorption-desorption hysteresis (in this case, the relative pressure of ~0.49) [153]. This behavior shows that the material had a narrow size distribution of large mesopores (see pore size distribution in Figure 2.18(b)) and the entrances to the mesopores were below 5 nm in diameter [153]. The specific surface area of this material was 213 m^2 g^{-1}, the total pore volume was 0.33 cm^3 g^{-1} and the micropore volume was 0.07 cm^3 g^{-1}. The low surface area and total pore volume can be attributed to the large shrinkage upon calcination (see above). The maximum on the pore size distribution was at 23 nm. The sample obtained after the acid treatment exhibited a steep capillary condensation step at a higher relative pressure (p/p_0 = ~0.937) and a relatively narrow hysteresis loop with the capillary evaporation at p/p_0 = ~0.8, which indicates a significant pore cage diameter enlargement (see Figure 2.18(b)) and a dramatic increase in the pore entrance size, which is likely to be close to the pore cage diameter [138]. The BET specific surface area was 251 m^2 g^{-1}, the total pore volume was 0.91 cm^3 g^{-1}, and there was no microporosity detectable using the α_s plot method. The maximum on the pore size distribution was at 32 nm (see Figure 2.18(b)). The pore diameter was also calculated using Equation 1 and reached 35.7 nm for the acid-treated material. The adsorption isotherms for the silicas prepared in the presence of ethylbenzene and the structural parameters derived from them were similar to those reported for the largest-pore ULP-FDU-12 silicas synthesized using xylenes as a swelling agent[138]. This demonstrates that ethylbenzene is another option for the synthesis of FDU-12 silicas with the highest attainable unit-cell sizes and pore diameters. The availability of several superior swelling agents for a particular surfactant has already been demonstrated to be

useful in the surfactant-templated synthesis of porous materials. Namely, an earlier study of organosilicas with 2-D hexagonal structures of very large cylindrical mesopores showed that although cyclohexane was suitable as a micelle expander for Pluronic P123 for several framework compositions, it did not work well for one important framework composition (phenylene-bridged organosilica) and its substitution with TIPB was crucial in obtaining well-defined products [139]. Moreover, unlike xylenes, which is a mixture of isomers without fully specified composition, ethylbenzene is a single compound available with high purity, which may potentially have an impact on the reproducibility of the synthesis. Our synthesis with xylenes was very well reproducible[138], but other composition of the isomer mixture may potentially afford slightly different results. To this end, TMB isomers were shown to yield somewhat different results in alkylammonium-templated synthesis [154].

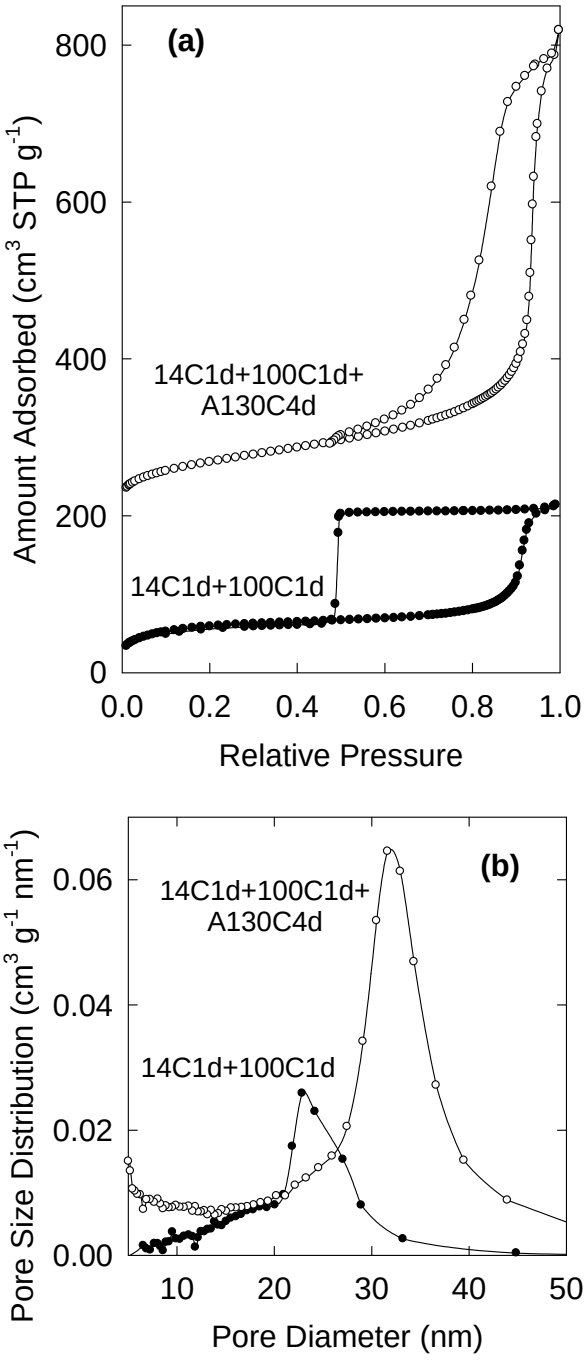

Figure 2.18. (a) Nitrogen adsorption isotherms and (b) pore size distributions for ULP-FDU-12. The isotherm for the acid treated sample was offset vertically by 200 cm^3 STP g^{-1}. [57]

2.3.2.2. Synthesis of closed-pore FDU-12 silica with ethylbenzene as micelle expander[57]

Shown in Figure 2.19 are SAXS patterns for FDU-12 silica prepared in the presence of ethylbenzene at low temperature only. The patterns correspond to as-synthesized sample and the samples derived from it through calcination at different temperatures in 300-650 °C range. All the SAXS patterns featured multiple peaks that are characteristic of a face-centered cubic structure, showing that the material retained its periodic structure over the entire temperature range. The unit-cell parameter for the as-synthesized sample was 52.3 nm (which is somewhat smaller than that for the hydrothermally treated as-synthesized material), and it decreased to 45.0, 42.8, 42.5, 41.6 and 40.3 after calcination at 300, 350, 400, 450 and 650 °C, respectively (Table 2.7). As seen in Figure 2.20, the material calcined at 300 and 350 °C exhibited adsorption isotherms characteristic of a large-pore material with spherical mesopores, the total pore volume of 0.32 and 0.29 cm^3 g^{-1}, respectively, the BET specific surface area of 300 and 265 m^2 g^{-1}, respectively, and the pore diameter was 22.2 and 21.4 nm, respectively. On the other hand, a low uptake of nitrogen was observed after calcination at a temperature of 400 °C or higher, thus showing the pore closing [44,138] around this temperature. The other ULP-FDU-12 sample prepared in the same manner exhibited the pore closing in 400-450 °C range (data not shown). The pore closing temperature for the present samples happens to be somewhat lower than the temperature of 450 °C reported earlier for the pore closing of ULP-FDU-12 prepared using xylenes as a swelling agent [138]. The present pore closing temperature approaches the temperature that was sufficient to derive closed-pore silicas from periodic mesoporous organosilicas with Fm3m structure (400 °C) [140], but in the latter case,

mesopore volumes were typically low and they would be further reduced as a result of shrinkage that leads to thermally-induced pore closing. Consequently, ULP-FDU-12 appears to be a better precursor to closed-pore silicas with appreciable mesopore volume. It should be noted that this volume cannot be directly assessed by gas adsorption, but can in some cases be obtained through extrapolation of data for open-pore materials [138,143]. It is also noteworthy that the periodic structure persisted at temperature of 650 °C, which is 250 °C above the pore closing temperature, showing that the loss of the pore connectivity is not a prelude to the sintering of the material.

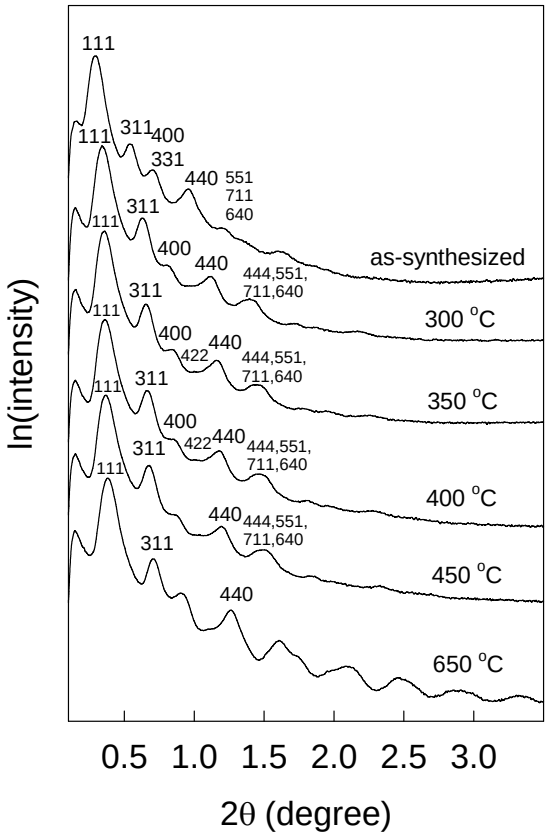

Figure 2.19. SAXS patterns for ULP-FDU-12 sample synthesized at 14 °C without subsequent hydrothermal treatment, either was as-synthesized or calcined at different temperatures. [57]

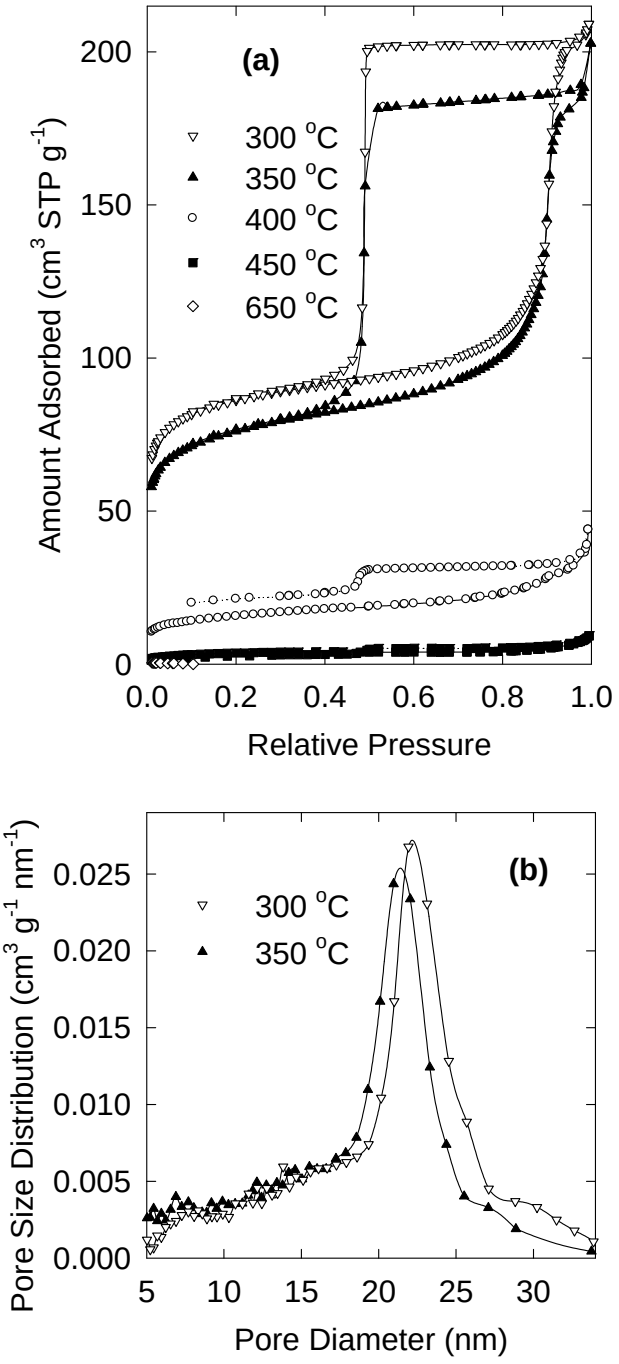

Figure 2.20. (a) Nitrogen adsorption isotherms and (b) pore size distributions for ULP-FDU-12 sample synthesized at 14 °C without subsequent hydrothermal treatment, which was calcined at different temperatures. [57]

Table 2.7. Structural parameters for FDU-12 silicas prepared with ethylbenzene and calcined at different temperatures[a]

Calcination temperature (^oC)	a_{as} (nm)	a_c (nm)	a_c/a_{as}	w_{KJS} (nm)	S_{BET} (m^2/g)	V_t (cm^3/g)
300C	52.3	45.0	0.86	22.2	300	0.32
350C	52.3	42.8	0.83	21.4	265	0.31
400C	52.3	42.5	0.81	NA[b]	55	0.065
450C	52.3	41.6	0.80	NA[b]	13	0.013
650C	52.3	40.3	0.77	NA[b]	0.04	NA[b]

[a] Notation: a_{as}, unit cell parameter for as-synthesized sample; a_c, unit cell parameter for calcined sample; w_{KJS}, pore diameter calculated by using KJS method; S_{BET}, BET specific surface area; V_t, total pore volume. [b] Pores were closed and no suitable data were available to determine the pore diameter or pore volume.

2.3.3. Conclusions[57]

Ethylbenzene was predicted to be a powerful swelling agent for the synthesis of ordered mesoporous silicas with spherical mesopores on the basis of its reported extent of solubilization in poly(ethylene oxide)-poly(propylene oxide)-based copolymer surfactants and of the known swelling agent performance of other alkyl-substituted benzenes. The application of ethylbenzene in the low-temperature synthesis involving Pluronic F127 block copolymer, which was similar to that originally developed for LP-FDU-12 using TMB and later improved through the use of xylenes, afforded ultra-large-pore FDU-12 silicas with unit-cell sizes and pore diameters matching those attained earlier for xylenes. Consequently, ethylbenzene-based synthesis was established as an alternative avenue to face-centered cubic silicas that exhibit the highest reported unit-cell sizes and diameters

of spherical mesopores. ULP-FDU-12 prepared at low temperature only exhibited the thermally-induced pore closing at 400-450 °C, which is very low. The suitability of individual xylene isomers as swelling agents was investigated and appeared to approach that of xylenes mixture and ethylbenzene. These results show that the performance of the alkyl-substituted benzenes as swelling agents primarily depends on the total number of carbon atoms in the alkyl substituents rather than on the details of the molecular structure.

Chapter 3. Grafting of Organic Groups in Nanopores of Ordered Mesoporous Silicas

3.1. Synthesis of mesoporous silica/polymer composites via "grafting from" method

3.1.1. Introduction

The polymer / solid composites combine the advantages of soft polymer and hard solid to create novel materials exhibiting beneficial mechanical properties and versatile functionalities. Various monomers have been successfully grafted from surfaces of nanoporous materials via surface-initiated atom transfer radical polymerization (SI-ATRP), including styrene[39,61,76], methyl methacrylate[61,76], n-isopropylacrylamide[64] and acrylonitrile[39,42] . Mesoporous silicas, including SBA-15[39,76], MCM-41[155], FDU-1[39] and mesocellular foam[64], have been used as the solid supports.

As discussed earlier, FDU-12 silicas have spherical pores and three-dimensional pore connectivity. Such pore connectivity provides advantages in mass transport because the local pore blocking in one place in the pore network shuts down only one of many possible transport pathways. Ultra-large-pore FDU-12 discussed above exhibits pore size up to 36 nm which is about 10 nm larger than the pore diameter of ultra-large pore SBA-15, and thus ULP-FDU-12 is a good candidate to serve as a solid support for polymer/silica composites. However, SI-ATRP has not been reported from the surfaces of FDU-12 silicas, except for the work described in the Ph.D. dissertation of Liang Cao on polymerization of acrylonitirle.[80] A possible reason is that in the synthesis of FDU-12 silica, a relatively large amount of inorganic salt (KCl) is typically used to facilitate the formation of the ordered structure, while only a catalytic amount of inorganic salt (NH_4F) is needed in the synthesis of large-pore SBA-15 silica. The residue of the inorganic salt in

the framework of FDU-12 silica appears to affect the process of SI-ATRP and prevent the growth of polymer as shown in the work of Dr. Liang Cao.[80] Secondly, the size of passages between the mesopores of FDU-12 is smaller than the size of pore cages. Such a structural feature increases the risk of pore blocking during the polymerization, if the structure of FDU-12 is not properly tailored to achieve a large pore entrance size. In such a case, the blocking of connections between the pores, or entrances on the outer surface of particles, will affect the accessibility of the pores in the matrix. From this point of view, the SI-ATRP in FDU-12 silicas is more complicated and challenging than in the case of cylindrical mesopores (such as SBA-15).

The combination of stimuli-responsive polymers and OMSs could produce interesting hybrid materials. For example, a pH sensitive polyzwitterionic brush was grafted from the surfaces of mesoporous silica film to mimic the function of pore-forming proteins.[156] The charges on the channels of mesoporous silica could be switched by adjusting the pH of the environment and thus the selective transport of ionic species was achieved. In our study, FDU-12 silicas were synthesized in the absence of inorganic salt, following prior work of Dr. L. Cao.[80] By carefully selecting the synthesis conditions, large-pore FDU-12 silicas were prepared with highly ordered face-centered cubic structure. The initiating sites were introduced by silylation reaction with bromoester-bearing organosilane. Bromoester-based initiator was successfully used in SI-ATRP[39,42,75,157-158]. Herein, thermoresponsive polymer was grafted from the surfaces of FDU-12 silicas via surface-initiated atom transfer radical polymerization (SI-ATRP) or surface-initiated atom transfer radical polymerization with activators regenerated by electron transfer (SI-

ARGET ATRP) to synthesize potentially thermoresponsive polymer/silica composites (Sheme 4).

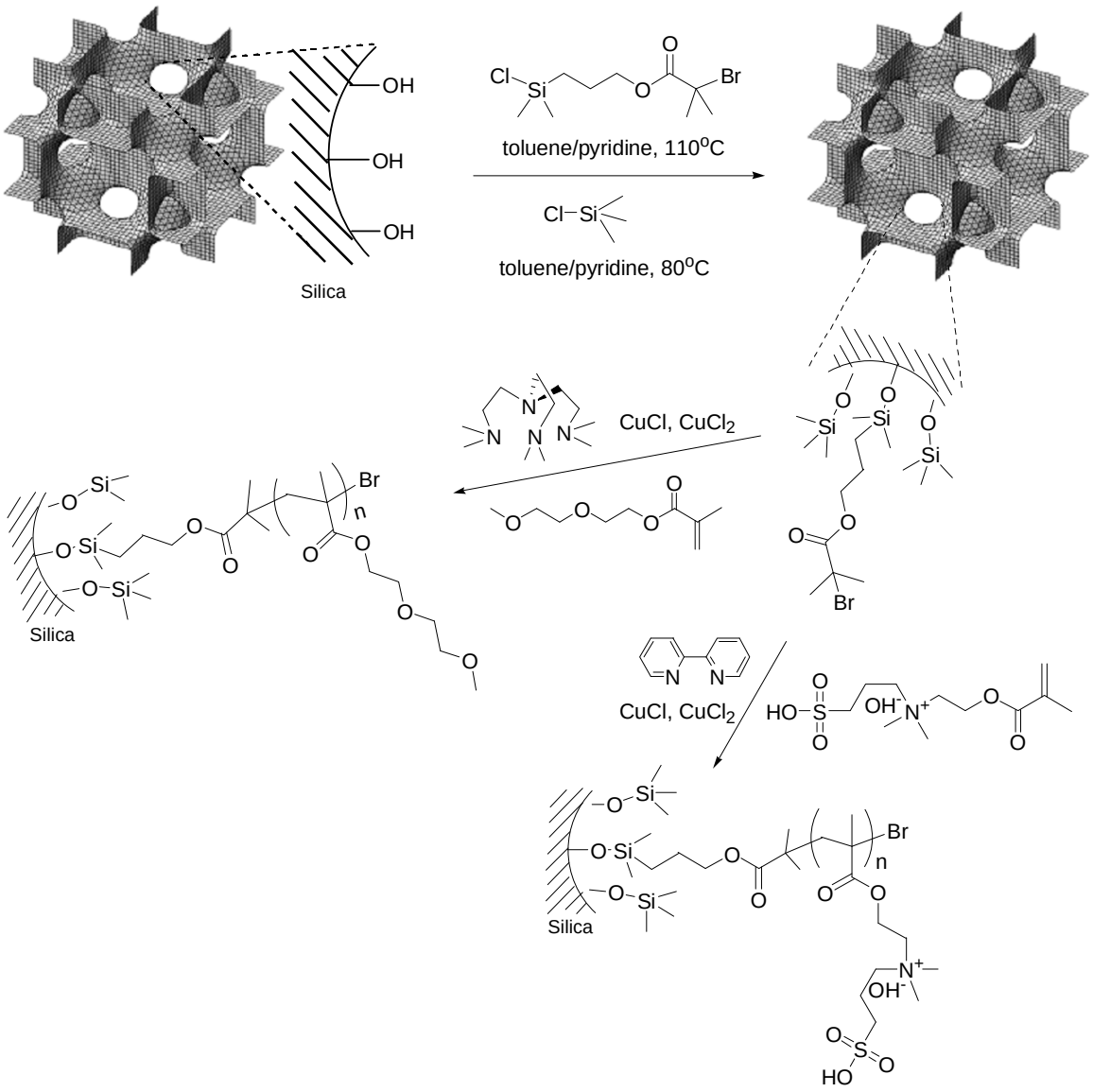

Scheme 4. Grafting poly [di(ethylene glycol) methyl ether methacrylate] and poly [2-(methacryloyloxy)ethyl]dimethyl(3-sulfopropyl)ammonium from concave surface of spherical mesopores of FDU-12 via normal atom transfer radical polymerization (ATRP)

3.1.2. Experimental section

3.1.2.1. Materials

The FDU-12 silica was prepared under salt-free conditions as introduced above and originally investigated by Liang Cao (Ph.D dissertation).[80] 1 g of F127 was dissolved in 60 mL of HCl at room temperature, and then the solution was brought to 14 ^{o}C. 3 hours later, 2.35 mL of xylenes were added to the solution. The mixture was stirred in a closed polypropylene bottle for 16.5 hours. Then 4.35 mL of TEOS was added and the mixture was stirred at 14 ^{o}C for 1 day. The mixture was moved to an oven set at 100^{o}C and kept for 1 day. Then the mixture was transferred to a Teflon-lined autoclave and heated at 130 °C for 2 days. The as-synthesized FDU-12 silica was recovered by filtration and dried at 60 ^{o}C under vacuum. The as-synthesized sample was calcined at 550 ^{o}C. Di(ethylene glycol) methyl ether methacrylate ($M(EO)_2MA$), [2-(methacryloyloxy)ethyl]dimethyl(3-sulfopropyl)ammonium hydroxide (MEDSAH), 1,1'-bipyridine (bpy) and tin(II) 2-ethylhexanoate ($Sn(EH)_2$) were purchased from Aldrich. $M(EO)_2MA$ was purified by passing through a column filled with basic alumina. Tris[2-(dimethylamino)ethyl]amine (Me_6TREN) was purchased from ATRP Solutions, Inc. and used as received. The initiator, 3-(chlorodimethylsilyl) propyl 2-bromoisobutyrate was synthesized as described elsewhere.[162] All other chemicals including solvents and copper salts were used as received.

3.1.2.2. Synthetic procedures

Grafting the initiator to the surface of FDU-12 silicas. 0.5 g of FDU-12 silica was dispersed in 10 ml of dry toluene in a round bottom flask. The mixture was stirred with

purging nitrogen for 30 minutes before 1 ml 3-(chlorodimethylsilyl) propyl 2-bromoisobutyrate was injected. Then 0.3 ml pyridine was injected. The mixture was refluxed for 1 day at 110 ^{o}C. Then the silica was recovered by filtration and washed thoroughly with toluene, ethanol and water. The sample was dried in a vacuum oven at 40 ^{o}C. Then a similar surface modification of the obtained sample was conducted as described above by using trimethylchlorosilane instead of 3-(chlorodimethylsilyl) propyl 2-bromoisobutyrate. The obtained sample was denoted FDU-12-BiB.

Grafting of M(EO)$_2$MA from the surface of FDU-12 via ATRP. [I] : [M] : [CuCl] : [$CuCl_2$] : [Me_6TREN] = 1 : 20 : 1 : 0.1 : 2.2. A typical procedure of ATRP was as follows. In the polymerization, the initiator-modified silica (50 mg, with 0.0355 mmol initiator), M(EO)$_2$MA monomer (0.13 ml, 0.71 mmol), a pre-mixed solution of $CuCl_2$ (0.5 mg, 0.00355 mmol) and Me_6TREN (9 mg, 0.0781 mmol) in anisole (1 ml) and anisole (4 ml) were added to a 10 ml Schlenk flask. The flask was sealed and oxygen was removed by subjecting the contents of the flask to three freeze-pump-thaw cycles. Then 3.5 mg of CuCl (0.0355 mmol) was added under nitrogen flow. The sealed and stirred flask was placed in an oil bath at 40 ^{o}C. The polymerization was terminated by opening the flask and exposing the catalyst to oxygen from the air. The polymer/silica composites were recovered by filtration, washed thoroughly with toluene, methanol and water and dried in a vacuum oven at 60 ^{o}C.

Grafting of M(EO)$_2$MA from the surface of FDU-12 via ARGET ATRP without deoxygenation. [I] : [M] : [$CuBr_2$] : [Me_6TREN] = 1 : 100 : 0.005 : 0.05. The initiator-modified silica (40 mg with 0.0331 mmol initiator), M(EO)$_2$MA monomer (0.61 ml,

3.310 mmol), a pre-mixed solution of $CuBr_2$ (0.0370 mg, 0.000166 mmol) and Me_6TREN (0.383 mg, 0.00166 mmol) in anisole (37 μl) and anisole (3.3 ml) were added to a 4 ml glass vial. Then vial was then sealed with a rubber septum. 47.6 mg $Sn(EH)_2$ was injected to the vial. The stirred vial was suspended in an oil bath at 40^{o}C. The polymerization was terminated by opening the vial and exposing the catalyst to oxygen from the air. The polymer/silica composites were recovered by filtration, washed thoroughly with toluene, methanol and water and dried in a vacuum oven at 60 ^{o}C.

Grafting of MEDSAH from the surface of FDU-12 via ATRP [I] : [M] : [CuCl] : [$CuCl_2$] : [bpy] = 1 : 20 : 1 : 0.1 : 2.5. A typical procedure of ATRP was as follows. The initiator-modified silica (50 mg, with 0.0355 mmol initiator), MEDSAH monomer (198 mg, 0.710 mmol), and methanol/water mixture (3.0 ml, 4/1 v/v) were added to a 10 mL Schlenk flask. The flask was sealed and oxygen was removed by subjecting the contents of the flask to three freeze-pump-thaw cycles. Then 3.5 mg of CuCl (0.0355 mmol) was added under nitrogen flow to a degassed solution of $CuCl_2$ (0.486 mg, 0.00355 mmol) and bpy (13.86 mg, 0.0888 mmol) in methanol (0.331 ml) and stirred at room temperature for 30 min. Afterwards, the solution of CuCl, $CuCl_2$ and bpy was transferred to the Schlenk flask containing silica initiator and monomer via a syringe. Then the stirred flask was placed in an oil bath at 25 ^{o}C. The polymerization was terminated by opening the flask and exposing the catalyst to oxygen from the air. The polymer/silica composites were recovered by filtration, washed thoroughly with toluene, methanol and water and dried in a vacuum oven at 60 ^{o}C.

3.1.2.3 Measurements

Small-angle X-ray scattering (SAXS) measurements were performed by using a Bruker Nanostar U SAXS/wide-angle X-ray scattering instrument with a rotating anode X-ray source and Vantec-2000 two-dimensional detector. Nitrogen adsorption measurements at -196 °C were carried out using a Micromeritics ASAP 2020 volumetric adsorption analyzer. Prior to the adsorption measurement, the samples were outgassed under vacuum at 200 °C (for silicas) or 80 °C (for modified silicas) in the port of the gas adsorption analyzer. FTIR spectra were collected on Bruker Vertex 70V FT-IR spectrometer, operating at 4 cm^{-1} resolution and 32 scans. Thermogravimetric analysis (TGA) was performed under flowing air from room temperature to 800 °C on Hi-Res 2950 thermogravimetric analyzer from TA Instruments. The heating rate was 5° C/min.

3.1.2.4 Calculations

The specific surface area was calculated from nitrogen adsorption isotherms using the BET method[3] in the relative pressure range from 0.04 to 0.2. The total pore volume[3] was estimated from the amount adsorbed at a relative pressure of 0.99. The pore size distribution (PSD) was calculated from adsorption branches of isotherms[144] using the BJH method (with KJS correction)[144,159] with the statistical film thickness curve for a macroporous silica gel.[142] The loading of surface-bound groups was calculated from TGA data under assumption that for all the samples, the residue at ~800 °C is dehydroxylated silica. In most cases, the weight percentage of the organic groups was estimated as a weight loss in the temperature range from 100 °C to ~800 °C.

3.1.3. Results and discussion

3.1.3.1. Grafting of P[M(EO)$_2$MA] from the surface of FDU-12 via SI-ATRP

The immobilization of the initiator on the surface of FDU-12 silica was confirmed by TGA (Figure 3.1), where a weight loss was seen in the 250-400 ^{o}C range from the weight change curve of FDU-12-BiB, which is primarily attributable to the decomposition and volatilization of the BiB groups. The weight loss for unmodified calcined silicas is small in the temperature range in which organic groups burn out and thus the weight loss can be associated with the loading of organic groups. The burning out of one mole of BiB moiety is related to a weight loss of 238 g. Therefore, 14.85 % weight loss corresponds to about 0.73 mmol of initiator groups per gram of FDU-12 silica and 0.97 groups per nm^2 on the surface for FDU-12-BiB^b (Table 3.1). The N_2 adsorption isotherm of FDU-12-BiB (Figure 3.2) showed lowering of the pore volume and the decrease in the S_{BET} (Table 3.1). The combination of these results points to a successful modification of the surface of the material with the initiator.

Poly di(ethylene glycol) methyl ether methacrylate (M(EO)$_2$MA) is a water-soluble thermoresponsive biocompatible polymer with the lower critical solution temperature (LCST) about 25 ^{o}C in water.[160] Below the LCST, the polymer chains swell and extend in water. Above the LCST, the polymer chains collapse and become hydrophobic. Comparing to the well-known temperature-responsive polymer, poly(N-isopropylacrylamide), (PNIPAAm), the reports on PM(EO)$_2$MA brushes were fewer.[161] Because PM(EO)$_2$MA is totally noncytotoxic, and the LCST of the copolymer of M(EO)$_2$MA and oligo (ethylene glycol) methyl ether methacrylate can be tuned between

25 to 90 ^{o}C[162-164], this composition of a stimuli-responsive polymer provides opportunities for biological applications[165-166] and smart nanomaterials[167-168]. PM(EO)$_2$MA brushes were grafted from flat surfaces[169], silicon wafers[167,170] and spherical nanoparticles[171] via SI-ATRP. However, a surface-initiated polymerization of PM(EO)$_2$MA in mesoporous structures has not been reported.

The polymerization of M(EO)$_2$MA was done at 40 ^{o}C. The control over the loading of polymer was proved by TGA (Figure 3.1). It should be noted that the polymerization time, the structural parameters measured by N_2 adsorption and the loading of polymer were summarized in Table 3.1. One-hour polymerization afforded 9.1 wt.% PM(EO)$_2$MA content in the silica / polymer composite. As the polymerization time increased to 2 and 3 hours, the loading of PM(EO)$_2$MA increased to 20.6 wt.% and 23.8 wt. %, respectively.

For the polymer contents of 9-21 wt.% in the composites, a decrease in the pore volume, surface area and pore diameter (based on capillary condensation pressure) were observed from N_2 adsorption analysis (Figure 3.2 and 3.3), which confirmed the successful grafting of PM(EO)$_2$MA in the pores. The pore diameter decreased about 1.1 nm after 9.1 wt.% PM(EO)$_2$MA grafted and about 2.0 nm when the loading doubled. The thickness of the polymer layer corresponded to the pore size decrease and was estimated to be ~0.5 and 1.0 nm for 9.1 and 20.6 wt.% loading, respectively. When the polymerization time was extended to 3 hours, the loading of PM(EO)$_2$MA slightly increased to 23.8 wt.%. However, N_2 adsorption analysis for this composite showed low pore volume, which implied that some of the mesopores might have been blocked or filled with the polymer. Taking into account that after 2-hour polymerization, a limited

fraction of the pore volume was available for further growth of the polymer, the diffusion of monomers, catalyst complex and deactivator complex in the pores would be more and more difficult after the extended time. Perhaps because of that, the polymerization slowed down. It should be noted that the adsorption isotherms for polymer-grafted samples were distorted due to the contribution of a moderate or mall specific area and small sample mass. The distortion manifested itself in a decrease in the gas uptake as the relative pressure increased, which is on artifact.

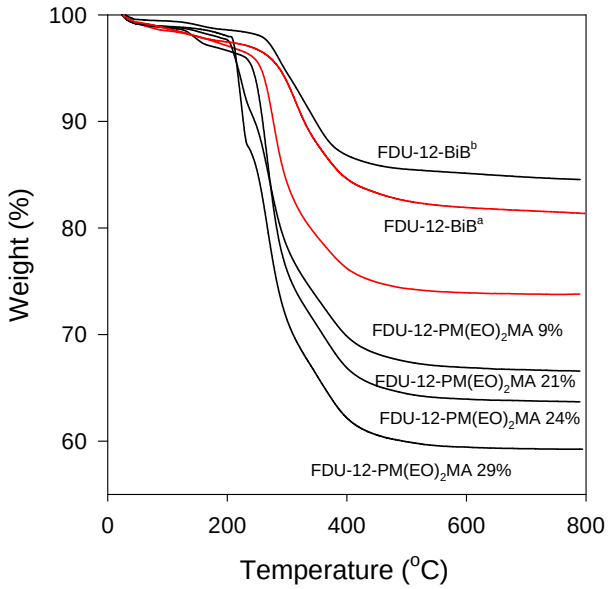

Figure. 3.1. Thermogravimetric weight change patterns for initiator-modified FDU-12 and $PM(EO)_2MA$ / FDU-12 composites (the loading of $PM(EO)_2MA$ in composites is shown in wt.%). The measurements were done under air.

When the concentrations of the reactants were doubled by decreasing the volume of the solvent in the reaction mixture, a loading of 29.2 wt.% was achieved after 2 hours. The higher concentration of monomer and initiator in the reaction mixture could accelerate

the polymerization rate. N_2 adsorption analysis for this composite showed no pores accessible for N_2 molecules.

Table 3.1. Structural parameters for polymer/silica composites

FDU-12 support, grafted polymer and its weight % in the composite	t (h)	S_{BET} (m^2 g^{-1})	V_t (cm^3 g^{-1})	w_{KJS} (nm)
FDU-12[a]	-	459	0.97	27.1
FDU-12-BiB[a]	-	172	0.54	25.8
FDU-12[a]-$PM(EO)_2MA$-9%	1	26	0.22	24.7
FDU-12[b]	-	458	1.20	27.6
FDU-12-BiB[b]	-	145	0.63	25.3
FDU-12[b]-$PM(EO)_2MA$-21%	2	20	0.13	23.3
FDU-12[b]-$PM(EO)_2MA$-24%	3	2	0.04	NA
FDU-12[b]-$PM(EO)_2MA$-29% [c]	2	0	NA	NA

Notation: [a] Samples were prepared by using the same batch of FDU-12 [a] silica. [b] Samples were prepared by using the same batch of FDU-12 [b] silica. [c]The total volume of the polymerization mixture was reduced to 50 % of the volume used for the other composites; w_{KJS}, pore diameter calculated by using KJS method; S_{BET}, BET specific surface area; V_t, total pore volume; NA was used where the data could not be measured as pores were blocked.

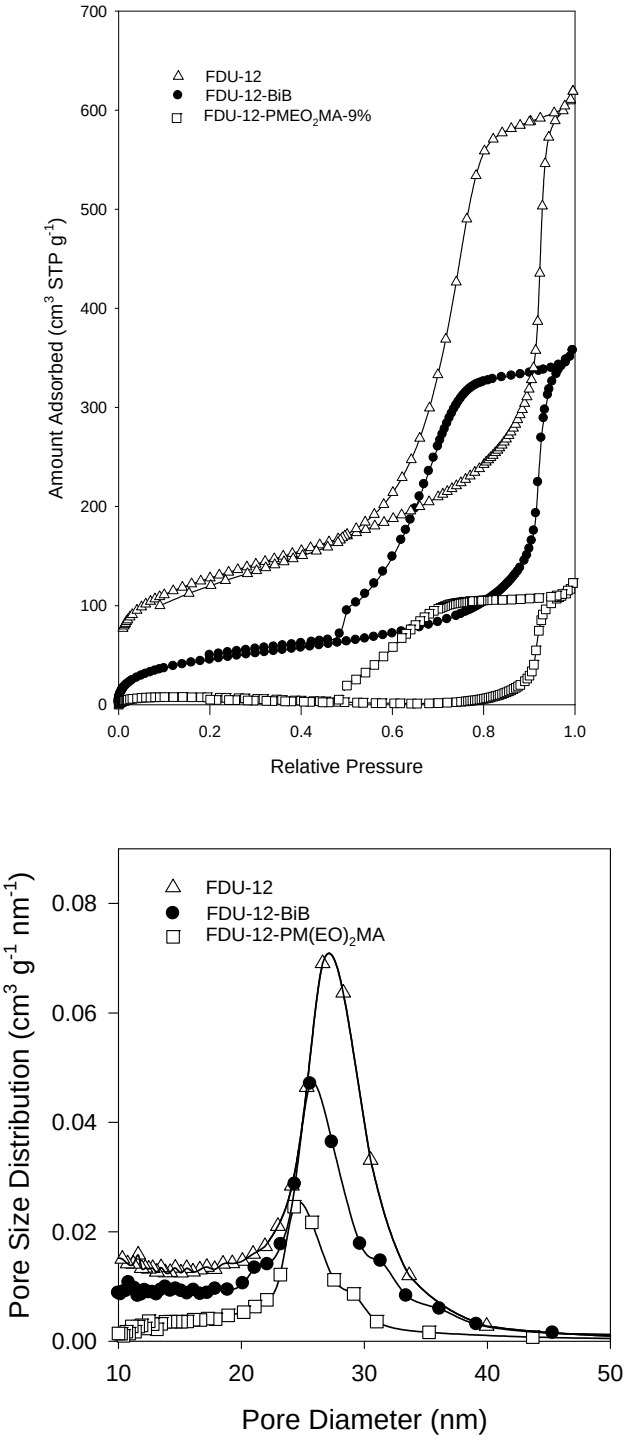

Figure 3.2. N_2 adsorption isotherms (top) and pore size distributions (bottom) for FDU-12 silicas before and after the attachement of initiator and the grafting of $PM(EO)_2MA$.

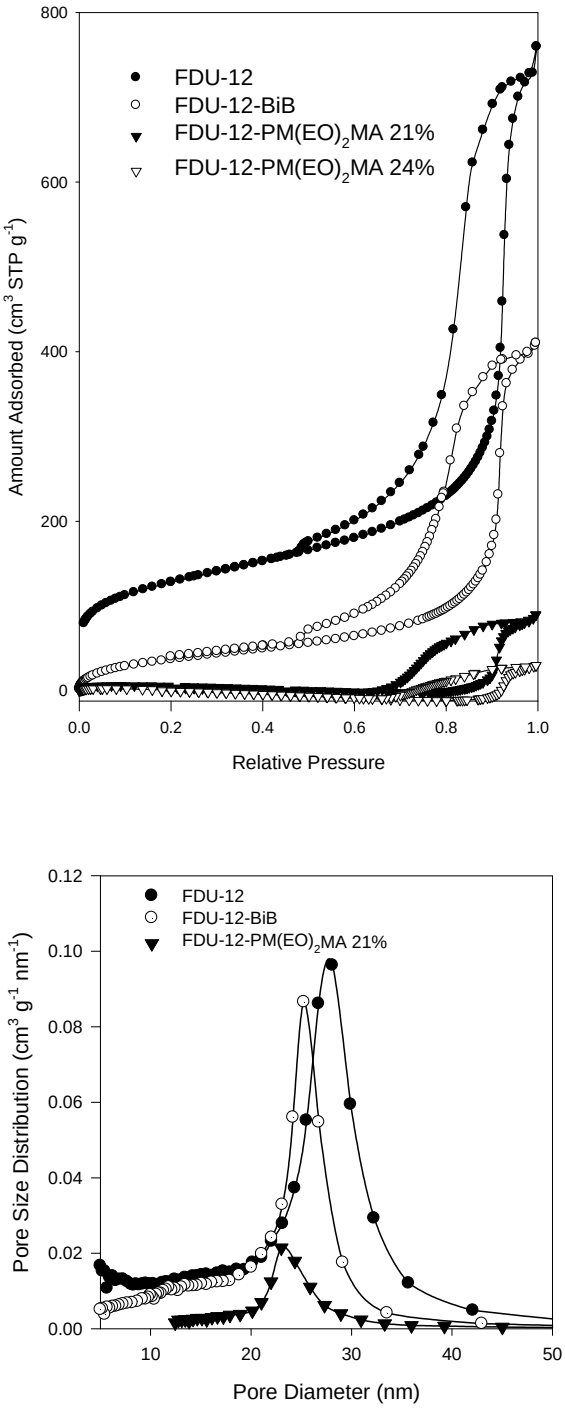

Figure 3.3. N_2 adsorption isotherms (top) and pore size distributions (bottom) for FDU-12 silicas before and after the attachement of initiator and the grafting of $PM(EO)_2MA$.

3.1.3.2. Grafting of $M(EO)_2MA$ from the surface of FDU-12 via ARGET ATRP

In ARGET ATRP, the molar ratio of reactants was [I] : [M] : [$CuBr_2$] : [Me_6TREN] : = 1 : 100 : 0.005 : 0.05. The initiator : catalyst ratio was 200-fold lower than that in normal ATRP (see above) and 2-fold lower than that in ARGET ATRP in solution studied by others.[172] The polymerizations were conducted without prior deoxygenation in a 4 mL glass vial. The reducing reagent was used to reduce Cu(II) to Cu(I) and to remove the oxygen (radical trap) through a cycle involving oxidation and reduction of copper species.

The successful grafting of $PM(EO)_2MA$ was inferred from N_2 adsorption analysis (Figure 3.4) and TGA (Figure 3.5). 7.0 wt.% and 33.5 wt.% of $PM(EO)_2MA$ content were achieved after 3 and 4 hours polymerization, respectively. Because the concentration of Cu(II) was very low, the depletion of oxygen could take some time. After the induction period, the polymerization proceeded at a considerable rate and the loading of $PM(EO)_2MA$ differed considerably (from 7.0 wt.% to 33.5 wt.%) when the polymerization time differed by just one hour. The loading of polymer continued to increase as the time of polymerization time increased. After 15 hours of polymerization, the loading of $PM(EO)_2MA$ reached 49 wt.%. FT-IR spectra of FDU-12 grafted with 33 wt.% $PM(EO_2)MA$ (Figure 3.6) showed a peak at 1727 cm^{-1} associated to the carbonyl group which was enhanced after the grafting of the polymer.

N_2 adsorption isotherm indicated a lower pore volume, surface area and pore diameter (based on capillary condensation pressure) after the loading of 7.0 wt.% polymer. The shape of the adsorption-desorption hysteresis loop was maintained after the grafting,

which indicated that the polymers were uniformly distributed on the inner surface of the mesopores. The pore size decreased 1.5 nm (Table 3.2). Therefore the thickness of the polymer layer could be ~0.7 nm. With 33.5 wt.% or more of $PM(EO)_2MA$ in the composite, the pores were inaccessible for N_2 molecules, and some polymer chains were most likely grown on the external surfaces of the solid support at longer polymerization time (15 hours).

Table 3.2. Structural parameters and TGA results for polymer/silica composites.

FDU-12 support, grafted polymer and its weight %	t (h)	S_{BET} ($m^2\ g^{-1}$)	V_t ($cm^3\ g^{-1}$)	w_{KJS} (nm)	weight loss (%)	residue (%)
FDU-12	-	458	0.94	27.1	-	-
FDU-12-BiB	-	172	0.54	25.8	17.33	81.82
FDU-12-$PM(EO)_2MA$-7%	3	95	0.37	24.3	23.07	75.78
FDU-12-$PM(EO)_2MA$-33%	4	NA	NA	NA	44.92	54.15
FDU-12-$PM(EO)_2MA$-39%	4.5	NA	NA	NA	49.11	45.75
FDU-12-$PM(EO)_2MA$-49%	15	NA	NA	NA	57.36	41.49

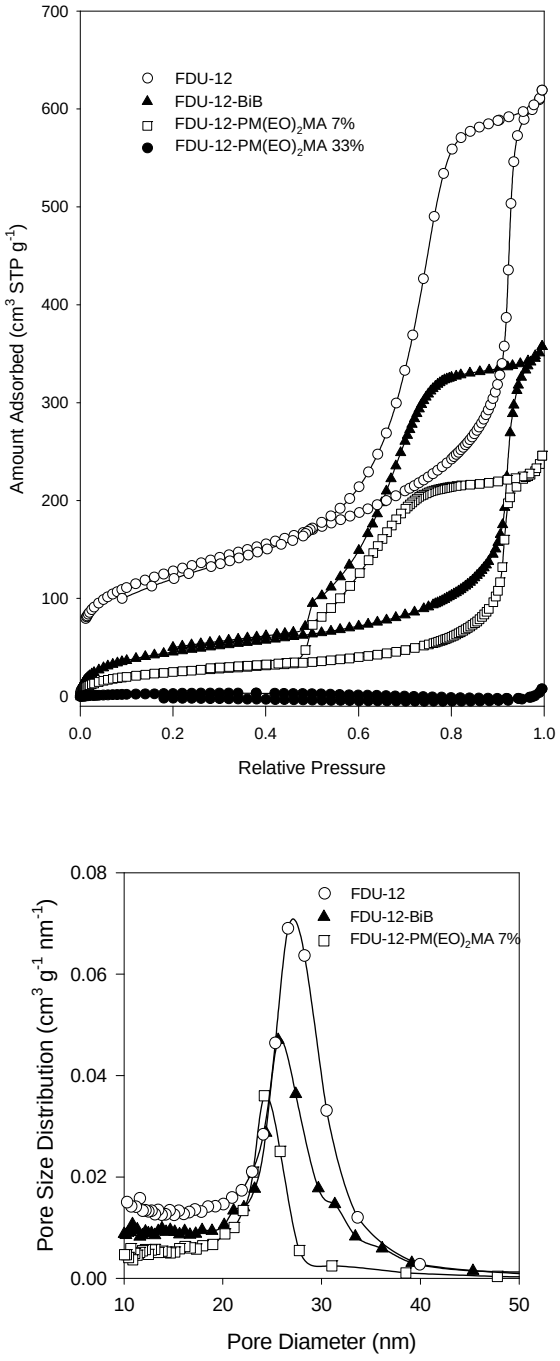

Figure. 3.4. (top) N_2 adsorption isotherms and (bottom) pore size distributions distributions for FDU-12 silicas before and after the attachement of initiator and the grafting of $PM(EO)_2MA$ via ARGET ATRP.

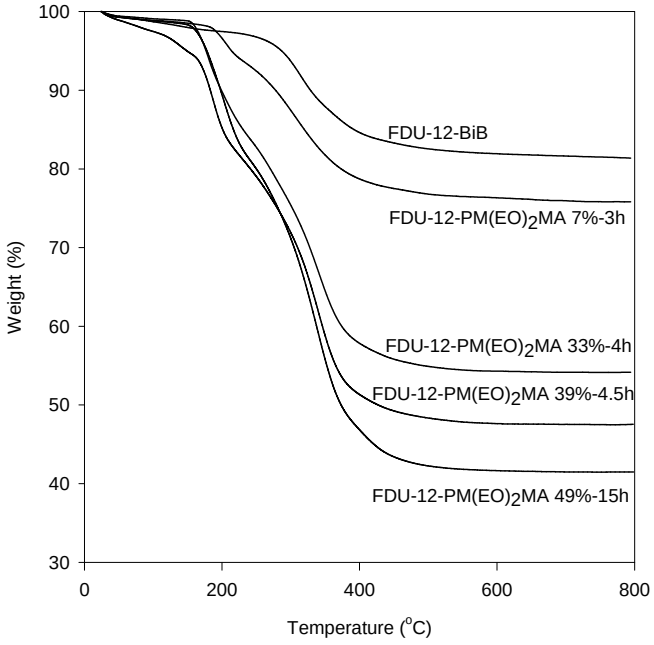

Figure 3.5. Thermogravimetric weight change patterns for initiator-modified FDU-12 and $PM(EO)_2MA$ / FDU-12 composites (the loading of $PM(EO)_2MA$ in composites is shown in wt.%).

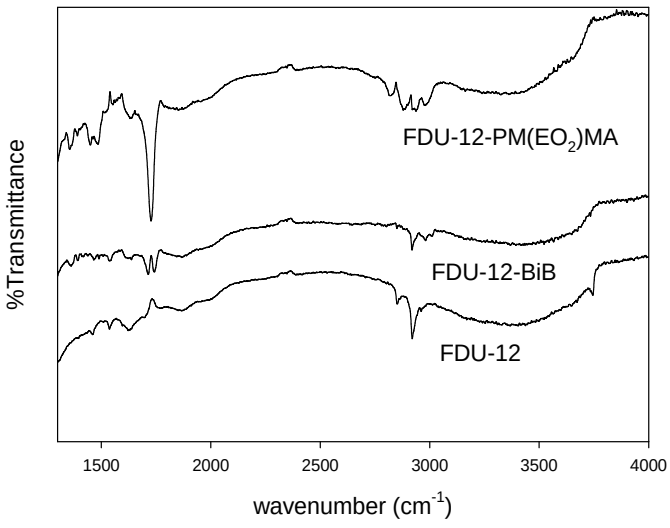

Figure. 3.6. FT-IR spectra of FDU-12, FDU-12 modified with 2-bromoisobutyrate group (FDU-12-BiB), and 33 wt% of $PM(EO_2)MA$.

3.1.3.3. Grafting of MEDSAH from the surface of FDU-12 via SI-ATRP

[2-(methacryloyloxy)ethyl]dimethyl(3-sulfopropyl)ammonium hydroxide (MEDSAH) (Scheme 4) is a zwitterionic monomer, which bears an anionic sulfonate group (SO_3^-) and a cationic quaternary ammounium group. The polymer of MEDSAH (PMEDSAH) is biocompatible and shows great potential for making surfaces resistant to non-specific protein adsorption. In addition, PMEDSAH exhibits interesting reversible self-association behavior in solution due to the strong inter- and intrachain ion-paring interactions. The self-association of PMEDSAH chains usually renders them insoluble, and only as the ionic interactions are broken at a sufficiently high temperature, the associated chains are isolated and the polyzwitterionic polymers become soluble.[173] Such hydrophobic-to-hydrophilic transition at an upper critical solution temperature (UCST) provides opportunities for creating thermoresponsive coatings.[174] The brushes of PMEDSAH were synthesized on surfaces of planar substrates,[173-176] and spherical nanoparticles,[177] while the grafting of PMEDSAH in nanopores has not been reported.

The SI-ATRP of MEDSAH was conducted in methanol/water mixture at room temperature by using the conditions reported for polymerization in solution.[174] Since the sulfobetaine monomer is able to coordinate to copper and form a stable complex, Cu(I) and Cu(II) were precoordinated with bipyridine before adding to the reaction mixture.[174] The polymerization of MEDSAH proceeded rapidly. TGA result (Figure 3.7) showed a loading of 20 wt% polymer was obtained after a 30-min polymerization. A major increase of loading took place during an hour, and then it slowed down. The N_2 adsorption measurement (Figure 3.8) revealed the growth of the polymer in the mesopores. After the half-hour polymerization, the pore volume and specific surface area

decreased significantly. The pore size shifted towards smaller value retaining the narrow distribution indicating that the inner pore surface was indeed grafted with the polymer. However, the magnitude of the pore volume decreased, when compared with original pore volume and the loading of organic groups, suggested that some pores were blocked by the grafted polymer.

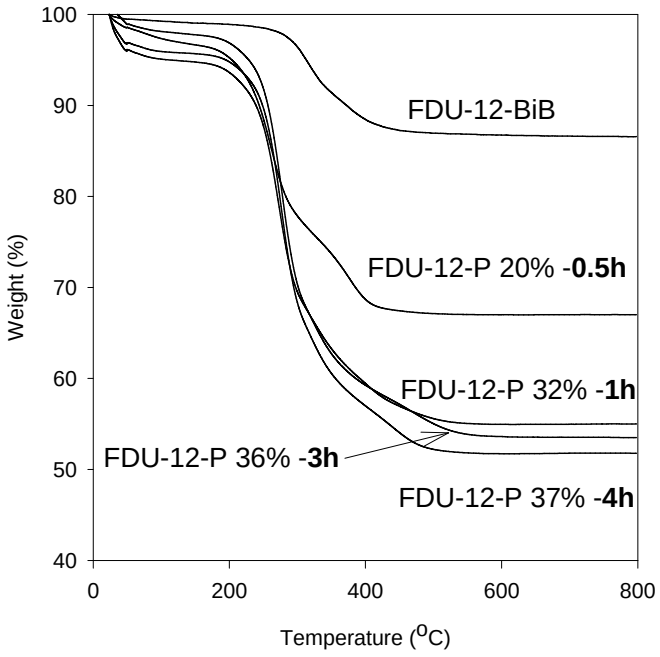

Figure 3.7. Thermogravimetric weight change patterns for initiator-modified FDU-12 and PMEDSAH / FDU-12 composites (the loading of PMEDSAH in composites is shown in wt.%).

As the loading of the polymer increased to 32 wt%, the pores were not accessible to N_2 molecules any more, which is expected as the organic group loading was close to that expected to completely fill the pores. The total pore volume of the unmodified FDU-12 was 0.97 cm^3/g (Table 3.3), so the silica support which constitutes 55 wt.% the material

has a pore volume of ~0.53 cm^3 per gram of the composite of FDU-12-PMEDSAH-32%. The organic group (PMEDSAH and initiator moiety) constitute 40 wt.%, and assuming that the density of the organic groups is 1.0 g/cm^3, the volume occupied by organic groups should be ~0.40 cm^3. Therefore, the pore volume of only about 0.13 cm^3 (0.53 cm^3-0.40 cm^3 = 0.13 cm^3) is expected to remain, which is a small fraction of original pore volume and access to it may be blocked by the polymer grown in the passages between the mesopores. At longer polymerization times, the polymer loading was very close to the maximum loading that can be accommodated in the material, assuming no major contribution from polymerization on the external surface of the particles.

The successful grafting of PMEDSAH was also confirmed from the peak that at 1720 cm^{-1} (Figure 3.9) which corresponds to the carbonyl group and has become much stronger comparing with the initiator-modified material, because carbonyl groups carried by the polymer chains were more numerous than those present in the initiator moieties.

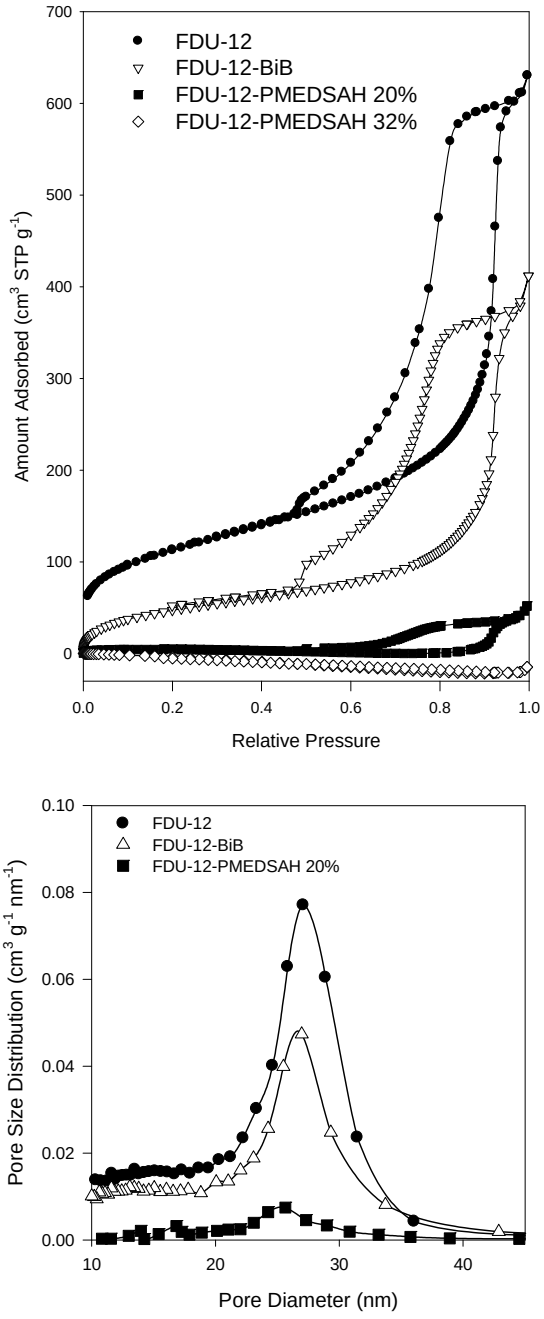

Figure 3.8. (top) N_2 adsorption isotherms and (bottom) pore size distributions distributions for FDU-12 silicas before and after the attachement of initiator and the grafting of PMEDSAH.

Table 3.3. Structural parameters and TGA results for polymer/silica composites.[a]

sample	t (h)	S_{BET} (m^2/g)	V_t (cm^3/g)	w_{KJS} (nm)	weight loss (%)	residue (%)	weight % of polymer
FDU-12	-	408	0.97	27.1	-	-	-
FDU-12-BiB	-	182	0.64	26.8	12.65	86.48	-
FDU-12 PMEDSAH - 21%	0.5	15	0.07	25.4	30.29	67.04	20.48
FDU-12 PMEDSAH - 32%	1	0.1	NA	NA	40.13	55.10	32.07
FDU-12 PMEDSAH - 36%	3	NA	NA	NA	43.87	52.55	36.18
FDU-12 PMEDSAH - 37%	4	NA	NA	NA	44.34	51.95	36.74

[a] Notation: t_1 polymerization time; w_{KJS}, pore diameter calculated by using KJS method; S_{BET}, BET specific surface area; V_t, total pore volume; NA was used where the data could not be measured due to the lack of pore accessibility.

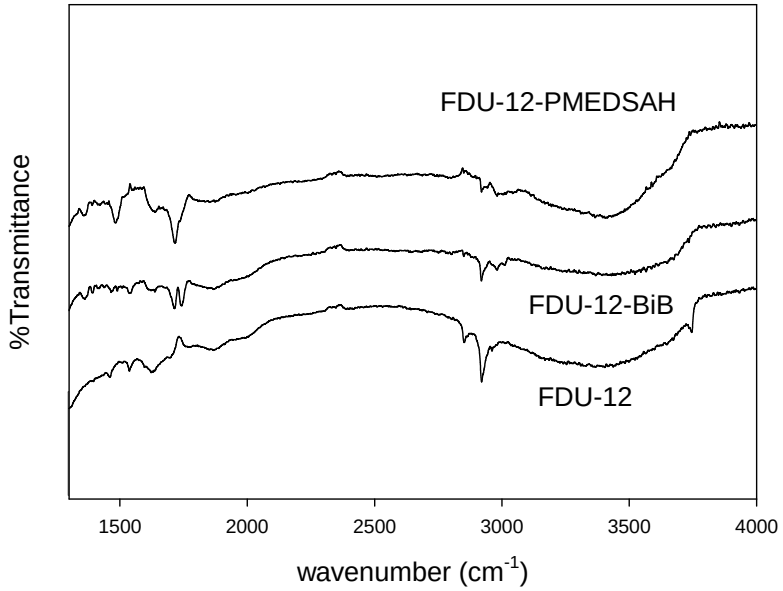

Figure 3.9. FT-IR spectra of FDU-12, FDU-12 modified with 2-bromoisobutyrate group (FDU-12-BiB), and the FDU-12 with 20 wt% of PMEDSAH.

3.1.4. Conclusions

The grafting of $PM(EO)_2MA$ from the concave surfaces of FDU-12 silicas was successful for both SI-ATRP and SI-ARGET ATRP. Without appreciable pore blocking, the loading of $PM(EO)_2MA$ reached 20 wt.% and the corresponding polymer layer thickness was about 1 nm via normal ATRP. The ARGET ATRP with very low amount of copper showed good control over the polymerization and achieved considerable polymer loading within short polymerization time. The SI-ATRP of PMEDSAH was successfully conducted in protic media, 20 wt. % of loading was achieved in 0.5 hour. Higher loadings were also readily achieved.

3.2. Synthesis of ordered mesoporous silica/polymer composites via "grafting to" method

3.2.1 Introduction

The results discussed above confirmed that the "grafting from" method is very effective for the synthesis of polymer brushes on the surface of nanopores, which was also shown in the earlier work.[39,42,76-77] However, the characterization of grafted polymers, such as determining molecular weight and polydispersity, is not convinent or in some cases not successful in the "grafting from" approach. For example, the conventional method to cleave grafted polymers from the silica support is to dissolve the silica by using HF acid, which is hazardous while this method does not work well in the case of cleaving highly hydrophobic polymers.[178] Another disadvantage of the grafting from approach lies in the fact that the grafted polymer may undergo covalent degradation in the process of removal from the silica. The analyzed cleaved product may therefore be different from the polymer that is grown from the silica. The "grafting to" method provides an alternative way to attach preformed polymers with known characteristics to solid supports. Due to the steric hindrance during the grafting, the grafting densities afforded by the "grafting to" approach are usually lower than those from the "grafting from" method. Therefore, developing new "grafting to" strategy by employing highly efficient coupling methods is very attractive to improve the performance of this approach.

The so-called "Click" chemistry is a set of powerful tools for jointing two units together and has been applied widely to the functionalization of flat surfaces,[110,179-186] surfaces of resins,[87,187] silica beads,[87,188] nanoparticles,[99,126-128,189-199] nanorods,[200] nanolayers,[94]

nanotubes,[201-202] and nanofibers[98,203] with molecules and biomolecules. The grafting of polymers to the concave surface is challenging because the attachment of polymers relies on the "point to point" coupling between the chain end and the functional group on the surface. The surface curvature and the low concentration of the chain end contribute to the difficulty during the grafting. Therefore, the orthogonal and highly efficient "click" reactions are very promising for grafting polymers to surfaces of mesopores.

3.2.2. "Click" Grafting to Surfaces of SBA-15 Silicas via Huisgen Cycloaddition Reaction[122]

Ordered mesoporous silicas (OMSs)[4,15,204] are attractive as media for immobilization of biomolecules[58-59] and polymers,[39,60-64,205] and they constitute an excellent model system to study the surface functionalization,[2,65-67] because the changes in the pore diameter, surface area, pore accessibility and surface properties can be readily followed.[39,68] Bein and coworkers[107] used large-pore SBA-15 silica with cylindrical mesopores synthesized using 1,3,5-trimethylbenzene as a micelle expander as a high-surface-area support for the introduction of protein molecules. The silica surface was modified with 3-chloropropylsilyl groups, in which chlorine was subsequently replaced with an azide group through the reaction with sodium azide. Thus prepared "clickable" porous silica was reacted with a protein functionalized with a propargyl group. A moderate loading of protein (~12 wt.%) was achieved and the protein exhibited an appreciable enzymatic activity. Another approach for the synthesis of "clickable" high-surface-area ordered mesoporous silica is to introduce the azide functionality through a co-condensation of azidopropyltrialkoxysilane with tetraethoxysilane (TEOS) in the presence of a surfactant template.[108,112] This synthesis affords the silica framework with azidopropyl groups attached through Si-C bonds and can

render a high loading of azide groups, which become readily accessibly to further functionalization after the extraction of the surfactant template. The Huisgen cycloaddition of several small molecules and biomolecules (monosaccharides) has been successfully achieved in thus obtained nanopores. Moreover, the saccharides on the external surface of the particles of the material were used to anchor Concanavalin-A protein. While the co-condensation approach to "clickable" OMSs is convenient, it restricts opportunities for the pore size and pore structure symmetry adjustment, unlike in the case of post-functionalization of pure-silica materials, the latter being available in a wide range of pore diameters and structure types. Indeed, the two reported co-condensation approaches both afforded azide-functionalized cylindrical pores of diameter ~6 nm.

Herein, an alternative approach to the synthesis of "clickable" high-surface-area OMS supports is proposed (see Scheme 5). It includes the post-synthesis modification of the silica surface leading to the introduction of propargyl groups. Unlike in the case of an earlier work,[107] this preparation does not involve basic compounds (i.e., NaN_3), which may potentially degrade the silica framework.[205] Consequently, the silica support remains intact throughout the functionalization process. The post-synthesis functionalization approach allowed us to select highly ordered large-pore SBA-15 silica as a support with very uniform cylindrical mesopores that can accommodate high loadings and appreciable thicknesses of layers of surface-bound groups without the pore blocking. It is demonstrated for the first time that the Huisgen cycloaddition can serve as a highly efficient method to attach polymers to the surface of ordered nanopores in the "grafting to" approach. Moreover, oligomers and monosaccharides can be immobilized in the nanopores with high loadings. In all these cases, functionalized, accessible nanopores were obtained, opening a

wide range of opportunities in the application of the high-surface-area materials synthesized through a proposed synthesis approach.

3.2.2.1. Experimental section

3.2.2.1.1. Materials

Pluronic P123 poly(ethylene oxide)-poly(propylene oxide)-poly(ethylene oxide) triblock copolymer $EO_{20}PO_{70}EO_{20}$ was provided by BASF as a free sample. TEOS was purchased from Aldrich. 3-aminopropyltriethoxysilane was acquired from Gelest. 4-pentynoyl chloride was synthesized by reacting 4-pentynoic acid with oxalyl chloride in methylene chloride, and isolated through evaporation of the solvent. D-galactose 1-[2-(2-azidoethoxy) ethoxyethyl]-2,3,4,6-tetra-O-acetate (protected D-galactose) was purchased from TCI. 1-[2-(2-azidoethoxy) ethoxyethyl] D-galactose (deprotected D-galactose) was prepared[182] by deprotecting D-galactose 1-[2-(2-azidoethoxy)ethoxyethyl]-2,3,4,6-tetra-O-acetate. Sodium ascorbate and copper (II) sulfate pentahydrate were purchased from Aldrich. 2-(2-(2-azidoethoxy)ethoxy)ethanol (later referred to as azido-oligo(ethylene glycol), OEG) was synthesized as originally reported elsewhere[206]. Azido-functionalized poly(methyl methacrylate) (PMMA) was synthesized via atom transfer radical polymerization (ATRP).[72] A procedure for a lower-molecular-weight PMMA (denoted PMMA-LMW) using an azide functionalized initiator[207] was as follows. A mixture of methyl methacrylate (1.07 mL, 10 mmol), anisole (2 mL), 2-(2-(2-azidoethoxy)ethoxy)ethyl 2-bromo-2-methylpropanoate (85 mg, 0.25 mmol; synthesized as reported elsewhere[206]) and PMDETA (21 μl, 0.1 mmol) in a 10 mL Schlenk tube was degassed by 3 freeze-pump- thaw cycles, and CuBr (14.3 mg, 0.1 mmol) was added to the frozen mixture under nitrogen flow. Then

the tube was closed, evacuated, and back-filled with nitrogen, and the reaction mixture was heated to 60 °C. After 4.5 h, the flask was removed from oil bath and opened. The resulting solution was diluted with THF, passed through a neutral alumina column to remove the catalyst, and precipitated into cold methanol to give PMMA. Number-average molecular weight, M_n, was 4008 g/mol, and polydispersity index (PDI) was 1.18.

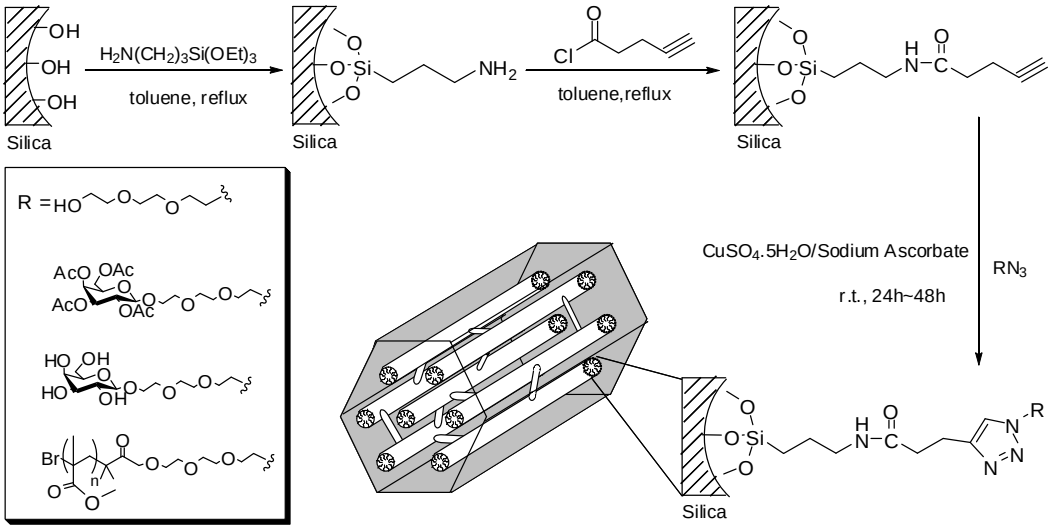

Scheme 5. "Click" grafting on the surface of ordered mesoporous silica via Huisgen cycloaddition reaction.[119]

3.2.2.1.2. Synthetic procedures

Synthesis of Large-pore SBA-15. Large-pore SBA-15 silica was synthesized as reported elsewhere.[52] Briefly, 2.4 g of P123 ($EO_{20}PO_{70}EO_{20}$) and 0.027 g of NH_4F were dissolved in 84.0 mL of 1.3 M HCl aqueous solution in a polypropylene (PP) bottle at room temperature. After all of the surfactant dissolved, the reaction container was moved to a water bath (nominal temperature accuracy of 0.01 °C) set at 17.00 °C. 5 hours later, a mixture of 5.5 mL tetraethyl orthosilicate (TEOS) and 1.5 g of 1,3,5-triisopropylbenzene (TIPB) was added to the solution. The molar composition of the synthesis mixture was

TEOS : P123 : TIPB : NH_4F : HCl : H_2O = 1 : 0.0168 : 0.297 : 0.0295 : 4.42 : 186. The synthesis mixture was stirred for 24 hours at 17 °C in the open PP bottle using a mechanical stirrer. The synthesis mixture was then heated in a closed container in an oven at 100 °C for 2 days. The resulting as-synthesized material was isolated by filtering and drying in a vacuum oven. Finally, the sample was calcined under air at 550 °C for 5 hours (heating ramp 2 °C min^{-1}).

"Click" Attachment to Surface of SBA-15. 0.2 g of calcined LP-SBA-15 was reacted with 1 mL 3-aminopropyltriethoxysilane in 10 mL of dry toluene under reflux for 24 hours.[68] The resulting white solid was filtered off, washed with toluene, ethanol and water, and dried under vacuum to isolate amino-functionalized SBA-15 (denoted as SBA-15-NH_2). Then 0.11 g (0.94 mmol) of 4-pentynoyl chloride was reacted with 0.35 g (0.56 mmol) of SBA-15-NH_2 in 20 mL dry toluene under the protection of N_2. After 24 hours of refluxing at 110 ^oC, the product was filtered and washed with toluene, ethanol and water, and then dried under vacuum. Then the product was reacted at room temperature for 24 hours with azido-saccharides, azido-oligo(ethylene glycol) or azido-poly(methyl methacrylate) in the presence of copper(I) catalyst (added as $CuSO_4 \cdot 5H_2O$) and L(+)-sodium ascorbate. Conditions used for click reactions are listed in Table 3.4. Afterward, the products were washed thoroughly with THF, methanol and water to remove the unreacted azide-functionalized molecules and the catalyst. Then the products were dried at 60 °C under vacuum.

Table 3.4. Conditions used in the "click" attachment of azide-functionalized compounds to the surface of SBA-15 silica.[a] [119]

SBA-15 support, grafted organic groups	Silica (mmol of propargyl groups)	Azide		Reaction time (d)
		Compound	Amount (mmol)	
SBA-15-PMMA-LMW[b]	0.0329	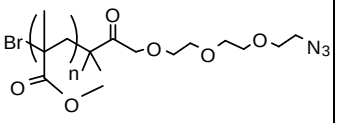	0.0382	2
SBA-15-PMMA-HMW[b]	0.0329	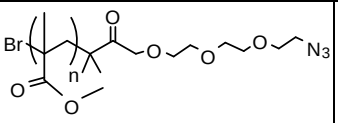	0.0093	2
SBA-15-GA-1[c]	0.0392	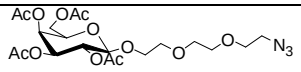	1.01	1
SBA-15-GA-2[c]	0.0392	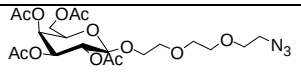	0.0989	1
SBA-15-GA-3[c]	0.0392	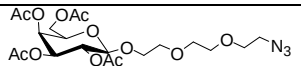	0.0396	1
SBA-15-DGA[d]	0.0392	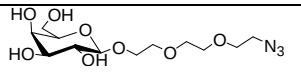	0.0297	1
SBA-15-OEG[c]	0.0392	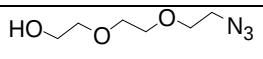	1.00	1

[a] Note: PMMA-LMW: poly(methyl methacrylate), M_n = 4008 g/mol, polydispersity index (PDI) = 1.18; PMMA-HMW: M_n = 8850 g/mol, PDI = 1.22; The reaction time for the "click" grafting of polymers was 48 hours, and for other azide molecules were 24 hours. GA: D-galactose 1-[2-(2-azidoethoxy)ethoxyethyl]-2,3,4,6-tetra-O-acetate; DGA: 1-[2-(2-azidoethoxy)ethoxyethyl] D-galactose; OEG: oligomeric ethylene glycol. The solvent used in the click reaction: [b] anisole/H_2O (9/1 v/v); [c] CH_3OH/H_2O (9/1 v/v); [c] CH_3CN/H_2O (9/1 v/v).

3.2.2.1.2. Measurements

See 3.1.2.3

3.2.2.1.3. Calculations

See 3.1.2.4

3.2.2.2. Results and discussion[119]

"Click" grafting of polymers. SAXS pattern of the SBA-15 silica (Figure 3.10) was characteristic of a highly ordered 2-D hexagonal structure. The unit-cell parameter, which in the case of SBA-15, corresponds to the distance between the centers of adjacent cylindrical pores, was 16.5 nm, as calculated from the (100) interplanar spacing determined by SAXS. Shown in Figure 3.11 are weight change patterns for SBA-15 after modification with aminopropyl groups, attachment of propargyl functional groups through a reaction of amino groups with 4-pentynoyl chloride, and "click" grafting of PMMA of molecular weight ~4000 g/mol (see Scheme 5). The polymer grafting was performed in the anisole/water mixture (volume ratio 9/1). The introduction of the organic groups on the silica surface resulted in a significant weight loss primarily in the temperature range from 200 to 600 °C, whereas the unmodified silica support (data not shown) exhibited a weight loss below 1 %. The attachment of PMMA caused a particularly large increase in the weight loss, corresponding to 25 wt.% of the polymer in the grafted SBA-15 (see Table 3.5).

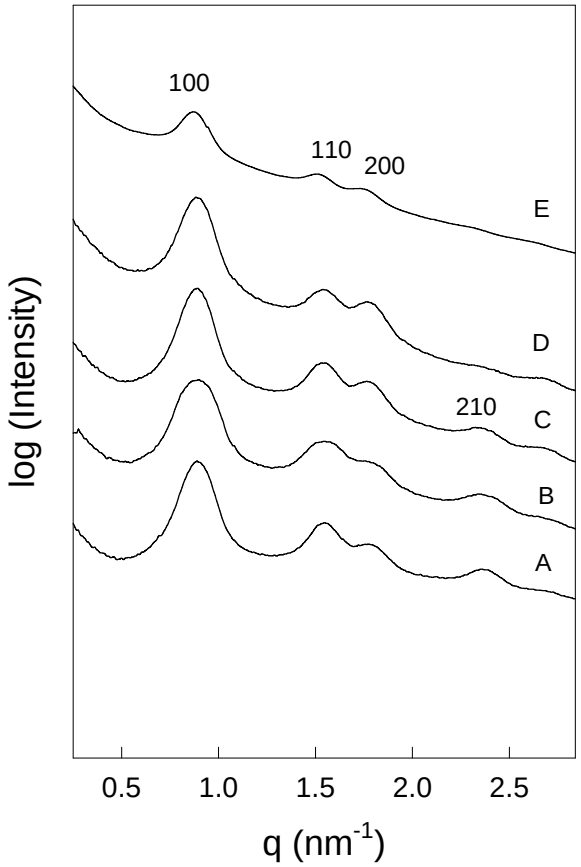

Figure 3.10. SAXS patterns for: (A) SBA-15 and (B) SBA-15-NH_2, (C) (-$NHCOC_4H_5$), (D)(-PMMA-HMW) and (E) (-PMMA-LMW).[119]

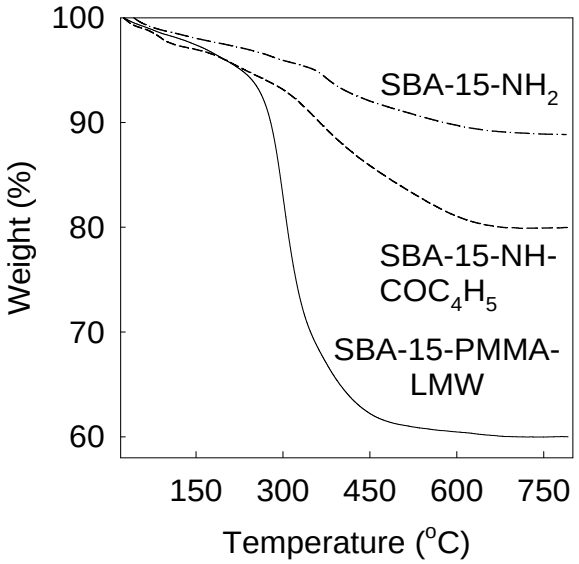

Figure 3.11. Weight change patterns recorded under air for unmodified SBA-15, and SBA-15 modified with aminopropyl groups (-NH_2), propargyl groups (-$NHCOC_4H_5$) and poly(methyl methacrylate) (-PMMA-LMW).[119]

Nitrogen adsorption isotherms (Figure 3.12 (top)) showed that all of the considered samples exhibited accessible mesopores with narrow size distribution, as inferred from the occurrence of steep capillary condensation steps on the isotherms. Pore size distributions (PSDs, Figure 3.12 (bottom)) calculated for the isotherms were narrow in all cases, and the position of the peak on PSD shifted to lower pore diameter values as the surface was functionalized first with aminopropyl groups, then with propargyl groups and finally with the polymer (see Table 3.6). The retention of narrow PSD after the attachment of PMMA at 25 wt.% loading is particularly noteworthy and indicative of the presence of a uniform polymer layer across the surface of the material. The thickness of the polymer film was about 2 nm, as estimated from the decrease in the pore radius after the "click" grafting. After the attachment of the polymer, the hysteresis loop on the nitrogen adsorption

isotherm broadened to some extent, but the capillary evaporation took place primarily above the lower limit of adsorption-desorption hysteresis[149] (relative pressure of 0.4-0.5). This behavior indicates that the polymer grafting introduced some constrictions in the pore structure, but their diameter was predominantly above 5 nm.[39,149] The specific surface area of the SBA-15/PMMA composite was ~70 m^2/g, whereas the pore volume was ~0.2 $cm^3 g^{-1}$. The loading of the polymer and the polymer layer thickness are comparable to the best reported results achieved using the "grafting from" method of functionalization of OMSs with polymers using controlled radical polymerization in 10-15 nm mesopores.[39,74-75] In the latter cases, the polymer loading up to 29 wt.% and the polymer layer thicknesses up to ~2 nm were achieved without making the pores inaccessible to nitrogen at -196 °C (higher loadings were also achieved,[39,42] but in these cases, the pores were not accessible to nitrogen). Similar or even higher loadings of the polymer on the silica support can be achieved for cross-linked polymer layers,[209] but in this case, a part of the polymer network is located in micropores and the thickness of the polymer layer on the surface of mesopores is on the order of 1 nm or less. The surface density of PMMA can be estimated to be 0.120 chains per nm^2. This grafting density was close to that achieved for PAN grafted via surface-initiated polymerization in ~10 -15 nm mesopores[39,210] Clearly, the "click" "grafting to" procedure provides an appreciable surface coverage of polymer chains.

Table 3.5. Thermogravimetric weight losses for surface-modified SBA-15 samples. [119]

Sample	Weight loss (%)	Residue (%)	Weight % of groups	Amount of groups (mmol per gram of silica)
SBA-15-NH_2 [a]	9.84	88.83	9.2 -$(CH_2)_3NH_2$	1.79
SBA-15-$NHCOC_4H_5$ [a]	17.75	79.96	8.9 -COC_4H_5	1.37
SBA-15-PMMA-LMW [a]	38.30	59.92	25.0 PMMA	0.10
SBA-15-PMMA-HMW [a]	33.01	65.84	18.4 PMMA	0.03
SBA-15-NH_2 [b]	9.83	88.27	9.2 -$(CH_2)_3NH_2$	1.80
SBA-15-$NHCOC_4H_5$ [b]	15.56	82.58	6.4 -COC_4H_5	0.95
SBA-15-GA-1 [b]	32.85	66.12	20.4 GA	0.61
SBA-15-GA-2 [b]	30.99	67.91	18.2 GA	0.53
SBA-15-GA-3 [b]	29.82	68.13	17.0 GA	0.49
SBA-15-DGA [b]	28.26	63.92	16.2 DGA	0.75
SBA-15-OEG [b]	24.54	71.56	11.1 OEG	0.88

[a,b] Samples were prepared using two different batches of SBA-15 silica denoted by letters “a” and “b”.

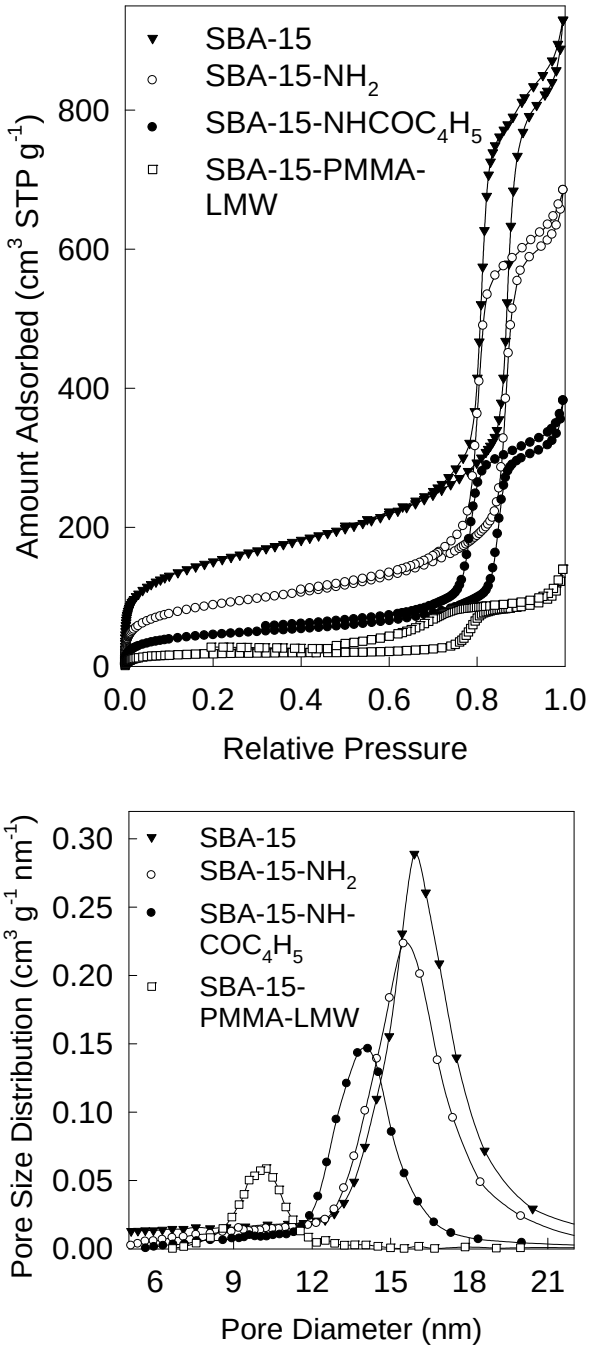

Figure 3.12. Nitrogen adsorption isotherms (top) and pore size distributions (bottom) for unmodified SBA-15 and SBA-15 modified with aminopropyl groups (-NH_2), propargyl groups (-$NHCOC_4H_5$) and poly(methyl methacrylate) (-PMMA-LMW).[119]

Table 3.6. Structural parameters of samples determined by nitrogen adsorption [119]

Sample	BET surface area (m^2 g^{-1})	Total pore volume (cm^3 g^{-1})	BJH pore diameter (nm)
SBA-15 [a]	524	1.37	15.9
SBA-15-NH_2 [a]	321	1.02	15.5
SBA-15-NH_2-CO-C_4H_5 [a]	158	0.55	13.9
SBA-15-PMMA-LMW [a]	66	0.19	10.2
SBA-15-PMMA-HMW [a]	147	0.45	12.4
SBA-15 [b]	653	1.68	15.4
SBA-15-NH_2 [b]	422	1.17	14.4
SBA-15-NH_2-CO-C_4H_5 [b]	284	0.86	13.6
SBA-15-GA-1 [b]	103	0.30	10.9
SBA-15-GA-2 [b]	111	0.32	11.2
SBA-15-GA-3 [b]	105	0.31	11.3
SBA-15-DGA [b]	178	0.56	12.2
SBA-15-OEG [b]	178	0.65	13.0

[a,b] Samples were prepared using two different batches of SBA-15 silica denoted by letters “a” and “b”.

Similar results were obtained for a higher-molecular-weight PMMA, but the loading of the polymer was somewhat lower (~18 wt.%) and the thickness of the polymer film was about 0.8 nm (Figure 3.13). The lower loading might have been due to more significant steric hindrance for attachment of larger macromolecules. FTIR spectra (Figure 3.14, a, b, c and g) for the PMMA-grafted samples and their precursors provided additional insight into

the "click" functionalization of SBA-15 surface with PMMA. In spectra g and h, the band centered at 1450 cm^{-1} can be attributed to C=N vibrations, which indicates the formation of 1,2,3-triazole after the "click" reaction. Moreover, the peak around 1720 cm^{-1} is assigned to the carbonyl groups in PMMA.

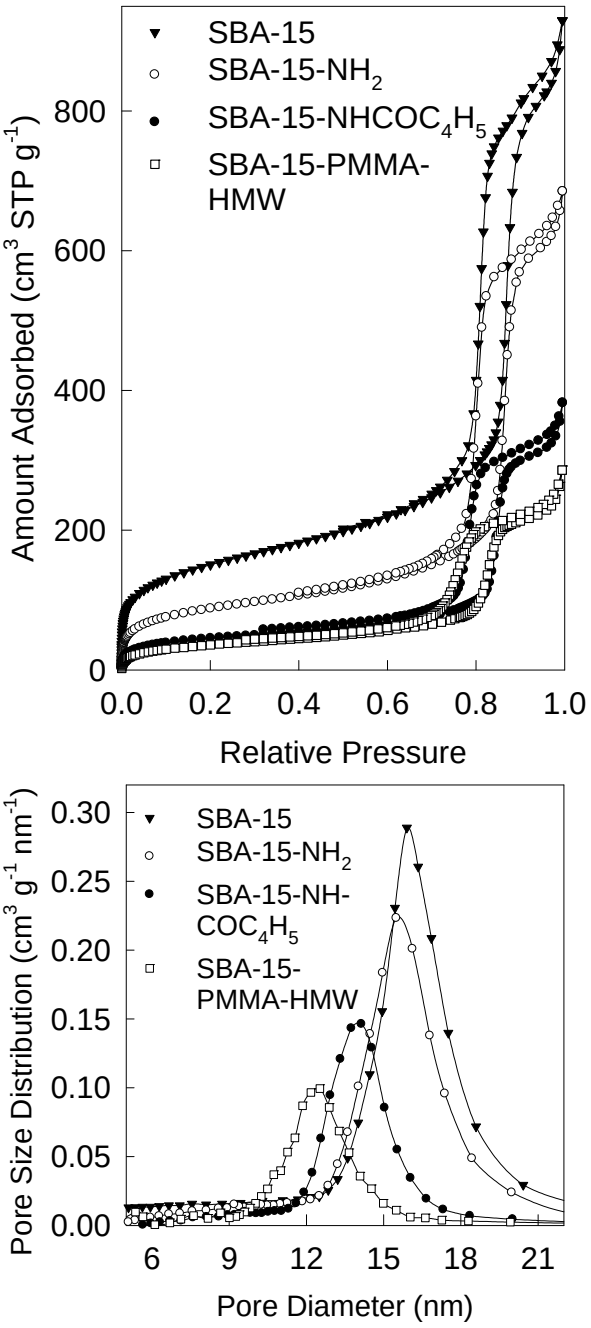

Figure 3.13. (top) Nitrogen adsorption isotherms and (bottom) pore size distributions for unmodified SBA-15 and SBA-15 modified with aminopropyl groups ($-NH_2$), propargyl groups ($-NHCOC_4H_5$) and poly(methyl methacrylate) (-PMMA-HMW).[119]

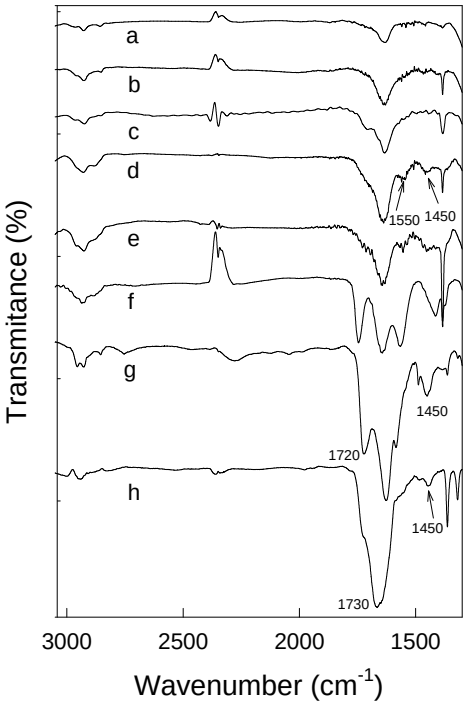

Figure 3.14. FT-IR spectra of **a**: SBA-15; **b**: SBA-15-NH_2; **c**: SBA-15-NH-CO-C_4H_5; **d**: SBA-15-OEG; **e**: SBA-15-DGA; **f**: SBA-15-GA; **g**: SBA-15-PMMA-LMW; **h**: SBA-15-PMMA-HMW.[119]

An oligomeric ethylene glycol (OEG) was also successfully attached to the surface of SBA-15. FTIR spectrum of the resulting material (Figure 3.14, spectrum d) featured bands centered at 1550 and 1450 cm^{-1} that can be attributed to C=C and C=N vibration bands, which indicate the formation of 1,2,3-triazole after the "click" reaction. The loading of OEG was ~12 wt.%, as determined from TGA (Figure 3.11). The "click" attachment of OEG resulted in the decrease in the adsorption capacity, but the hysteresis loop on the nitrogen adsorption isotherm remained narrow, suggesting that the attachment did not lead to an introduction of any constrictions in the pore structure of the material. PSD shifted to lower pore diameter values, but remained narrow. Thus, the "click" "grafting to" method

for the synthesis of polymer brushes on the nanopore surface allows one to introduce moderate to high loadings of well-defined oligomers and polymers covalently attached to the silica surface. Therefore, the present "grafting to" method for the covalent attachment of polymers to the surface of nanoporous materials is an attractive alternative of the "grafting from" approach, that is, surface-initiated polymerization,[39,62,74-77,210] allowing one to synthesize a polymer in solution or bulk and thoroughly characterize it prior to the surface attachment. On the other hand, the surface-initiated polymerization allows one to control the polymer loading and molecular weight through the adjustment of synthesis parameters,[39,76-77] while the characterization of the molecular weight and polydispersity of the grafted polymer is quite inconvenient.

"Click" grafting of monosaccharides. The "click" functionalization of the large-pore SBA-15 support with monosaccharides was also studied. In particular, a protected D-galactose azide was reacted with propargyl groups on the silica surface to obtain monosaccharide-functionalized high-surface-area material. As inferred from TGA data (Figure 3.15), the loading of 20 wt.% (see Table 3.5) was achieved with a twenty-five-fold excess of the sugar azide with respect to propargyl groups. The loading decreased only slightly (to 17-18 wt.%; see Table 3.5) when a 2.5 fold excess and stoichiometric amount of the azide were used. With one equivalent of D-galactose azide used, 52 % of alkyne groups on the silica surface participated in the triazole-forming reaction. With 2.5 and twenty-five-fold excess of galactose, 56 and 64 % of alkyne groups reacted. Nitrogen adsorption isotherms (Figure 3.16) and pore size distributions (Figure 3.17) showed a similar decrease in adsorption capacity and pore diameter for monosaccharide-functionalized samples synthesized with different relative amounts of the azide. Clearly, a

high loading was achievable even with a stoichiometric amount of the azide with respect to the propargyl groups on the surface. While the loading corresponds to 52-64 % of propargyl groups reacted, and thus there was no quantitative conversion, it needs to be realized that the protected D-galactose is a quite bulky group, so the steric hindrance is likely to limit the loading on the concave surface of the pores of SBA-15. The thickness of the monosaccharide layer on the pore surface was about 1 nm. Deprotected D-galactose was also attached to the surface of SBA-15 via "click" chemistry with the loading of 16.2 wt.% (see TGA data in Figure 3.15), which corresponds to 0.69 molecule/nm^2. An actual coverage of the surface of mesopores is likely to be even higher, because micropores in SBA-15 framework that provide appreciable contribution to the specific surface area[18] are likely to exhibit a lower surface coverage.

It should be noted that others attached monosacharides to the surface of "clickable" SBA-15 with pores of diameter ~ 5 nm, achieving moderate to high loadings.[112] However, no information about the pore accessibility after the "click" functionalization was reported.

In the case of deprotected D-galactose, 0.76 equivalent of deprotected galactose was used and yet 79 % of alkyne groups were converted, which is slightly above 100% efficiency. Perhaps the weighing error for the amount (10 mg) of DGA azide used or inaccuracy in weight loss readings contributed to this result, which should be considered as an indication of quantitative (or nearly quantitative) surface attachment, which is in line with the "click" mannose attachment in the pores of small-unit-cell SBA-15 that proceeded with 55-79 % efficiency.[112] The deprotected D-galactose showed higher grafting efficiency than the protected D-galactose, which is likely to be due to a smaller molecular size and thus a lower steric hindrance for the attachment at high surface density. Nitrogen

adsorption data (Figures 3.16 and 3.17) showed a decrease in adsorption capacity and decrease in pore diameter after the D-galactose attachment, but the resulting sugar-functionalized material still had a significant pore volume (above 0.5 cm^3 g^{-1}) and large pore diameter (~12 nm). With a proper selection of sugar moiety, such large-pore sugar-functionalized materials would accommodate large molecules, including proteins, and thus would offer advantages in protein binding over previously reported mannose-functionalized SBA-15 of smaller unit-cell parameter.[112]

For monosaccharide-functionalized materials, FTIR spectra (Figure 3.14) featured bands centered at 1550 and 1450 cm^{-1} (spectrum (e)) and 1565 and 1415 cm^{-1} (spectrum (f)) that can be attributed to the C=C and C=N vibration bands, which indicate the formation of 1,2,3-triazole after the "click" reaction. In spectrum (f), the strong peak at 1750 cm^{-1} is the vibration of acetate groups which indicates the successful grafting of D-galactose 1-[2-(2-azidoethoxy)ethoxyethyl]-2,3,4,6-tetra-O-acetate. As seen in Figure 3.10, SAXS patterns did not change to any appreciable extent throughout the grafting process, as expected from the fact that the chemistry used is not likely to modify the silica framework.

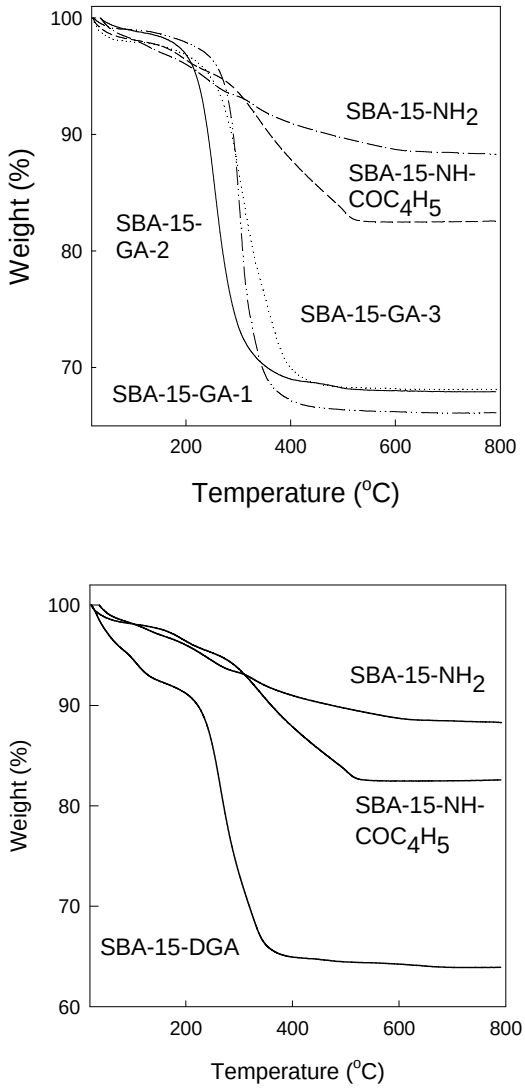

Figure 3.15. Weight change patterns recorded under air for SBA-15 modified with aminopropyl groups ($-NH_2$), propargyl groups ($-NHCOC_4H_5$), protected galactose (-GA-1, -2, -3) and deprotected galactose (-DGA).[119]

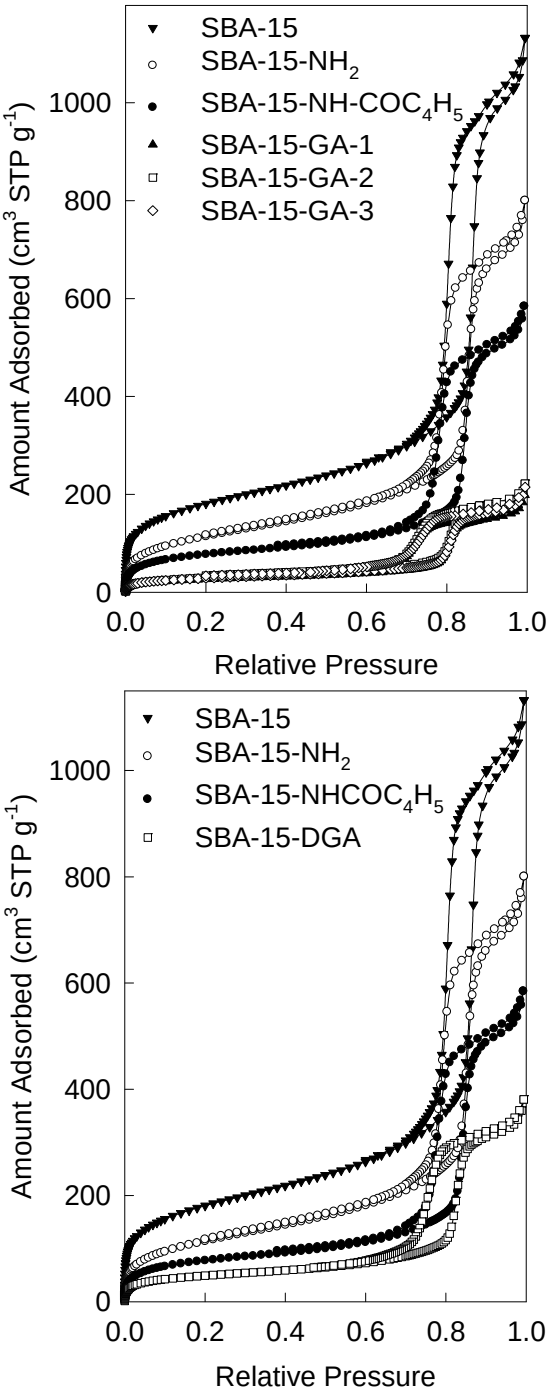

Figure 3.16. Nitrogen adsorption isotherms for unmodified SBA-15, and SBA-15 modified with aminopropyl groups (-NH_2), propargyl groups (-$NHCOC_4H_5$), protected galactose (-GA-1, -2, -3) and deprotected galactose (-DGA).[119]

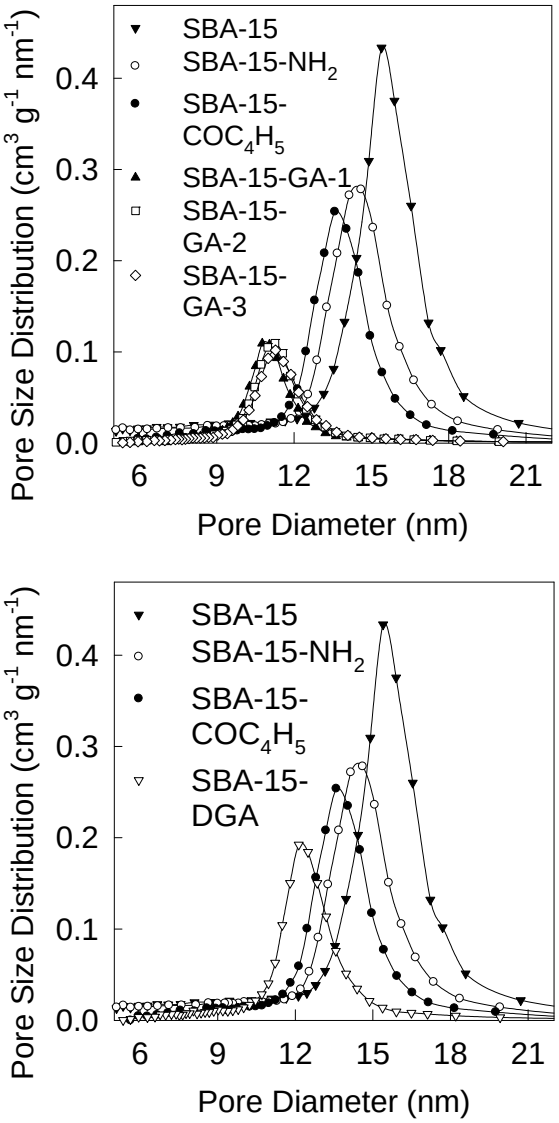

Figure 3.17. Pore size distributions for unmodified SBA-15, and SBA-15 modified with aminopropyl groups (-NH_2), propargyl groups (-$NHCOC_4H_5$), protected galactose (-GA-1, -2, -3) and deprotected galactose (-DGA).[119]

3.2.2.3. Conclusions[119]

The Huisgen cycloaddition reaction was found to be a powerful method for the functionalization of the surface of porous silicas without compromising the accessibility of the pores. A significant loading (17 wt.%) of surface-bound monosaccharide was achieved

even when stoichiometric amounts of the azide-functionalized monosaccharide were used. Moreover, the use of the "click" reaction allowed us to introduce oligomers and polymers on the pore surface via the "grafting to" approach. Moderate to high loadings of polymer (up to 25 wt.%) were introduced without the pore blocking and the polymer layer thickness up to about 2 nm has been achieved. In all cases, the surface modification proceeded uniformly on the surface of the high-surface-area silica support resulting in a material with narrow pore size distribution. These beneficial properties make the "grafting to" strategy based on the Huisgen cycloaddition an attractive alternative to the "grafting from" pathway to polymer-grafted surfaces.

.

3.2.3. "Click" Grafting to Surfaces of SBA-15 Silicas via Thiol-ene Reaction

Although the thiol-ene reaction has been discovered over one hundred years ago[122], and has been widely used in synthesis of polymers and materials, its "click" characteristics was popularized recently.[123] Compared to the well-known Huisgen cycloaddition "click" reaction, thiol-ene reaction stands out because of its "metal-free" property, which offers advantage for the applications in the biomedical area. For high-surface-area OMSs materials, which tend to adsorb copper ions and thus the residue of copper catalyst used in Huisgen cycloaddition may contaminate the final composites, it is desirable to develop thiol-ene "click" grafting approach in the nanopores. Currently only one study has reported the attachment of molecules on OMSs via thiol-ene reaction.[120] Sen Gupta and co-workers reported functionalization of SBA-15 silicas using thiol-ene "click" reaction via nucleophile-mediated pathway. Their results were considered as the first thiol-ene "click" reaction on OMSs materials. A variety of thiol containing molecules were attached to the methacrylate-functionalized SBA-15, including small thiols, ferrocene-containing thiol and disulfide-containing substances (cystine and biotin-labeled cystine). In the presence of tris-2-carboxyethylphosphine, the disulfide bonds were cleaved, which was followed by thiol-ene reaction between the produced thiol and the vinyl groups on surfaces. The electrochemical properties and the affinity binding of proteins of the ferrocene or biotin- functionalized SBA-15 were tested, although insufficient information of structural parameters of these two hybrid materials was provided and the distribution and accessibility of pores after grafting was not elucidated.

In our study, ultra-large-pore SBA-15 with cylindrical pores and ordered 2-D hexagonal structure was used as the solid support, which was able to accommodate macromolecules. The funcionalization of SBA-15 silica is shown in Scheme 6. First, the "clickable" SBA-15 was prepared by reacting with the commercially available chlorodimethylvinylsilane. Then 1-hexanethiol and thiol-functionalized polystyrene were grafted to the "clickable" SBA-15 by adding azobisisobutyronitrile (AIBN) as the radical source. Our results demonstrated thiol-ene "click" reaction as another viable "grafting to" approach for attaching macromolecules in nanopores.

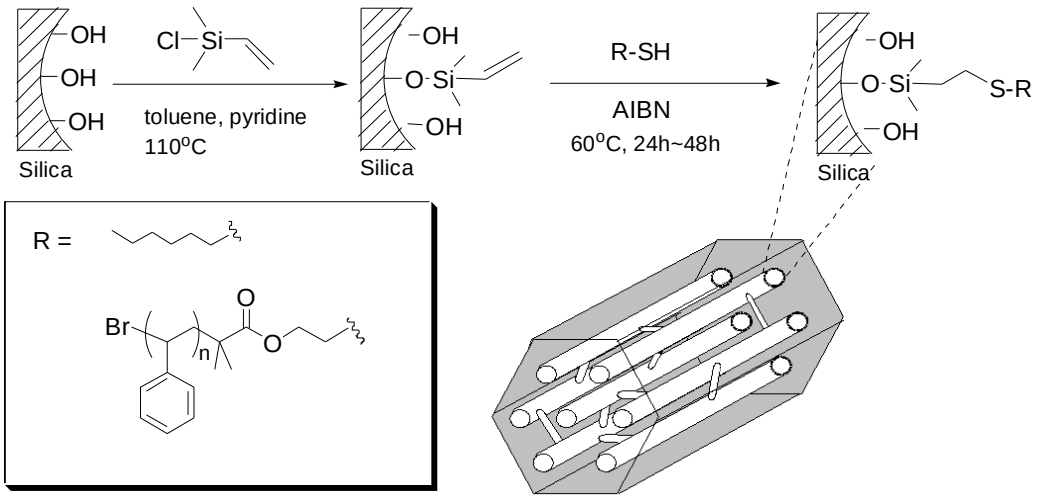

Scheme 6. Grafting on the surface of ordered mesoporous silica via thiol-ene "click" reaction.

3.2.3.1. Experimental section

3.2.3.1.1. Materials

1-hexanethiol, 1,3,5-triisopropylbenzene (TIPB) and styrene were purchased from Acros. Styrene was purified by passing through a basic alumina column to remove the inhibitor. Chlorodimethylvinylsilane was acquired from Gelest. Tributylphosphine was purchased from TCI. Bis(2-[2'-bromoisobutyryloxy]ethyl)disulfide was purchased from ATRP Solutions Inc.

3.2.3.1.2. Synthetic procedures

Synthesis of ultra-large-pore SBA-15. SBA-15 silicas were synthesized using the reported method[52] (with some modification following Ph.D. Dissertation of Liang Cao)[80] by using Pluronic P123 as a template and 1,3,5-triisopropylbenzene (TIPB) as a micelle expander. 2.4 g P123 and 0.027 g NH_4F were dissolved in 84.0 mL of 1.30 M aqueous HCl solution at room temperature. Then the solution was transferred to a water bath at a temperature 12.5 ^oC and after one hour, a mixture of 5.5 mL TEOS and 3.6 mL (3.0 g) TIPB was added. The solution was stirred for 24 hours at 12.5 ^oC in an open container using a mechanical stirrer. Then the solution was transferred to a Teflon-lined autoclave and heated at 130 °C for 1 day. As-synthesized material was filtered and dried at ~60 ^oC in a vacuum oven. Finally, the sample was calcined under air at 550 °C for 5 hours (heating ramp 2 °C/min).

Synthesis of vinyl-functionalized SBA-15 (SBA-15-Vinyl) SBA-15 (0.50 g), chloro(dimethyl)vinylsilane (0.3 mL) and pyridine (1 mL) were added to 10 mL dry toluene in a round bottom flask. The solution was refluxed with stirring for 24 hours.

Then the powder was filtered, washed thoroughly with toluene, ethanol and water and dried at 60^{o}C under vacuum.

Synthesis of disulfide-containing polystyrene (PS-SS-PS). Disulfide-containing PS was synthesized via ARGET ATRP. A procedure for a lower-molecular-weight PS-SS-PS was as follows. A mixture of styrene (5.04 mL, 44.0 mmol), anisol (4.5 mL), bis(2-[2'-bromoisobutyryloxy]ethyl)disulfide (46.1 mg, 0.10 mmol), $CuCl_2$ (0.27 mg, 0.0020 mmol) and Me_6TREN (4.7 mg, 0.020 mmol) was placed in a 25 mL Schlenk tube. The Schlenk flask was degassed by 3 freeze-pump-thaw cycles, and $Sn(EH)_2$ (2.9 mg, 0.020 mmol) in 0.5 mL anisole was added to the frozen mixture under nitrogen flow. Then the tube was closed, evacuated, and back-filled with nitrogen, and the reaction mixture was heated to 110 °C. After 1 h, the flask was removed from oil bath and opened. The resulting solution was diluted with THF, passed through a neutral alumina column to remove the catalyst, and precipitated into cold methanol to give PSt-SS-PSt. Number-average molecular weight, M_n, was 5343 g/mol, and polydispersity index (PDI) was 1.13.

Cleavage of disulfide bond in PS-SS-PS. The disulfide bond was then cleaved by using tributylphosphine to produce the thiol-containing PS (HS-PS).[211] 0.4 g PS-SS-PS was dissolved in 6 mL THF and 0.05 mL Bu_3P was added. The solution was stirred at room temperature for 2 hours. The HS-PS was recovered by precipitating in methanol.

Thiol-ene "click" grafting to SBA-15-Vinyl. The SBA-15-Vinyl was reacted at 60 °C for 24 to 48 hours with 1-hexanethiol or HS-PS in the presence of AIBN. Conditions used for click reactions are listed in Table 3.7. Afterwards, the products were washed

thoroughly with toluene, ethanol and water to remove the unreacted thiol molecules and the radical initiator. Then, the products were dried at 60 °C under vacuum.

Table 3.7. Conditions used in the "click" attachment of thiol-containing molecules to the surface of SBA-15 silica.

Sample	SBA-15-Vinyl	Thiol			Solvent
	mmol of vinyl groups	Compound	Mass		
			(mg)	mmol	
SBA-15-HEXT	0.0575	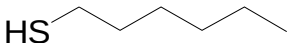	43.0	0.364	Anisole
SBA-15-PS-1	0.0575	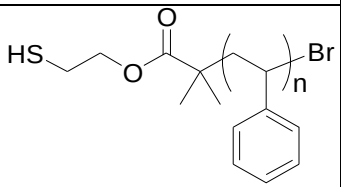	233	0.0162	Anisole
SBA-15-PS-2	0.0575	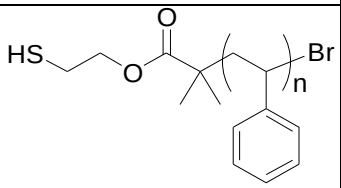	120	0.0479	Anisole

Note: HS-PS-1, Mn = 14419 g/mol, PDI = 1.16; HS-PS-2, Mn = 2507 g/mol, PDI = 1.38.

3.2.3.1.2. Measurements.

See 3.1.2.3

3.2.3.1.3. Calculations.

See 3.1.2.4.

3.2.3.2. Results and discussion

Synthesis and characterization of SBA-15-Vinyl. The successful functionalization of SBA-15 with vinyl groups was first confirmed by the TGA results (Figure 3.18). After the reaction with chloro(dimethyl)vinylsilane, the weight loss was 3.82 wt%. Considering the removal of every vinyl group accompanying with two methyl groups, is likely to be accompanied by a gain of three bonds with oxygen for the silicon atom and thus the gain of 3/2 oxygen atom. Therefore, 3.82 wt% corresponds to 1.15 mmol of vinyl groups per gram of SBA-15-Vinyl. The loading of vinyl groups was not high because chloro(dimethyl)vinylsilane only has one reactive site and the advantage of using such organosilane is to avoid the multilayer grafting. The N_2 adsorption measurement (Figure 3.19) provided evidence of the decreases in the pore volume, surface areas and pore diameter after the grafting of vinyl groups in the mesopores. Narrow pore size distribution indicating the uniform monolayer of grafted vinyl groups on the surfaces. The FT-IR spectra of SBA-15-Vinyl (Figure 3.20) displayed absorption bands at 3020 and 3059 cm^{-1}, corresponding to the vinylic C-H bond. The band that appeared at 2974 cm^{-1} was assigned to stretching vibrations of C-H bonds in methyl groups of the grafted organosilane.

Thiol-ene "click" grafting of 1-hexanethiol to SBA-15-Vinyl. After the grafting of 1-hexanethiol, the product was denoted as SBA-15-HEXT. TGA result showed a loading of 4.84 wt.% thiol molecules in the product, indicating 36 % of the vinyl groups reacted in the thiol-ene grafting. This conversion is not much lower than the value achieved by grafting cystine to methacrylate-functionalized SBA-15.[120] The grafting density was ~0.65 molecule/nm^2. The peaks for vinylic C-H almost disappeared in the FT-IR spectra

of SBA-15-HEXT (Figure 3.20), indicating the addition of 1-hexanethiol to the alkene groups. The N_2 adsorption isotherm (Figure 3.19) of SBA-15-HEXT showed decreased pore volume and BET specific surface area due to the grafted thiol molecules in the pores. However, the pore diameter shifted slightly to the larger size. While the reason for this behavior is not fully clear, it might be due to the change of the surface property of SBA-15 from weakly hydrophobic to highly hydrophobic after the attachment of 1-hexanthiol molecules. This might lead to the decreased film thickness of the adsorbed N_2 molecules on the surface, possibly leading to a higher capillary condensation pressure corresponding to a larger pore diameter calculated. Consequently, the apparent increase in the pore diameter might be on artifact of the pore size calculation method.

Table 3.8. Thermogravimetric weight losses for surface-modified SBA-15 samples.

Sample	Weight loss (%)	Residue (%)	Weight % of groups	mmol of groups / gram of silica
SBA-15-Vinyl	3.82	95.47	3.82 $-CH_3$, $-C_2H_3$	1.15
SBA-15-HEXT	8.49	91.18	4.84 $-C_6H_{13}SH$	0.41
SBA-15-PS-1	10.62	88.64	7.07 –PS-1	0.005
SBA-15-PS-2	10.56	88.23	7.03 –PS-2	0.028

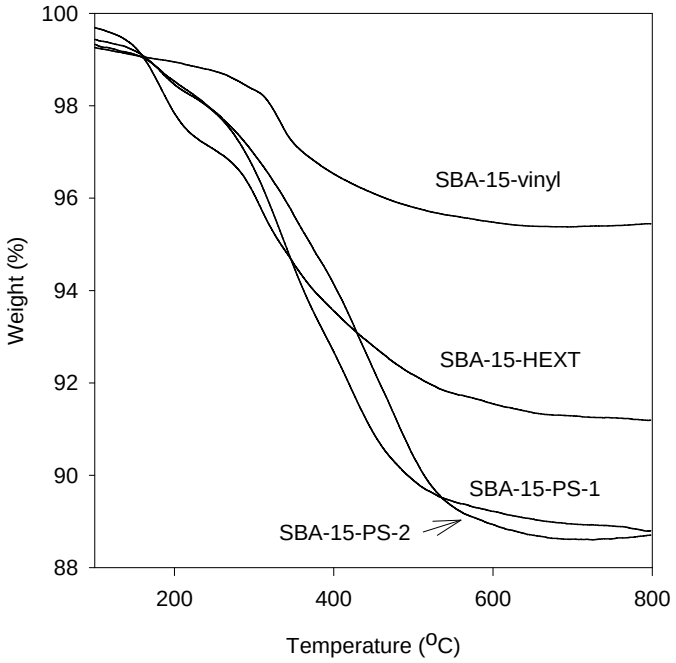

Figure 3.18. Weight change patterns recorded under air for SBA-15 modified with vinyl groups, 1-hexanethiol and thiol-functionalized polystyrene with different molecular weights.

Thiol-ene "click" grafting of thiol-containing polystyrene to SBA-15-Vinyl. High molecular weight and low molecular weight thiol-containing polystyrenes were employed in the thiol-ene "click" grafting. TGA results (Figure 3.18) confirmed the attachment of these polymers to SBA-15. The grafting density of low-molecular-weight PS was 0.045 chains/nm^2. The FT-IR spectra of SBA-15 grafted with low-molecular-weight PS (Figure 3.20, SBA-15-PS-2) clearly showed a new peak at 2000 cm^{-1}, which indicated the aromatic rings from polystyrene.

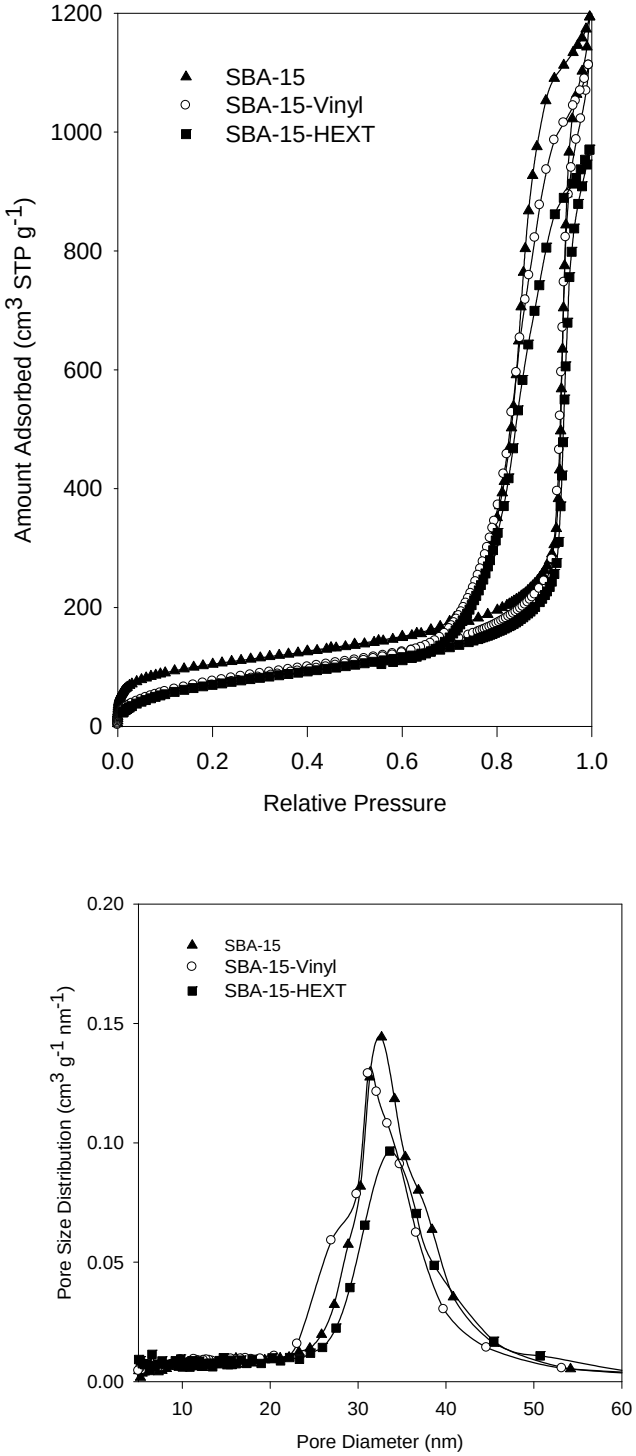

Figure 3. 19. Pore size distributions for unmodified SBA-15, and SBA-15 modified with vinyl groups and 1-hexanethiol.

The grafting of high-molecular-weight PS resulted in a very low grafting density of ~0.008 chains/nm^2. The pore diameter did not change after the grafting, while pore volume and surface areas decreased (Figure 3.21). It is possible that the high-molecular-weight PS attached primarily on the external surfaces of the material and blocked some mesopores. The successful attachment of low-molecular-weight PS can also be confirmed from the N_2 adsorption measurement (Figure 3.22). The pore diameter shifted to a smaller size by 0.9 nm indicating uniform distribution of polystyrene on the surfaces in the mesopores.

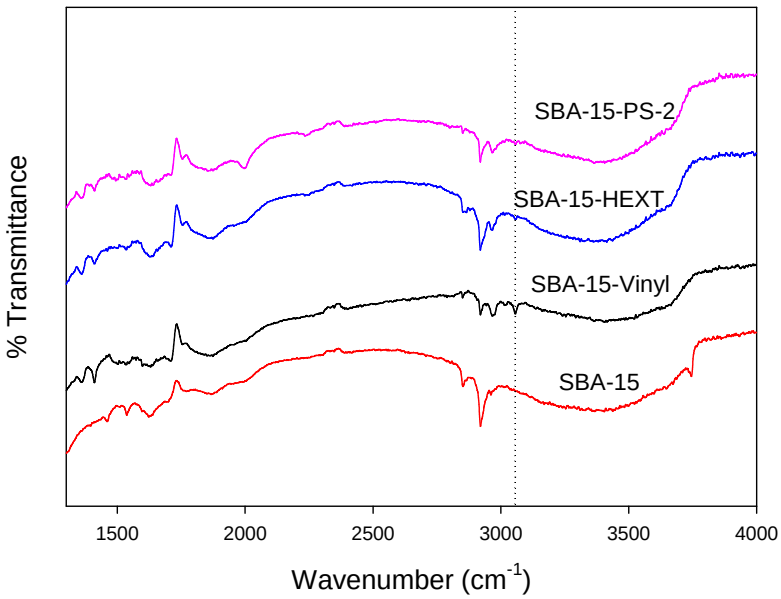

Figure 3.20. FT-IR spectra of SBA-15, SBA-15 modified with vinyl group (SBA-15-vinyl), 1-hexanethiol (SBA-15-HEXT) and HS-PS (SBA-15-PS-2).

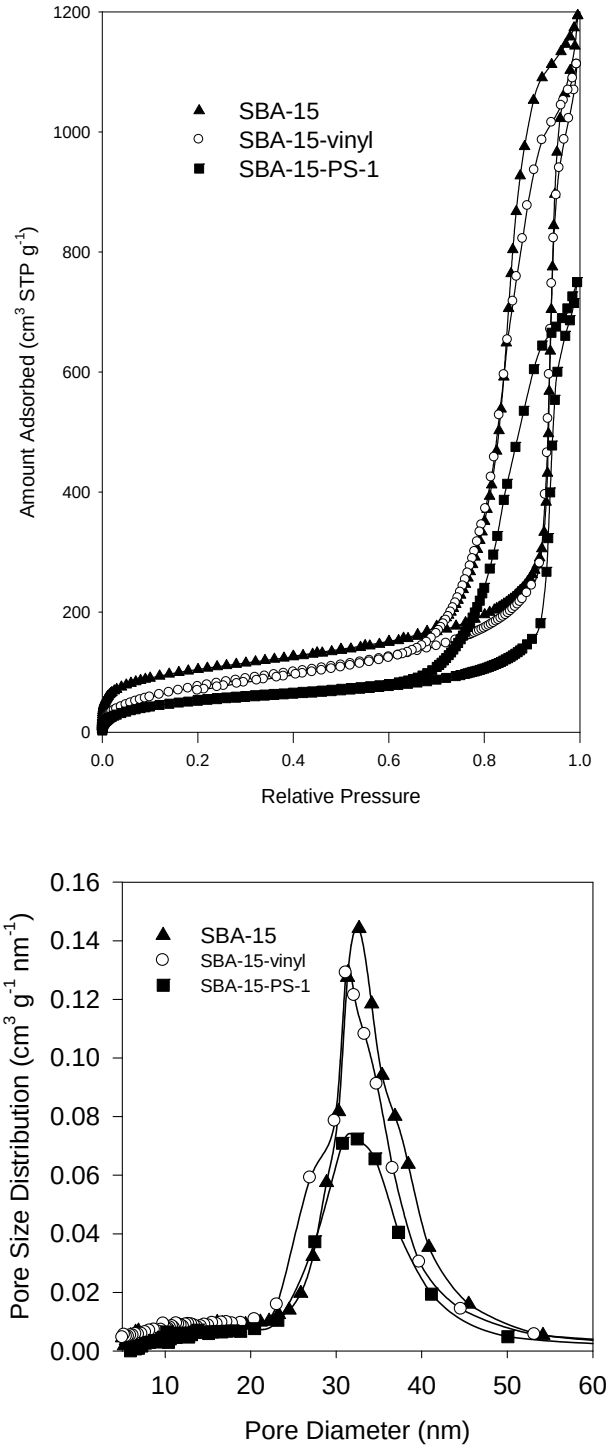

Figure 3.21. Pore size distributions for unmodified SBA-15, and SBA-15 modified with vinyl groups and HS-PS-1 (Mn = 14419 g/mol, PDI=1.16).

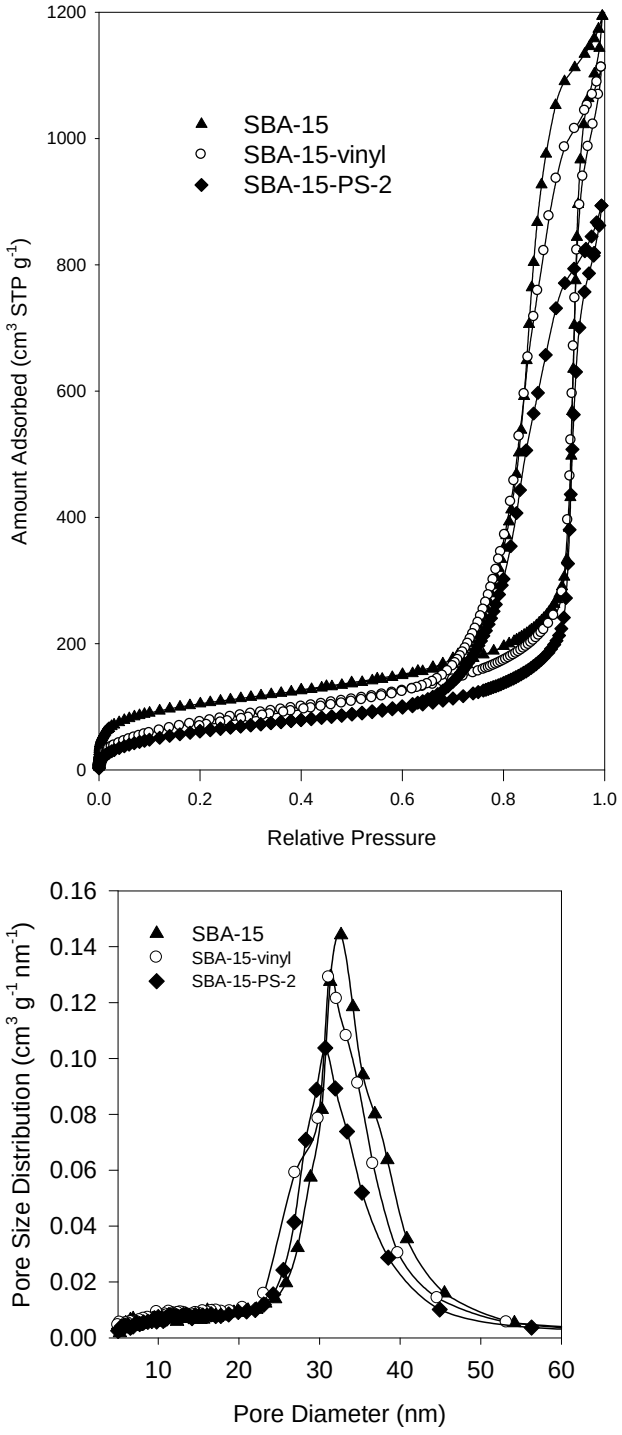

Figure 3.22. Pore size distributions for unmodified SBA-15, and SBA-15 modified with vinyl groups and HS-PS-2 (Mn = 2507 g/mol, PDI=1.38).

Table 3.9. Structural parameters of samples determined by nitrogen adsorption

Sample	BET surface area (m^2 g^{-1})	Total pore volume (cm^3 g^{-1})	BJH pore diameter (nm)
SBA-15	378	1.77	32.4
SBA-15-Vinyl	296	1.65	31.5
SBA-15-HEXT	275	1.46	33.3
SBA-15-PS-1	199	1.11	31.5
SBA-15-PS-2	236	1.33	30.6

3.2.3.3. Conclusion

As the first example of thiol-ene "click" grafting of polymers to the pores of OMSs, the exploration of new "grafting to" method was quite successful. The attachment of thiol-containing substances was confirmed by TGA, FT-IR and N_2 adsorption. Thiol-ene "click" worked and a reasonable conversion of alkene groups was achieved when small thiol molecules were used. The grafting of polymers showed quite low loadings and grafting densities. The molecular weight of polymers affected the grafting efficiency in a similar way as in the study of Huisgen cycloaddition "click" grafting approach, that is, the efficiency decreased as the molecular weight of polymer increased. However, the thiol-ene "click" appeared to be much less effective for polymer attachment than the azide-alkyne "click". It should be noted that lower efficiency may stem from the use of a vinyl group located right at the silica surface without any spacer, which might have hindered the access of polymer to the vinyl groups on the surface.

Chapter 4. Conclusions

This dissertation is devoted to exploring of a novel method to synthesize ordered mesoporous silicas with ultra-large mesopores (Chapter 2) and to functionalize the surfaces of the latter and other related ordered mesoporous silicas with small molecules and polymers (Chapter 3).

The approaches established herein were facile, reproducible, effective and versatile. Xylenes (mixture of isomers) was successfully identified as a superior swelling agent, which worked perfectly with the commercially available surfactant, Pluronic F127 ($EO_{106}PO_{70}EO_{106}$), to achieve ordered mesoporous silicas with desired face-centered cubic structure and very large pore diameter. The ultra-large pore FDU-12 silicas exhibited unit-cell parameters (up to 56 nm) and pore diameters (up to 36 nm) comparable to the highest values for Fm3m silica structures templated by custom-made surfactants, which were reported in the literature. The library of the swelling agents with superior performance was extended to xylene isomers and ethylbenzene. In particular, ethylbenzene was proven to be another powerful micelle expander to create ultra-large pore FDU-12 silicas, being as effective as xylenes (isomer mixture) and seemingly somewhat more effective than individual xylene isomers.

Highly ordered closed-pore FDU-12 silicas were prepared via a simple thermally-induced pore closure process at temperatures as low as 400-450 °C. These closed-pore silicas possessed appreciable pore volumes as determined from extrapolation of pore volume vs. unit-cell volume relation for open pore materials. These results suggested that low dielectric constant closed-pore materials with and appreciable pore volume can be prepared through the thermally-induced pore closure process.

Diverse surface modification methods were studied to introduce organic groups to the surfaces of ordered mesoporous silicas, including "grafting from" and "grafting to" approaches. In the "grafting from" approach, polymers grow from the initiation sites on the surface via surface-initiated polymerization. In the "grafting to" approach, molecules or pre-formed polymers are attached to the surface by forming covalent bond between the functional groups on the surface and the attachment points (functional groups) on grafted molecules.

FDU-12 silica with 3-D pore system was used as the solid support for the surface-initiated grafting of temperature-responsive polymers. Silica/polymer composites with different polymer loadings were obtained by surface-initiated atom transfer radical polymerization (SI-ATRP) or surface-initiated atom transfer radical polymerization with activators regenerated by electron transfer (SI-ARGET ATRP). Good control of the polymerizations was observed in organic and protic media. The composites with as high as ~20 wt.% poly [di(ethylene glycol) methyl ether methacrylate] (PM(EO_2)MA) and poly [2-(methacryloyloxy)ethyl]dimethyl(3-sulfopropyl)ammonium (PMEDSAH) showed accessible mesopores.

The Huisgen azide-alkyne cycloaddition "click" reaction and thiol-ene "click" reaction were employed as coupling methods for grafting organic groups to the surfaces of cylindrical mesopores of SBA-15 silicas. Oligomers, monosaccharides, and poly(methyl methacrylate) were attached to the nanopores via Cu(I) catalyzed Huisgen cycloaddition "click" grafting. Moderate to high grafting densities were achieved. Especially for low-molecular weight PMMA, the grafting density reached ~0.12 chains/nm^2, which is quite high as for the "grafting to" attachment. The distribution of attached molecules was

uniform on the surfaces of mesopores. All the functionalized silicas showed accessible pores. Thiol-ene “click” reaction also found suitable for the grafting of a small thiol molecule and low-molecular weight polystyrene. Although the grafting density was lower than the value achieved by Huisgen cycloaddition “click” grafting of polymers, the “metal-free” feature of this method is known to be especially valuable for applications in the biomedical area. Both “click” reactions demonstrated applicability of the “grafting to” method in the confined spaces and provided robust and convenient alternative approaches to construct ordered mesoporous silica/polymer composites.

Bibliography

(1) Wan, Y.; Zhao, D. *Chem. Rev.* **2007**, *107*, 2821.

(2) Hoffmann, F.; Cornelius, M.; Morell, J.; Froeba, M. *Angew. Chem. Int. Ed.* **2006**, *45*, 3216.

(3) Sing, K. S. W.; Everett, D. H.; Haul, R. A. W.; Moscou, L.; Pierotti, R. A.; Rouquerol, J.; Siemieniewska, T. *Pure Appl. Chem.* **1985**, *57*, 603.

(4) Inagaki, S.; Fukushima, Y.; Kuroda, K. *J. Chem. Soc., Chem. Commun.* **1993**, 680.

(5) Kresge, C. T.; Leonowicz, M. E.; Roth, W. J.; Vartuli, J. C.; Beck, J. S. *Nature* **1992**, *359*, 710.

(6) Huo, Q.; Margolese, D. I.; Ciesla, U.; Demuth, D. G.; Feng, P.; Gier, T. E.; Sieger, P.; Firouzi, A.; Chmelka, B. F. *Chem. Mater.* **1994**, *6*, 1176.

(7) Flodström, K.; Wennerström, H.; Teixeira, C. V.; Amenitsch, H.; Lindén, M.; Alfredsson, V. *Langmuir* **2004**, *20*, 10311.

(8) Huo, Q.; Margolese, D. I.; Stucky, G. D. *Chem. Mater.* **1996**, *8*, 1147.

(9) Beck, J. S.; Vartuli, J. C.; Roth, W. J.; Leonowicz, M. E.; Kresge, C. T.; Schmitt, K. D.; Chu, C. T. W.; Olson, D. H.; Sheppard, E. W. *J. Am. Chem. Soc.* **1992**, *114*, 10834.

(10) Huo, Q.; Margolese, D. I.; Ciesla, U.; Feng, P.; Gier, T. E.; Sieger, P.; Leon, R.; Petroff, P. M.; Schueth, F.; Stucky, G. D. *Nature* **1994**, *368*, 317.

(11) Sakamoto, Y.; Kaneda, M.; Terasaki, O.; Zhao, D. Y.; Kim, J. M.; Stucky, G.; Shin, H. J.; Ryoo, R. *Nature* **2000**, *408*, 449.

(12) Huo, Q.; Leon, R.; Petroff, P. M.; Stucky, G. D. *Science* **1995**, *268*, 1324.

(13) Sayari, A.; Liu, P.; Kruk, M.; Jaroniec, M. *Chem. Mater.* **1997**, *9*, 2499.

(14) Bagshaw, S. A.; Prouzet, E.; Pinnavaia, T. J. *Science* **1995**, *269*, 1242.

(15) Zhao, D.; Feng, J.; Huo, Q.; Melosh, N.; Frederickson, G. H.; Chmelka, B. F.; Stucky, G. D. *Science* **1998**, *279*, 548.

(16) Zhao, D.; Yang, P. D.; Melosh, N.; Feng, Y. L.; Chmelka, B. F.; Stucky, G. *Adv. Mater.* **1998**, *10*, 1380.

(17) Kruk, M.; Jaroniec, M.; Ko, C. H.; Ryoo, R. *Chem. Mater.* **2000**, *12*, 1961.

(18) Ryoo, R.; Ko, C. H.; Kruk, M.; Antochshuk, V.; Jaroniec, M. *J. Phys. Chem. B* **2000**, *104*, 11465.

(19) Zhao, D.; Huo, Q.; Feng, J.; Chmelka, B. F.; Stucky, G. D. *J. Am. Chem. Soc.* **1998**, *120*, 6024.

(20) Sakamoto, Y.; Diaz, I.; Terasaki, O.; Zhao, D.; Perez-Pariente, J.; Kim, J. M.; Stucky, G. D. *J. Phys. Chem. B* **2002**, *106*, 3118.

(21) Yu, C.; Yu, Y.; Zhao, D. *Chem. Commun.* **2000**, 575.

(22) Matos, J. R.; Kruk, M.; Mercuri, L. P.; Jaroniec, M.; Zhao, L.; Kamiyama, T.; Terasaki, O.; Pinnavaia, T. J.; Liu, Y. *J. Am. Chem. Soc.* **2003**, *125*, 821.

(23) Fan, J.; Yu, C.; Gao, F.; Lei, J.; Tian, B.; Wang, L.; Luo, Q.; Tu, B.; Zhou, W.; Zhao, D. *Angew. Chem. Int. Ed.* **2003**, *42*, 3146.

(24) Kleitz, F.; Liu, D.; Anilkumar, G. M.; Park, I.-S.; Solovyov, L. A.; Shmakov, A. N.; Ryoo, R. *J. Phys. Chem. B* **2003**, *107*, 14296.

(25) Fan, J.; Yu, C.; Lei, J.; Zhang, Q.; Li, T.; Tu, B.; Zhou, W.; Zhao, D. *J. Am. Chem. Soc.* **2005**, *127*, 10794.

(26) Monnier, A.; Schuth, F.; Huo, Q.; Kumar, D.; Margolese, D.; Maxwell, R. S.; Stucky, G. D.; Krishnamurty, M.; Petroff, P.; Firouzi, A.; Janicke, M.; Chmelka, B. F. *Science* **1993**, *261*, 1299.

(27) Chan, Y.-T.; Lin, H.-P.; Mou, C.-Y.; Liu, S.-T. *Chem. Commun.* **2002**, 2878.

(28) Kleitz, F.; Choi, S. H.; Ryoo, R. *Chem. Commun.* **2003**, 2136.

(29) Kim, T.-W.; Kleitz, F.; Paul, B.; Ryoo, R. *J. Am. Chem. Soc.* **2005**, *127*, 7601.

(30) Che, S.; Garcia-Bennett, A. E.; Liu, X.; Hodgkins, R. P.; Wright, P. A.; Zhao, D.; Terasaki, O.; Tatsumi, T. *Angew. Chem. Int. Ed.* **2003**, *42*, 3930.

(31) Han, Y.; Lee, S. S.; Ying, J. Y. *Chem. Mater.* **2006**, *18*, 643.

(32) Yang, H.; Li, J.; Yang, J.; Liu, Z.; Yang, Q.; Li, C. *Chem. Commun.* **2007**, 1086.

(33) Shui, W.; Fan, J.; Yang, P.; Liu, C.; Zhai, J.; Lei, J.; Yan, Y.; Zhao, D.; Chen, X. *Anal. Chem.* **2006**, *78*, 4811.

(34) Yang, P.; Zhao, D.; Chmelka, B. F.; Stucky, G. D. *Chem. Mater.* **1998**, *10*, 2033.

(35) El-Safty, S. A.; Hanaoka, T.; Mizukami, F. *Chem. Mater.* **2005**, *17*, 3137.

(36) Fan, J.; Lei, J.; Wang, L.; Yu, C.; Tu, B.; Zhao, D. *Chem. Commun.* **2003**, 2140.

(37) Hudson, S.; Cooney, J.; Hodnett, B. K.; Magner, E. *Chem. Mater.* **2007**.

(38) Urrego, S.; Serra, E.; Alfredsson, V.; Blanco, R. M.; Díaz, I. *Microporous and Mesoporous Mater.* **2010**, *129*, 173.

(39) Kruk, M.; Dufour, B.; Celer, E. B.; Kowalewski, T.; Jaroniec, M.; Matyjaszewski, K. *Macromolecules* **2008**, *41*, 8584.

(40) Yiu, H. H. P.; Niu, H.-j.; Biermans, E.; Tendeloo, G. v.; Rosseinsky, M. J. *Adv. Funct. Mater.* **2010**, published on Web.

(41) Tian, B.; Liu, X.; Yang, H.; Xie, S.; Yu, C.; Tu, B.; Zhao, D. *Adv. Mater.* **2003**, *15*, 1370.

(42) Kruk, M.; Dufour, B.; Celer, E. B.; Kowalewski, T.; Jaroniec, M.; Matyjaszewski, K. *J. Phys. Chem. B* **2005**, *109*, 9216.

(43) Yu, K.; Hurd, A. J.; Eisenberg, A.; Brinker, C. J. *Langmuir* **2001**, *17*, 7961.

(44) Kruk, M.; Hui, C. M. *J. Am. Chem. Soc.* **2008**, *130*, 1528.

(45) Smarsly, B.; Xomeritakis, G.; Yu, K.; Liu, N.; Fan, H.; Assink, R. A.; Drewien, C. A.; Ruland, W.; Brinker, C. J. *Langmuir* **2003**, *19*, 7295.

(46) Yu, K.; Smarsly, B.; Brinker, C. J. *Adv. Funct. Mater.* **2003**, *13*, 47.

(47) Yu, K.; Wu, X.; Brinker, C. J.; Ripmeester, J. *Langmuir* **2003**, *19*, 7282.

(48) Sayari, A.; Yang, Y.; Kruk, M.; Jaroniec, M. *J. Phys. Chem. B* **1999**, *103*, 3651.

(49) Jana, S. K.; Nishida, R.; Shindo, K.; Kugita, T.; Namba, S. *Microporous and Mesoporous Mater.* **2004**, *68*, 133.

(50) Kruk, M.; Cao, L. *Langmuir* **2007**, *23*, 7247.

(51) Kruk, M.; Hui, C. M. *Microporous and Mesoporous Mater.* **2008**, *114*, 64.

(52) Cao, L.; Man, T.; Kruk, M. *Chem. Mater.* **2009**, *21*, 1144.

(53) Nagarajan, R. *Colloid. Surface. B* **1999**, *16*, 55.

(54) Nagarajan, R.; Barry, M.; Ruckenstein, E. *Langmuir* **1986**, *2*, 210.

(55) Lettow, J. S.; Han, Y. J.; Schmidt-Winkel, P.; Yang, P.; Zhao, D.; Stucky, G. D.; Ying, J. Y. *Langmuir* **2000**, *16*, 8291.

(56) Schmidt-Winkel, P.; Lukens, W. W.; Zhao, D.; Yang, P.; Chmelka, B. F.; Stucky, G. D. *J. Am. Chem. Soc.* **1999**, *121*, 254.

(57) Huang, L.; Kruk, M. *J. Colloid Interface Sci.* **2012**, *365*, 137.

(58) Yiu, H. H. P.; Wright, P. A. *J. Mater. Chem.* **2005**, *15*, 3690.

(59) Hartmann, M. *Chem. Mater.* **2005**, *17*, 4577.

(60) Wu, C. G.; Bein, T. *Science* **1994**, *264*, 1757.

(61) Save, M.; Granvorka, G.; Bernard, J.; Charleux, B.; Boissiere, C.; Grosso, D.; Sanchez, C. *Macromol. Rapid Commun.* **2006**, *27*, 393.

(62) Moreno, J.; Sherrington, D. C. *Chem. Mater.* **2008**, *20*, 4468.

(63) Fu, Q.; Rao, G. V. R.; Ista, L. K.; Wu, Y.; Andrzejewski, B. P.; Sklar, L. A.; Ward, T. L.; Lopez, G. P. *Adv. Mater.* **2003**, *15*, 1262.

(64) Zhou, Z.; Zhu, S.; Zhang, D. *J. Mater. Chem.* **2007**, *17*, 2428.

(65) Moller, K.; Bein, T. *Chem. Mater.* **1998**, *10*, 2950.

(66) Sayari, A.; Hamoudi, S. *Chem. Mater.* **2001**, *13*, 3151.

(67) Stein, A.; Melde, B. J.; Schroden, R. C. *Adv. Mater.* **2000**, *12*, 1403.

(68) Jaroniec, C. P.; Kruk, M.; Jaroniec, M.; Sayari, A. *J. Phys. Chem. B* **1998**, *102*, 5503.

(69) Wei, J.; Wang, H.; Deng, Y.; Sun, Z.; Shi, L.; Tu, B.; Luqman, M.; Zhao, D. *J. Am. Chem. Soc.* **2011**.

(70) Suzuki, N.; Kiba, S.; Yamauchi, Y. *Mater. Lett.* **2011**, *65*, 544.

(71) Zou, H.; Wu, S.; Shen, J. *Chem. Rev.* **2008**, *108*, 3893.

(72) Matyjaszewski, K.; Xia, J. *Chem. Rev.* **2001**, *101*, 2921.

(73) Edmondson, S.; Osborne, V. L.; Huck, W. T. S. *Chem. Soc. Rev.* **2004**, *33*, 14.

(74) Cao, L.; Kruk, M. *Polym. Prepr.* **2008**, *49(2)*, 294.

(75) Cao, L.; Dufour, B.; Matyjaszewski, K.; Kruk, M. *Polym. Prepr.* **2009**, *50*, 348.

(76) Cao, L. K., M. *Polym. Chem.* **2010**, *1*, 97.

(77) Martin, A.; Morales, G.; Martinez, F.; van Grieken, R.; Cao, L.; Kruk, M. *J. Mater. Chem.* **2010**, *20,8026*.

(78) Nguyen, J. V. J., C. W. *Macromolecules* **2004**, *37*.

(79) Jakubowski, W.; Matyjaszewski, K. *Angew. Chem. Int. Ed.* **2006**, *45*, 4482.

(80) Cao, L. *Dissertation*, the Graduate Center, the City University of New York, **2010**.

(81) Kolb, H. C.; Finn, M. G.; Sharpless, K. B. *Angew. Chem. Int. Ed.* **2001**, *40*, 2004.

(82) Lutz, J.-F. *Angew. Chem. Int. Ed.* **2007**, *46*, 1018.

(83) Johnson, J. A.; Finn, M. G.; Koberstein, J. T.; Turro, N. J. *Macromol. Rapid Commun.* **2008**, *29*, 1052.

(84) Binder, W. H.; Sachsenhofer, R. *Macromol. Rapid Commun.* **2007**, *28*, 15.

(85) Binder, W. H.; Sachsenhofer, R. *Macromol. Rapid Commun.* **2008**, *29*, 952.

(86) Meldal, M.; Tornoe, C. W. *Chem. Rev.* **2008**, *108*, 2952.

(87) Tornoe, C. W.; Christensen, C.; Meldal, M. *J. Org. Chem.* **2002**, *67*, 3057.

(88) Malkoch, M.; Thibault, R. J.; Drockenmuller, E.; Messerschmidt, M.; Voit, B.; Russell, T. P.; Hawker, C. J. *J. Am. Chem. Soc.* **2005**, *127*, 14942.

(89) Opsteen, J. A.; van Hest, J. C. M. *Chem. Commun.* **2005**, 57.

(90) Gao, H.; Matyjaszewski, K. *Macromolecules* **2006**, *39*, 4960.

(91) Gondi, S. R.; Vogt, A. P.; Sumerlin, B. S. *Macromolecules* **2007**, *40*, 474.

(92) Lin, W.; Fu, Q.; Zhang, Y.; Huang, J. *Macromolecules* **2008**, *41*, 4127.

(93) Quemener, D.; Davis, T. P.; Barner-Kowollik, C.; Stenzel, M. H. *Chem. Commun.* **2006**, 5051.

(94) Tasdelen, M. A.; Van Camp, W.; Goethals, E.; Dubois, P.; Du Prez, F.; Yagci, Y. *Macromolecules* **2008**, *41*, 6035.

(95) Shi, W.; Dolai, S.; Rizk, S.; Hussain, A.; Tariq, H.; Averick, S.; L'Amoreaux, W.; El Idrissi, A.; Banerjee, P.; Raja, K. *Org. Lett.* **2007**, *9*, 5461.

(96) Kaltgrad, E.; Sen Gupta, S.; Punna, S.; Huang, C.-Y.; Chang, A.; Wong, C.-H.; Finn, M. G.; Blixt, O. *ChemBioChem* **2007**, *8*, 1455.

(97) Bruckman, M. A.; Kaur, G.; Lee, L. A.; Xie, F.; Sepulveda, J.; Breitenkamp, R.; Zhang, X.; Joralemon, M.; Russell, T. P.; Emrick, T.; Wang, Q. *ChemBioChem* **2008**, *9*, 519.

(98) Landis, E. C.; Hamers, R. J. *Chem. Mater.* **2009**, *21*, 724.

(99) Brennan, J. L.; Hatzakis, N. S.; Tshikhudo, T. R.; Razumas, V.; Patkar, S.; Vind, J.; Svendsen, A.; Nolte, R. J. M.; Rowan, A. E.; Brust, M. *Bioconjugate Chem.* **2006**, *17*, 1373.

(100) Punna, S.; Kaltgrad, E.; Finn, M. G. *Bioconjugate Chem.* **2005**, *16*, 1536.

(101) Vundyala, N.; Sun, C.; Sidime, F.; Shi, W.; L'Amoreaux, W.; Raja, K.; Peetz, R. M. *Tetrahedron Lett.* **2008**, *49*, 6386.

(102) Jiang, X.; Lok, M. C.; Hennink, W. E. *Bioconjugate Chem.* **2007**, *18*, 2077.

(103) Rostovtsev, V. V.; Green, L. G.; Fokin, V. V.; Sharpless, K. B. *Angew. Chem. Int. Ed.* **2002**, *41*, 2596.

(104) Slater, M.; Snauko, M.; Svec, F.; Frechet, J. M. J. *Anal. Chem.* **2006**, *78*, 4969.

(105) Slater, M. D.; Fréchet, J. M. J.; Svec, F. *J. Sep. Sci.* **2009**, *32*, 21.

(106) Britcher, L.; Barnes, T. J.; Griesser, H. J.; Prestidge, C. A. *Langmuir* **2008**, *24*, 7625.

(107) Schlossbauer, A.; Schaffert, D.; Kecht, J.; Wagner, E.; Bein, T. *J. Am. Chem. Soc.* **2008**, *130*, 12558.

(108) Nakazawa, J.; Stack, T. D. P. *J. Am. Chem. Soc.* **2008**, *130*, 14360.

(109) Ciampi, S.; Bocking, T.; Kilian, K. A.; Harper, J. B.; Gooding, J. J. *Langmuir* **2008**, *24*, 5888.

(110) Lummerstorfer, T.; Hoffmann, H. *J. Phys. Chem. B* **2004**, *108*, 3963.

(111) Goto, Y.; Sato, H.; Shinkai, S.; Sada, K. *J. Am. Chem. Soc.* **2008**, *130*, 14354.

(112) Malvi, B.; Sarkar, B. R.; Pati, D.; Mathew, R.; Ajithkumar, T. G.; Sen Gupta, S. *J. Mater. Chem.* **2009**, *19*, 1409.

(113) Kacprzak, K. M.; Maier, N. M.; Lindner, W. *Tetrahedron Lett.* **2006**, *47*, 8721.

(114) Meng, J.-C.; Averbuj, C.; Lewis, W. G.; Siuzdak, G.; Finn, M. G. *Angew. Chem. Int. Ed.* **2004**, *43*, 1255.

(115) Meng, J.-C.; Siuzdak, G.; Finn, M. G. *Chem. Commun.* **2004**, 2108.

(116) Gadzikwa, T.; Lu, G.; Stern, C. L.; Wilson, S. R.; Hupp, J. T.; Nguyen, S. T. *Chem. Commun.* **2008**, 5493.

(117) Kar, M.; Malvi, B.; Das, A.; Panneri, S.; Gupta, S. S. *J. Mater. Chem.* **2011**, *21*, 6690.

(118) Fried, D. I.; Schlossbauer, A.; Bein, T. *Microporous and Mesoporous Mater.* **2012**, *147*, 5.

(119) Huang, L.; Dolai, S.; Raja, K.; Kruk, M. *Langmuir* **2009**, *26*, 2688.

(120) Kumari, S.; Malvi, B.; Ganai, A. K.; Pillai, V. K.; Sen Gupta, S. *J. Phys. Chem. C* **2011**, *115*, 17774.

(121) Lowe, A. B. *Polymer Chem.* **2010**, *1*, 17.

(122) Posner, T.; Dtsch, B. *Chem. Ges.* **1905**, *38*, 646.

(123) Killops, K. L.; Campos, L. M.; Hawker, C. J. *J. Am. Chem. Soc.* **2008**, *130*, 5062.

(124) Chen, G.; Amajjahe, S.; Stenzel, M. H. *Chem. Commun.* **2009**, 1198.

(125) Campos, L. M.; Killops, K. L.; Sakai, R.; Paulusse, J. M. J.; Damiron, D.; Drockenmuller, E.; Messmore, B. W.; Hawker, C. J. *Macromolecules* **2008**, *41*, 7063.

(126) Goldmann, A. S.; Walther, A.; Nebhani, L.; Joso, R.; Ernst, D.; Loos, K.; Barner-Kowollik, C.; Barner, L.; Müller, A. H. E. *Macromolecules* **2009**, *42*, 3707.

(127) van Berkel, K. Y.; Piekarski, A. M.; Kierstead, P. H.; Pressly, E. D.; Ray, P. C.; Hawker, C. J. *Macromolecules* **2009**, *42*, 1425.

(128) Connal, L. A.; Kinnane, C. R.; Zelikin, A. N.; Caruso, F. *Chem. Mater.* **2009**, *21*, 576.

(129) Triola, G.; Brunsveld, L.; Waldmann, H. *J. Org. Chem.* **2008**, *73*, 3646.

(130) Jones, M. W.; Mantovani, G.; Ryan, S. M.; Wang, X.; Brayden, D. J.; Haddleton, D. M. *Chem. Commun.* **2009**, 5272.

(131) Boyer, C.; Davis, T. P. *Chem. Commun.* **2009**, 6029.

(132) Fiore, M.; Marra, A.; Dondoni, A. *J. Org. Chem.* **2009**, *74*, 4422.

(133) Hong, V.; Kislukhin, A. A.; Finn, M. G. *J. Am. Chem. Soc.* **2009**, *131*, 9986.

(134) Ma, G.; Yan, X.; Li, Y.; Xiao, L.; Huang, Z.; Lu, Y.; Fan, J. *J. Am. Chem. Soc.* **2010**, *132*, 9596.

(135) Roux, E. L.; Liang, Y.; Storz, M. P.; Anwander, R. *J. Am. Chem. Soc.* **2010**, *132*, 16368.

(136) Deng, Y.; Yu, T.; Wan, Y.; Shi, S.; Meng, Y.; Gu, D.; Zhang, L.; Huang, Y.; Liu, C.; Wu, X.; Zhao, D. *J. Am. Chem. Soc.* **2007**, *129*, 1690.

(137) Tian, B.; Liu, X.; Yu, C.; Gao, F.; Luo, Q.; Xie, S.; Tu, B.; Zhao, D. *Chem. Commun.* **2002**, 1186.

(138) Huang, L.; Yan, X.; Kruk, M. *Langmuir* **2010**, *26*, 14871.

(139) Mandal, M.; Kruk, M. *J. Mater. Chem.* **2010**, *20*, 7506.

(140) Mandal, M.; Kruk, M. *J. Phys. Chem. C* **2010**, *114*, 20091.

(141) Zhou, X.; Qiao, S.; Hao, N.; Wang, X.; Yu, C.; Wang, L.; Zhao, D.; Lu, G. Q. *Chem. Mater.* **2007**, *19*, 1870.

(142) Jaroniec, M.; Kruk, M.; Olivier, J. P. *Langmuir* **1999**, *15*, 5410.

(143) Kruk, M.; Hui, C. M. *In Hybrid Nanomaterials: Synthesis, Characterization, and Applications*; Chauhan, B. P. S., Ed.; Wiley: 2011, p 285.

(144) Kruk, M.; Jaroniec, M.; Sayari, A. *Langmuir* **1997**, *13*, 6267.

(145) Ravikovitch, P. I.; Neimark, A. V. *Langmuir* **2002**, *18*, 1550.

(146) Yuan, P.; Sun, J.; Xu, H.; Zhou, L.; Liu, J.; Zhang, D.; Wang, Y.; Jack, K. S.; Drennan, J.; Zhao, D.; Lu, G.; Zou, X.; Zou, J.; Yu, C. *Chem. Mater.* **2010**, *23*, 229.

(147) Yu, T.; Zhang, H.; Yan, X.; Chen, Z.; Zou, X.; Oleynikov, P.; Zhao, D. *J. Phys. Chem. B* **2006**, *110*, 21467.

(148) Yang, C.-M.; Schmidt, W.; Kleitz, F. *J. Mater. Chem.* **2005**, *15*, 5112.

(149) Kruk, M.; Jaroniec, M. *Chem. Mater.* **2003**, *15*, 2942.

(150) Broekhoff, J. C. P.; De Boer, J. H. *J. Catal.* **1968**, *10*, 153.

(151) Schmidt, W. *Microporous and Mesoporous Mater.* **2009**, *117*, 372.

(152) Kruk, M.; Hui, C. M. *J. Am. Chem. Soc.* **2008**, *130*, 1528.

(153) Kim, T. W.; Ryoo, R.; Kruk, M.; Gierszal, K. P.; Jaroniec, M.; Kamiya, S.; Terasaki, O. *J. Phys. Chem. B* **2004**, *108*, 11480.

(154) Che, S.; Li, H.; Lim, S.; Sakamoto, Y.; Terasaki, O.; Tatsumi, T. *Chem. Mater.* **2005**, *17*, 4103.

(155) Q. Fu, G. V. R. R., L.K. Ista, Y. Wu, B.P. Andrzejewski, L.A. Sklar, T.L. Ward, G.P.Lopez. *Adv. Mater.* **2003**, *15*, 1262.

(156) Calvo, A.; Yameen, B.; Williams, F. J.; Soler-Illia, G. J. A. A.; Azzaroni, O. *J. Am. Chem. Soc.* **2009**, *131*, 10866.

(157) Save, M. G., G.; Bernard, J.; Charleux, B.; Boissiere, C.; Grosso, D.; Sanchez, C. *Macromol. Rapid Commun.* **2006**, *27*, 393.

(158) Calvo, A. Y., B.; Williams, F. J.; Azzaroni, O.; Soler-Illia, G. J. A. A. *Chem. Commun.* **2009**, 2553.

(159) Barrett, E. P.; Joyner, L. G.; Halenda, P. P. *J. Am. Chem. Soc.* **1951**, *73*, 373.

(160) Lutz, J.-F.; Hoth, A. *Macromolecules* **2005**, *39*, 893.

(161) Yamamoto, S.-i.; Pietrasik, J.; Matyjaszewski, K. *Macromolecules* **2008**, *41*, 7013.

(162) Han, S.; Hagiwara, M.; Ishizone, T. *Macromolecules* **2003**, *36*, 8312.

(163) Ali, M. M.; Stöver, H. D. H. *Macromolecules* **2004**, *37*, 5219.

(164) Dong, H.; Matyjaszewski, K. *Macromolecules* **2010**, *43*, 4623.

(165) Wischerhoff, E.; Uhlig, K.; Lankenau, A.; Börner, H. G.; Laschewsky, A.; Duschl, C.; Lutz, J.-F. *Angew. Chem. Int. Ed.* **2008**, *47*, 5666.

(166) Glinel, K.; Jonas, A. M.; Jouenne, T.; Leprince, J. r. m.; Galas, L.; Huck, W. T. S. *Bioconjugate Chem.* **2008**, *20*, 71.

(167) Jonas, A. M.; Hu, Z.; Glinel, K.; Huck, W. T. S. *Nano Lett.* **2008**, *8*, 3819.

(168) Jonas, A. M.; Hu, Z.; Glinel, K.; Huck, W. T. S. *Macromolecules* **2008**, *41*, 6859.

(169) Laloyaux, X.; Mathy, B.; Nysten, B.; Jonas, A. M. *Langmuir* **2009**, *26*, 838.

(170) Jonas, A. M. G., K.; Oren, R.; Nysten, B.; Huck, W. T. S. *Macromolecules* **2007**, *40*, 4403.

(171) Li, D.; Jones, G. L.; Dunlap, J. R.; Hua, F.; Zhao, B. *Langmuir* **2006**, *22*, 3344.

(172) Yamamoto, S.-i.; Matyjaszewski, K. *Polym. J.* **2008**, *40*, 496.

(173) Cheng, N.; Brown, A. A.; Azzaroni, O.; Huck, W. T. S. *Macromolecules* **2008**, *41*, 6317.

(174) Azzaroni, O.; Brown, A. A.; Huck, W. T. S. *Angew. Chem. Int. Ed.* **2006**, *45*, 1770.

(175) Zhang, Z.; Chao, T.; Chen, S.; Jiang, S. *Langmuir* **2006**, *22*, 10072.

(176) Ladd, J.; Zhang, Z.; Chen, S.; Hower, J. C.; Jiang, S. *Biomacromolecules* **2008**, *9*, 1357.

(177) Polzer, F.; Heigl, J.; Schneider, C.; Ballauff, M.; Borisov, O. V. *Macromolecules* **2011**, *44*, 1654.

(178) Xu, L.; Ye, Z.; Cui, Q.; Gu, Z.; Mercier, L. *Polymer* **2011**, *52*, 5961.

(179) Zhang, Y.; Luo, S.; Tang, Y.; Yu, L.; Hou, K.-Y.; Cheng, J.-P.; Zeng, X.; Wang, P. G. *Anal. Chem.* **2006**, *78*, 2001.

(180) Michel, O.; Ravoo, B. J. *Langmuir* **2008**, *24*, 12116.

(181) Ostaci, R.-V.; Damiron, D.; Capponi, S.; Vignaud, G.; Leger, L.; Grohens, Y.; Drockenmuller, E. *Langmuir* **2008**, *24*, 2732.

(182) Fazio, F.; Bryan, M. C.; Blixt, O.; Paulson, J. C.; Wong, C.-H. *J. Am. Chem. Soc.* **2002**, *124*, 14397.

(183) Collman, J. P.; Devaraj, N. K.; Chidsey, C. E. D. *Langmuir* **2004**, *20*, 1051.

(184) Haensch, C.; Erdmenger, T.; Fijten, M. W. M.; Hoeppener, S.; Schubert, U. S. *Langmuir* **2009**, *25*, 8019.

(185) Paxton, W. F.; Spruell, J. M.; Stoddart, J. F. *J. Am. Chem. Soc.* **2009**, *131*, 6692.

(186) Sun, X.-L.; Stabler, C. L.; Cazalis, C. S.; Chaikof, E. L. *Bioconjugate Chem.* **2006**, *17*, 52.

(187) Chen, G.; Tao, L.; Mantovani, G.; Ladmiral, V.; Burt, D. P.; Macpherson, J. V.; Haddleton, D. *Soft Matter.* **2007**, *3*, 732.

(188) Guo, Z.; Lei, A.; Liang, X.; Xu, Q. *Chem. Commun.* **2006**, 4512.

(189) White, M. A.; Johnson, J. A.; Koberstein, J. T.; Turro, N. J. *J. Am. Chem. Soc.* **2006**, *128*, 11356.

(190) An, Z.; Tang, W.; Wu, M.; Jiao, Z.; Stucky, G. D. *Chem. Commun.* **2008**, 6501.

(191) Zhou, Y.; Wang, S.; Xie, Y.; Guan, W.; Ding, B.; Yang, Z.; Jiang, X. *Nanotechnology* **2008**, *19*, 175601.

(192) Fleming, D. A.; Thode, C. J.; Williams, M. E. *Chem. Mater.* **2006**, *18*, 2327.

(193) Binder, W. H.; Sachsenhofer, R.; Straif, C. J.; Zirbs, R. *J. Mater. Chem.* **2007**, *17*, 2125.

(194) Hayashi, K.; Moriya, M.; Sakamoto, W.; Yogo, T. *Chem. Mater.* **2009**, *21*, 1318.

(195) Ranjan, R.; Brittain, W. J. *Macromolecules* **2007**, *40*, 6217.

(196) Ranjan, R.; Brittain, W. J. *Macromol. Rapid Commun.* **2007**, *28*, 2084.

(197) Evans, C. E.; Lovell, P. A. *Chem. Commun.* **2009**, 2305.

(198) Huang, C.-J.; Chang, F.-C. *Macromolecules* **2009**, *42*, 5155.

(199) Polito, L.; Monti, D.; Caneva, E.; Delnevo, E.; Russo, G.; Prosperi, D. *Chem. Commun.* **2008**, 621.

(200) Gole, A.; Murphy, C. J. *Langmuir* **2008**, *24*, 266.

(201) Li, H.; Cheng, F.; Duft, A. M.; Adronov, A. *J. Am. Chem. Soc.* **2005**, *127*, 14518.

(202) Zhang, Y.; He, H.; Gao, C. *Macromolecules* **2008**, *41*, 9581.

(203) Fu, G. D.; Xu, L. Q.; Yao, F.; Zhang, K.; Wang, X. F.; Zhu, M. F.; Nie, S. Z. *ACS Appl. Mater. Interfaces* **2009**, *1*, 239.

(204) Beck, J. S.; Vartuli, J. C.; Roth, W. J.; Leonowicz, M. E.; Kresge, C. T.; Schmitt, K. D.; Chu, C. T. W.; Olson, D. H.; Sheppard, E. W.; McCullen, S. B.; Higgins, J. B.; Schlenker, J. L. *J. Am. Chem. Soc.* **1992**, *114*, 10834.

(205) Kruk, M.; Dufour, B.; Celer, E. B.; Kowalewski, T.; Jaroniec, M.; Matyjaszewski, K. *J. Phys. Chem. B* **2005**, *109*, 9216.

(206) Asefa, T.; Kruk, M.; MacLachlan, M. J.; Coombs, N.; Grondey, H.; Jaroniec, M.; Ozin, G. A. *Adv. Funct. Mater.* **2001**, *11*, 447.

(207) Sen Gupta, S.; Raja, K. S.; Kaltgrad, E.; Strable, E.; Finn, M. G. *Chem. Commun.* **2005**, 4315.

(208) Mantovani, G.; Ladmiral, V.; Tao, L.; Haddleton, D. *Chem. Commun.* **2005**, 2089.

(209) Choi, M.; Kleitz, F.; Liu, D.; Lee, H. Y.; Ahn, W.-S.; Ryoo, R. *J. Am. Chem. Soc.* **2005**, *127*, 1924.

(210) Kruk, M.; Dufour, B.; Celer, E. B.; Kowalewski, T.; Jaroniec, M.; Matyjaszewski, K. *Polym. Mater. Sci. Eng.* **2007**, *97*, 274.

(211) Tsarevsky, N. V.; Matyjaszewski, K. *Macromolecules* **2005**, *38*, 3087.